

Copyright is owned by the Author of the thesis. Permission is given for a copy to be downloaded by an individual for the purpose of research and private study only. The thesis may not be reproduced elsewhere without the permission of the Author.

Design and Development of a Low-Cost Hybrid Wheeled-Leg for an Agricultural Robot

A thesis presented in partial fulfilment of the
requirements for the degree of

**Master of Engineering
in
Mechatronics**

at
Massey University, Manawatū Campus
Palmerston North
New Zealand

William T. Wilkinson
July 2020

Abstract

Currently, New Zealand is financially dependent on its agricultural industry quite heavily. However, the agricultural sector faces several problems such as labour shortages, environmental issues and increasing costs. In other industries, robotics and automation have been used to combat these issues successfully. Yet, in agriculture, robotics and automation have only been adopted in horticulture but not in pastoral farming (dairy, sheep, and cattle). This is because the tasks and terrain in horticulture are well defined and structured, whereas, in pastoral farming, the terrain and tasks are unstructured and dynamic. The locomotion used by current horticulture robots is either not capable of operating in unstructured terrain or are inefficient. Therefore, pastoral farming will need to adopt new forms of locomotion in automation platforms.

In this thesis, it is proposed that hybrid wheel-leg locomotion will enable robots to operate in unstructured and dynamic environments. With this in mind, a low-cost prototype hybrid wheeled leg has been designed and built. The leg has been designed to specifications which were developed based on the tasks that a multipurpose horticultural and pastoral farming robot is expected to do.

A joint actuator is extremely influential towards the performance of any robotic leg. Due to the unstructured terrain, in which the leg will operate, it was concluded, that a mechanically compliant actuator is required. Because of the prohibitive cost of commercially available actuators, a prototype high torque, low-cost mechanically compliant actuator was designed and built to meet the specified torque requirements. This was in addition to the design and fabrication of the leg itself.

Once the leg was assembled, the sensors, actuators and the motor were interfaced with ROS™ (Robot Operating System). ROS makes it easy to coherently control each leg's DOF (Degrees of Freedom) and makes it easy to combine and control multiple legs into a robot. Testing of the leg produced very encouraging results, but there were two issues with the performance of the actuator. The first issue is due to the poor implementation of the position control algorithm that came standard with the actuator motor driver. The problem can be resolved through software or the purchase of a different motor driver. The second issue is that the actuator only outputs 23 Nm of torque, but the motor used is rated at 50 Nm. This is due to the cheap drill motor used which is from an unknown brand; it is hoped that a more powerful drill motor from a well known reputable brand will be able to output its rated torque.

Acknowledgements

I would like to thank my supervisor Prof. Gourab Sen Gupta and my co-supervisor Ken Mercer for their guidance and support throughout.

I would also like to acknowledge Dr. Morio Fukuoka for his input, and the workshop staff, Ian Thomas, Clive Bardell and Anthony Wade, for their guidance, manufacturing of the components used in the project, conversation and company.

Thanks also goes out to Nick Look for setting up a SolidWorks simulation server, IT support and conversation, and thanks to Tobin Hall for his knowledge and guidance on BLDC motor control, and for being there to bounce ideas off.

I would also like to thank my close friends Pulathisi Wickramanayake, Robbie Cartwright, Ryan Simpson, Reid Atkinson and Adam Bartlett for their friendship, support, encouragement and company throughout my studies.

Thanks of course to my parents and family for their support and encouragement throughout my undergraduate and postgraduate journey.

I would like to extend a special thanks to Sonja Willemse for her unwavering love and support throughout this thesis. Her research competence and reviewing abilities have been invaluable in the completion of this thesis.

Table of Contents

ABSTRACT	I
ACKNOWLEDGEMENTS.....	III
TABLE OF CONTENTS	V
LIST OF FIGURES	X
LIST OF TABLES.....	XIV
LIST OF ABBREVIATIONS.....	XV
1 INTRODUCTION	1
1.1 RATIONALE AND IMPORTANCE OF RESEARCH.....	1
1.2 SCOPE OF RESEARCH	3
2 REVIEW OF MOBILE ROBOT LOCOMOTION.....	5
2.1 BACKGROUND	5
2.2 ROBOTS IN INDOOR AGRICULTURE	5
2.3 ROBOTS IN OUTDOOR FARMING	6
2.4 ROBOT LOCOMOTION	11
2.4.1 <i>Wheeled locomotion</i>	11
2.4.2 <i>Tracked locomotion</i>	12
2.4.3 <i>Legged locomotion</i>	13
2.4.4 <i>Wheel-track hybrid locomotion</i>	14
2.4.5 <i>Leg-track hybrid</i>	14
2.4.6 <i>Leg-wheel hybrid</i>	15
2.4.7 <i>Leg –wheel-track hybrid</i>	16
2.4.8 <i>Locomotion selection</i>	17
2.5 LEG ACTUATORS.....	18
2.6 ADJUSTABLE COMPLIANCE ACTUATOR DESIGNS	19
2.6.1 <i>Equilibrium-controlled Stiffness</i>	19
2.6.2 <i>Antagonistic-controlled stiffness</i>	19
2.6.3 <i>Structure-controlled stiffness</i>	20
2.6.4 <i>Mechanically controlled stiffness</i>	22
2.7 ROBOT CONTROL SOFTWARE/MANAGEMENT SOFTWARE.....	23
2.7.1 <i>ROCK and YARP</i>	24
2.7.2 <i>ROS</i>	25

3	REQUIREMENTS AND SPECIFICATIONS OF ROBOT PROTOTYPE	26
3.1	OVERVIEW	26
3.2	TASKS AND REQUIREMENTS	26
3.2.1	<i>Arable farming</i>	26
3.2.2	<i>Livestock farming</i>	27
3.2.3	<i>Additional requirements and constraints</i>	28
3.3	LOAD-CARRYING ABILITY	28
3.3.1	<i>Frame and components</i>	28
3.3.1.1	Momaro.....	29
3.3.1.2	MAMMOTH	30
3.3.1.3	Additional components	31
3.3.1.4	Example Frame	32
3.3.1.5	Final chassis weight	33
3.3.2	<i>Robot arm</i>	33
3.3.3	<i>Temporary electric fences</i>	35
3.3.4	<i>Targeted weed spraying</i>	36
3.3.5	<i>Manual weeding</i>	37
3.3.6	<i>Seeding planting equipment</i>	37
3.3.7	<i>Livestock monitoring and herding</i>	38
3.3.8	<i>Final hybrid robot weight specification</i>	39
3.4	LEG HEIGHT RANGE	39
3.4.1	<i>Going under single wire temporary electric fences</i>	39
3.4.2	<i>Crop and pasture heights for weeding</i>	40
3.4.3	<i>Delta robot clearance</i>	41
3.4.4	<i>Overall height specification</i>	42
4	MECHANICAL DESIGN OF HYBRID LEG.....	43
4.1	CONCEPT DESIGNS	43
4.1.1	<i>Linear actuation</i>	43
4.1.2	<i>Rotary actuation</i>	44
4.1.3	<i>Concept selection</i>	45
4.2	MECHANICAL DESIGN	47
4.2.1	<i>Base link</i>	48
4.2.2	<i>Femur link</i>	49
4.2.3	<i>Tibia link</i>	50
4.3	DESIGN ANALYSIS	51
4.3.1	<i>Possible configurations</i>	51
4.3.2	<i>Possible Loading</i>	51
4.3.3	<i>Finite Element Analysis</i>	54

4.3.3.1	Weight loading	54
4.3.3.2	Impact loading.....	55
4.4	COMPONENTS	57
4.4.1	<i>Joint actuator</i>	57
4.4.2	<i>Motorised wheel</i>	58
4.4.3	<i>Turning servo</i>	59
4.4.4	<i>Bearings</i>	60
4.5	FINDINGS AND RECOMMENDATIONS	62
4.5.1	<i>Base link</i>	62
4.5.2	<i>Femur link brace</i>	62
5	ACTUATOR DESIGN AND CONTROL.....	66
5.1	REQUIREMENTS	66
5.1.1	<i>Cost</i>	66
5.1.2	<i>Torque</i>	67
5.1.3	<i>Compliance</i>	69
5.1.4	<i>Modularity</i>	69
5.1.5	<i>Low power consumption</i>	70
5.2	MECHANICAL DESIGN.....	70
5.2.1	<i>Compliant drive link</i>	71
5.2.2	<i>Actuator chassis</i>	72
5.2.3	<i>Actuator stub axles</i>	73
5.2.4	<i>Bearing housings</i>	75
5.2.5	<i>Gearbox mount and motor guide</i>	75
5.2.6	<i>Encoder mounts</i>	76
5.3	ANALYSIS	77
5.3.1	<i>Torsional stiffness</i>	77
5.3.2	<i>Strength</i>	78
5.3.2.1	Compliant drive link	78
5.3.2.2	Gearbox mount	79
5.4	COMPONENTRY	80
5.4.1	<i>Bearings</i>	80
5.4.2	<i>Motor</i>	81
5.4.3	<i>Joint encoder</i>	83
5.4.1	<i>Motor encoder</i>	84
5.4.1.1	PCB	85
5.4.2	<i>Motor Driver</i>	85
5.4.3	<i>Micro-controller</i>	88
6	TESTING AND RESULTS	90

6.1	COMPLIANCE	91
6.2	CONTROL	92
6.2.1	<i>Actuators</i>	93
6.2.1.1	Momentum changes	95
6.2.1.2	Varying steady-state error.....	96
6.2.1.3	Noisy at set point	99
6.2.1.4	Joint position	99
6.2.1.5	Conclusion	101
6.2.2	<i>Steering servo</i>	102
6.2.3	<i>Driven wheel</i>	102
6.2.4	<i>ROS</i>	103
6.3	ACTUATOR PERFORMANCE	104
6.4	COST	105
6.4.1	<i>Comparison to commercial robots</i>	107
7	CONCLUSIONS AND FUTURE WORK	108
8	BIBLIOGRAPHY	111

List of Figures

Fig. 1. a) The ‘Scout’ UAV from American Robotics [15]. b) A seed spreading, weed control, and soil sampling robot from Rabbit Tractors [16].	1
Fig. 2. The cattle herding robot ‘Swagbot’ [23].	2
Fig. 3. Lely© Astronaut™AMS milking a cow [8].	6
Fig. 4. The cattle-herding robot ‘Swagbot’ [23].	8
Fig. 5. The Robot ‘BoniRob’ [41].	9
Fig. 6. a) The robot ‘Aramdillo’ [43]. b) The different configuration of the robot ‘Thorvald II’ [44].	10
Fig. 7. The robot ‘Mero’ [45].	10
Fig. 8. Locomotion types and how they are related [24].	11
Fig. 9. a) The robot ‘shrimp’[46]. b) The robot ‘Scarab’ [47].	12
Fig. 10. a) The robot ‘ROBHAZ-DT3’ [49]. b) The robot ‘Nnokhod’ [50].	13
Fig. 11. a) The robot ‘Bigdog’ [51]. b) The robot ‘HRP-4-humanoid’ [52]. c) The robot ‘COMET-I’ [53].	14
Fig. 12. a) The wheel-track hybrid robot ‘NEZA’ [56]. b) The wheel-track hybrid robot ‘RHMBot’ [57].	14
Fig. 13. a) A leg-track hybrid robot developed by Fujita et al. [58]. b) A leg-track hybrid robot developed by Yokota,et al. [59]. c) The leg-track hybrid robot ‘TITAN X’ [60].	15
Fig. 14. a) The wheeled leg hybrid robot ‘ATHLETE’ [62]. b) The leg wheel hybrid robot ‘HyTRO-I’ [63]. c) A leg-wheel hybrid robot developed by Tadakuma et al. [61].	16
Fig. 15. The leg wheel hybrid robot ‘Momaro’ [64].	16
Fig. 16. a) The leg-wheel-track robot ‘AZIMUT’ [66]. b) A leg-wheel-track robot developed by Zhou et al. [65].	17
Fig. 17. Unstructured terrain, and speed and efficiency performance of all the locomotion types [24].	18
Fig. 18. a) Workings of an antagonistic joint with series elasticity [74]. b) Workings of the antagonistic, variable stiffness actuator developed by Tonietti, et al. [76].	20
Fig. 19. The ‘MerRIA’ structure-controlled variable impedance actuator [78].	21
Fig. 20. a) The structure controlled variable stiffness mechanism developed by Choi et al. [79]. b) Diagram of the linkage used to change the effective length of the spring from the mechanism in a) [79].	22
Fig. 21. Diagram showing the ‘MACCEPA’ working principle [71].	23
Fig. 22. The robot ‘Momaro’ [64].	30
Fig. 23. The robot ‘MAMMOTH’ [68].	31
Fig. 24. Example frame for a final hybrid robot.	32

Fig. 25. Height of common crops. Data retrieved from [120].	40
Fig. 26. Common pasture heights. Data retrieved from [120].	41
Fig. 27. a) Linear actuation concept using a single cylinder. b) Linear actuation concept using dual cylinders.	44
Fig. 28. a) Concept (a) single bearing joint with overlapping links. b) Concept (b) dual bearing joint with motor at a right angle to the axis of rotation. c) Concept (c) dual bearing joint with inline motor drive.	46
Fig. 29. Overview of the prototype hybrid wheeled leg. (Render from SolidWorks Composer).	47
Fig. 30. Parts of the base link intended for testing. (Render from SolidWorks Composer).	48
Fig. 31. Parts of the Femur link. (Render from SolidWorks Composer).	49
Fig. 32. Parts of the Tibia link. (Render from SolidWorks Composer).	50
Fig. 33. Exaggerated leg deformation from a pure weight loading with a) tall height configuration, b) neutral height configuration and c) short height configuration.	52
Fig. 34. Exaggerated leg deformation from weight and head-on collision loading in a narrow stance with a) tall height configuration, b) neutral height configuration and c) short height configuration.	52
Fig. 35. Exaggerated leg deformation from weight and head-on collision loading in an in-between stance with a) tall height configuration, b) neutral height configuration and c) short height configuration.	53
Fig. 36. Exaggerated leg deformation from weight and head-on collision loading in a wide stance with a) tall height configuration, b) neutral height configuration and c) short height configuration.	53
Fig. 37. Simplified leg model used in the leg analysis simulations. (Same model used in section 4.3.2 above).	54
Fig. 38. Weight loading simulation results of the leg in a neutral height configuration: a) stress results, b) factor of safety results, and c) displacement results.	55
Fig. 39. Custom prototype joint actuator.	58
Fig. 40. Wheel with integrated hub motor used on the hybrid wheeled leg [126].	58
Fig. 41. ASMC-04B 12-24V servo used for steering [129].	60
Fig. 42. a) current Femur link brace showing points of high stress in the centre during a wide stance, head-on collision simulation. b) Solid Femur link brace showing no points of high stress during a wide stance, head-on collision simulation.	63
Fig. 43. a) Topology optimisation result. b) Femur link brace design based on the topology optimisation result.	64
Fig. 44. Femur link before (a) and after (b) topology optimisation. Green and yellow areas indicate stress concentrations.	65
Fig. 45. The ANYdrive actuator [84, 132].	67
Fig. 46. Calculation of distance x using equation (7).	68

Fig. 47. Leg configuration that has the largest x value.....	69
Fig. 48. Overview of the prototype custom compliant actuator.	70
Fig. 49. Parts of the Compliant drive link.....	71
Fig. 50. Parameters of the Compliant drive link used in equation (10).	72
Fig. 51. a) Knee joint Actuator chassis. b) Hip joint Actuator chassis.	73
Fig. 52. a) Shoulder joint actuator through drive-side stub axle. b) Shoulder joint actuator non-drive-side stub axle. c) Knee joint actuator through drive-side stub axle. d) Knee joint actuator non-drive-side stub axle.	74
Fig. 53. a) Drive side bearing housing. b) Non-drive side bearing housing.....	75
Fig. 54. a) Gearbox mount. b) Motor guide.	76
Fig. 55. a) Motor position encoder mount. b) Joint position encoder mount.	76
Fig. 56. Compliant drive link simulation displacement result.....	77
Fig. 57. Torsional stiffness of Compliant drive link calculated using SolidWorks simulation and equation 10.	78
Fig. 58. Compliant drive link FOS results with 147 Nm torque applied.	79
Fig. 59. Gearbox mount FOS with a 147 Nm torque applied.	79
Fig. 60. Demonstration of how a moment causing load F is converted into two equal but opposite radial loads F_r	80
Fig. 61. Certa 18V cordless drill motor and gearbox.....	82
Fig. 62. Calt HAE18U5V12 SSI absolute encoder [135].	83
Fig. 63. Calt HAE18U5v12 encoder SSI data format and timing [135].	83
Fig. 64. AS5047P encoder SPI data timing [136].	85
Fig. 65. a) Custom AS5047P encoder PCB layout. b) Custom AS5047P encoder PCB schematic.....	85
Fig. 66. VESC communication and control flow diagram.....	87
Fig. 67. VESC HW version 4.12 I/O [142].	87
Fig. 68. Arduino communication and control flow diagram.	88
Fig. 69. Available I/O on the Arduino Uno microcontroller.	89
Fig. 70. Final prototype hybrid wheeled leg.	90
Fig. 71. a) Bench testing rig with test pipe connected. b) Bench testing with Tibia link attached.....	91
Fig. 72. Actuator compliance.	92
Fig. 73. Single PID control loop setpoint change response.....	94
Fig. 74. Cascaded P-PID control loop setpoint change response.....	94
Fig. 75. Actuator motor's ability to follow commanded ramp profile.....	95
Fig. 76. Steady state error at 30 degrees.....	97
Fig. 77. Steady-state error at 45 degrees.	97
Fig. 78. Fourier transform of motor current while following the ramp profile. The red dots represent the chosen dominant frequencies (harmonics of the stator slots and motor poles).	98

Fig. 79. The blue plot is motor current while following the ramp profile. The orange plot is the inverse Fourier transform of the chosen dominant frequencies shown in Fig 78.....	98
Fig. 80. Raw encoder noise before and after filtering.....	99
Fig. 81. Relationship between joint position and motor position to a low-frequency sinusoidal command.	100
Fig. 82. Relationship between joint position and motor position to a high-frequency sinusoidal command.	100
Fig. 83. High ERPM steady-state speed control performance.	102
Fig. 84. Low ERPM steady-state speed control performance.	102
Fig. 85. Leg spawned in a Gazebo simulation.	103
Fig. 86. Leg visualised in RVIZ.....	103
Fig. 87. The lifting torque of the actuator being tested.....	104

List of Tables

Table 1. Momaro component weights.	29
Table 2. MAMMOTHs component weights.	31
Table 3. Final frame and components weight.	33
Table 4. Weight of robot in different configurations.....	39
Table 5. Leg height requirements.	42
Table 6. Possible leg configurations on the final agricultural robot.	51
Table 7. Leg collision stiffness (N/m) in various stances without added compliance....	56
Table 8. Estimated maximum allowable leg collision force.....	57
Table 9. Approximate maximum allowable leg stiffness to withstand a 5 km/h head-on collision.....	57
Table 10. Motorised wheel specifications.	59
Table 11. Steering servo specifications.	60
Table 12. Certa motor and gearbox specifications.	82
Table 13. Calt HAE18U5v12 encoder specifications.	84
Table 14. AS5047P encoder specifications.	84
Table 15. VESC specifications.	88
Table 16. Arduino Uno specifications.	89
Table 17. Cost of parts required to build the custom compliant actuator.	105
Table 18. Cost of parts required to build the leg.....	106

List of Abbreviations

3D	3-Dimensional
ABS	Acrylonitrile Butadiene Styrene
ADC	Analogue-to-Digital Converter
AMS	Automated Milking System
ATV	All-terrain Vehicle
BLDC	Brushless Direct Current
CAN	Controller Area Network
CLARAty	Coupled Layer Architecture for Robotic Autonomy
CNC	Computer Numerical Control
DARPA	Defence Advanced Research Projects Agency
DC	Direct Current
DOF	Degrees of Freedom
ERPM	Electrical Revolutions per Minute
ESC	Electronic Speed Controller
FEA	Finite Element Analysis
FOC	Field-oriented Control
FOS	Factor of Safety
GDP	Gross Domestic Product
GmbH	Company with Limited Liability
GPS	Global Positioning System
HW	Hardware
I ² C	Inter-Integrated Circuit
IC	Integrated Circuit
ID	Internal Diameter
IMU	Inertial Measurement Unit
LIDAR	Light Detection and Ranging
MATLAB	Matrix Laboratory
MIT	Massachusetts Institute of Technology
MRDS	Microsoft Robotics developer Studio
NASA	National Aeronautics and Space Administration
NZ	New Zealand
NZD	New Zealand Dollar
OD	Outside Diameter
P-PID	Proportional-Proportional Integral Derivative
PCB	Printed Circuit Board
PID	Proportional Integral Derivative
PLA	Polylactic Acid
PPR	Pulses per Revolution
RGB	Red Green Blue

RGB-D	Red Green Blue - Depth
ROCK	Robot Construction Kit
RPM	Revolutions per Minute
RTK	Real-time Kinetic
SEA	Series Elastic Actuator
SPI	Serial Peripheral Interface
SSI	Synchronous Serial Interface
UART	Universal Asynchronous Receiver-Transmitter
UAV	Unmanned Aerial Vehicle
UK	United Kingdom
USB	Universal Serial Bus
USD	United States Dollar
UV	Ultraviolet
VESC	Vedder Electronic Speed Controller
YARP	Yet Another Robot Platform

1 Introduction

1.1 Rationale and importance of research

Agriculture is an important factor for New Zealand's economy. The value of the New Zealand agribusiness is valued at 33.4 billion NZD, meaning that agriculture and its related products and services account for 12.4% of the NZ traded GDP [1]. However, the New Zealand farming industry has a labour shortage, and farming is fraught with dangerous occupation activities [2, 3]. It exposes its workers to large machinery and livestock, and workers are required to work alone, often in isolated and rugged terrain [3]. There have also been questions raised about the viability and affordability of farming with current practices as the cost of critical inputs such as viable land, labour, energy, water and fertilisers continue to rise [4, 5]. Additionally, farming faces criticism for its negative environmental impacts [4]. The manufacturing industry dealt with similar problems through automation and robotics, which allowed them to reduce labour costs and profit losses due to human error, while at the same time increasing precision, production volume and safety [6].

In the 1960s, automation in agriculture started with the partial automation of tractors [7] and has progressed to specific tasks that resemble manufacturing tasks in both indoor and outdoor agriculture. Such tasks include milking and feeding, weeding, phenotyping and planting. Examples of specific robots are automated milking systems (AMS) [8], automatic feeding systems [9], and robots for harvesting apples (Abundant Robotics) [10] and strawberries (Agrobot) [11], robot for manoeuvring between rows of corn (Rowbot) [12], autonomous surveying with drones (American Robotics) [13], seed spreading, weed control, and soil sampling with the small robots of Rabbit Tractors [14].

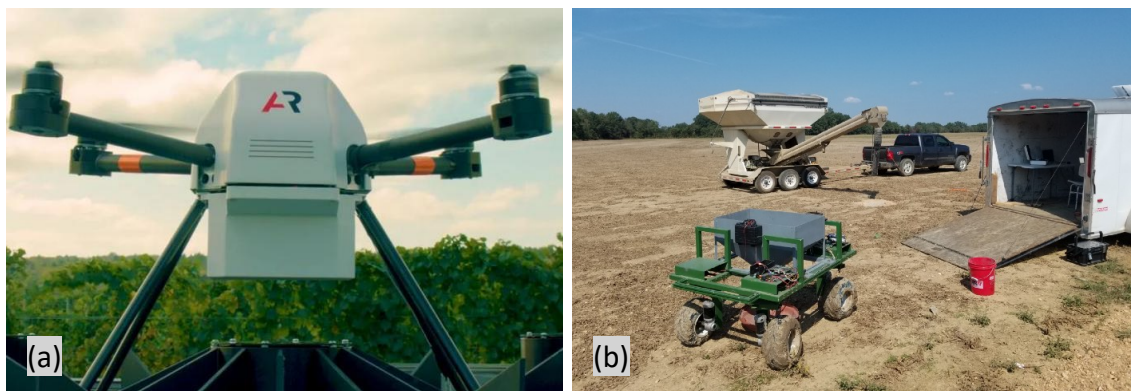


Fig. 1. a) The 'Scout' UAV from American Robotics [15]. b) A seed spreading, weed control, and soil sampling robot from Rabbit Tractors [16].

Automation in agriculture has paved the way for smaller machinery and thus more targeted operations. For example, targeted spraying can reduce herbicide use by as much as 90% [17], not only tailoring to plant-specific needs, but also reducing environmental impact [18]. The use of smaller robots, instead of large tractors, has enabled a reduction in soil compaction and thus energy consumption and operating costs [19]. These tasks either require a robot to be stationary or the path and the terrain which the robot navigates need to be easy and well defined.

However, in New Zealand, the majority of farms are dairy-based, followed by sheep and beef [20], and the livestock is predominantly pasture-fed [21]. New Zealand pastures are vast and located on rugged terrain, which has meant there have been hardly any robots developed for the kiwi market that can perform tasks in pastures with unstructured terrain, such as weeding, break feeding and livestock herding. A solution would be a robust, versatile and modular robot, able to traverse the rough terrain of many New Zealand farms.

Once a robot can traverse the unstructured terrain found on New Zealand farms, it can be outfitted to perform a variety of tasks in multiple categories of farming, such as crops, fruit orchards and pastures. Only one robot called “Swagbot” has been developed for pasture related tasks in rough terrain. Swagbot is intended for pasture and livestock monitoring research and can navigate undulating and hilly terrain [22]. However, Swagbot does appear vulnerable to getting stuck without a means of freeing itself, and it cannot be easily adapted to perform completely different tasks.



Fig. 2. The cattle herding robot ‘Swagbot’ [23].

Traversing rough terrain is a difficult challenge. The attributes that need to be investigated for the design of a versatile, multipurpose agricultural robot for undulating terrain are, amongst others: obstacle detection, navigation, customisability and connectivity. Yet the main attribute that requires investigation is locomotion. There are several types of locomotion a robot can use, with the three main types being wheeled,

tracked and legged locomotion. From these three main types, hybrids can be produced that combine the abilities and eliminate the disadvantages of the parent types.

The chosen locomotion must be highly efficient at covering large distances on structured terrain, such as farm raceways, but at the same time is capable in the unstructured terrain found in paddocks. Wheeled locomotion is the most efficient way of covering vast distances in structured terrain, and legged locomotion is the most capable in unstructured terrain [24]. From this, it follows that hybrid wheeled leg locomotion would be the right choice for a versatile farm robot in the mixed terrain and vastness of New Zealand farms.

When focussing on leg design, the leg actuator is an important aspect that needs to be tuned to the intended terrain of the agricultural robot. An actuator can be hydraulically, pneumatically or electrically actuated; linearly or rotationally. Due to the dynamic interactions the leg has with unstructured terrain, compliance in the actuator also needs to be considered. Compliance in an actuator can lower peak output gear forces, turn the force control into a position control problem, and the springs can briefly store energy from shock loads [25].

Crucial in robot control is “middleware”, which allows for efficient management of individual actuators and wheel motors in a leg, and subsequent efficient management of the individual legs in the robot. The purpose of middleware is to manage all the low-level communications with many sensors and controllers; then provide the user with a central, standardised way to run applications that use the sensor data and send commands to the controllers. This simplifies the integration of hardware and software and means the interface of only one leg must be developed, which can then be instantiated for each of the legs on the final robot.

1.2 Scope of research

This research aims to design and develop a prototype hybrid wheeled leg for a robot capable of traversing challenging terrain while remaining as efficient as wheeled locomotion on structured terrain. The robot is expected to complete a variety of tasks, explicitly tailored to farming in New Zealand. In order to achieve this aim, the following goals are established:

1. Investigate the current agricultural robots for both indoor and outdoor farming. Identify what the capabilities of the different robot locomotion types in challenging and structured terrain are. Identify what the benefits are of adding compliance to an actuator intended for a robot leg, and what the most

appropriate type of compliance is. Identify what the benefits are of using a robot middleware, and determine which middleware is most appropriate.

2. Determine the weight the proposed robot is required to carry and the height necessary in order to perform the tasks it is expected to do on NZ farms. From this, the leg strength and height requirements can be calculated.
3. Design a prototype hybrid wheeled leg to meet the weight carrying and height requirements. The budget to build a prototype of the designed leg is 3000 NZD.
4. Design an adjustable mechanically compliant leg actuator that meets the torque requirements, while staying within the budget of the whole leg.
5. Manufacture and assemble a physical prototype of the custom compliant actuator for proof of concept, torque output testing, compliance testing, development of the middleware interface driver and tuning of the positional control.
6. Manufacture and assemble a physical leg prototype for proof of concept with all moving joints (apart from the Hip orientation joint) capable of being controlled by the robot middleware.

Although the leg is intended for use on a four-legged agricultural robot, the design of the entire agricultural robot is not within the scope of this research. In order to determine the required specifications of the leg, a mock-up chassis is designed. The weight of the mock-up chassis and its components are based on the estimated payload the robot will have to carry and the tasks it has to perform. Therefore, the resulting mock-up chassis is not necessarily indicative of how the chassis of the final robot will look. Additionally, since the design of the final robot is not within the scope of this research, the leg orientation axis joint was not designed because it is heavily influenced by the design of the final robot's chassis.

2 Review of mobile robot locomotion

2.1 Background

Modern agriculture is a highly industrialised business. As with any modern business, the aim is to make the largest profit with the least amount of expenses. There have been questions as to the viability and affordability of farming with current practices as the cost of critical inputs such as viable land, labour, energy, water and fertilisers continue to rise [4]. The way that manufacturing dealt with the increased cost of critical inputs was to embrace robotics and automation. It allowed them to reduce labour costs and profit losses due to human error while at the same time increasing precision, production volume and safety [6].

2.2 Robots in indoor agriculture

A similarity between a dairy shed or feed barn and a factory can be found; they are both controlled environments where many repetitive tasks present themselves. Automated milking systems (AMS) have been developed [8], [26], [27] (Fig. 3) as have automatic feeding systems [9],[28] for dairy sheds and feed barns. Both these systems currently rely on the animals using them voluntarily and can only serve one animal at a time. Fitted with the correct sensors, an AMS can cater to the different needs of each animal and gather data about the animal. The voluntary nature of these systems makes them perfect for cows housed in barns since they get their food at the same place where they get milked. In some parts of Europe, 80% of the cows are housed in barns, especially during winter [29], making Europe one of the biggest adopters of these systems.

The robots mentioned above are fixed in position and rely on the livestock moving to them to use them, this works because the livestock are housed inside with the robots and have been trained to use them. If the livestock are grazing outside on pastures the robots that care for them are required to move around, since the livestock are not forced to be within the vicinity of the robot. In indoor agriculture, there already exist robots that can move around in greenhouses. In greenhouses, the robots must be able to move around because the plants cannot. An example of such a robot is Fitorobot [30] which can do several tasks within a greenhouse such as spraying, pruning and crop transport. Although Fitorobot is intended for greenhouses, it is not that different from the equivalent robots intended for outdoor crops since the plants are still stationary, and the terrain is comparable but can be slightly more difficult because it can get muddy outside.



Fig. 3. Lely© Astronaut™AMS milking a cow [8].

2.3 Robots in outdoor farming

In New Zealand, cows live outdoors on pastures and have to walk to and from the milking shed twice daily, which can be up to three kilometres away [31]. Here the cows do not eat next to where they get milked therefore are reluctant to walk to the dairy shed if it is too far away. Instead, they must be herded to the milking shed which is a task that can be done by an autonomous robot with excellent uneven terrain traversing capabilities due to the unstructured terrain on a farm and random location of the herd. Once at the shed, a voluntary AMS cannot milk the cows fast enough since only one cow at a time can be milked. A system currently being developed to allow more than one cow to be milked at a time is called Scott® Milktech [32] which replaces a worker fitting and removing the cups on a conventional rotary milking platform with a robot manipulator.

The challenge for engineers in an outdoor farming setting is that crops are stationary in an unknown reference frame and livestock move over vast distances in a dynamic environment and unknown reference frame. In both scenarios, an autonomous robot is required that is capable in uneven terrain and changing conditions [33]. However, a robot meant for livestock agriculture needs to be able to traverse the same terrain as an animal, but wheeled locomotion will suffice for robots only meant for crops and orchards because the terrain in which crops and orchards are planted is chosen so that wheeled machinery can get access for planting and harvesting. This has made crops and orchards the target of nearly all the current agricultural robots since either current machinery can be modified to be autonomous or purpose-built robots can use wheeled locomotion successfully.

Research starting in the 1960s looked at guidance systems in tractors to take control of steering adjustments for the operator, leaving them to only concentrate on implement adjustment, thus enabling the field speed to increase without a reduction in steering accuracy or implement performance [7]. Blackmore, et al. [34] were early to realise fully autonomous tractors. They used a deterministic approach for route planning and found that route of the robot can be calculated so that the distance the tractor travels is minimised, depending on the field shape and implement size. They were able to calculate an optimised and more efficient route, but the approach was not able to react to unknown situations or obstacles. This technology has now matured with commercially available tractors that have autonomous feature but still require an operator for supervision as their response to unknown situations and obstacles are still unpredictable [35].

Modifying conventional machinery is an easy way to develop autonomous agricultural robots. However, these conventional machines have started getting larger to take advantage of economies of scale because by getting larger, they can cover more land per hour the operator works [18]. Autonomous robots are not paid for their operating time and their running costs scale with size, this has led researchers to investigate what advantages, if any, smaller autonomous agricultural robots have over conventional agricultural equipment. A review by Pedersen, et al. (2008) [18] found that the use of micro spraying by smaller autonomous robots can decrease the use of herbicides by up to 90% and operations can be better tailored to plant needs, both reducing the environmental impact. Also, since it has been shown that 50% of a tractor's power is used for overcoming its wheel compaction [19], using a lighter machine will reduce soil compaction and thus reduce energy consumption.

Smaller autonomous agricultural robots are the future but most of the research and the resulting prototype robots that have been built, have been for a single purpose and designed towards undertaking a single task. However, many of these single, high volume tasks are seasonal, which means the robot will be unused for much of the year. If these robots are to be more appealing and persuade the farmer to choose them over conventional agricultural equipment, they need to have clear benefits such as the ability to automate more than just one task [36], but moreover, they need to be low-cost [33].

There have been a few attempts to make small agricultural robots for more than just one task. Agribot [37] is a robot designed to plough and then sow seeds, and Agrobot [38] is a robotic platform that has not been designed for any specific farming operation. The designers of Agribot [37] report that so far, they have just designed and implemented an autonomous robot platform that can be used in an agricultural setting but are yet to use it for any specific operation. They managed to keep the costs of the robot under \$2000. Agrover Gen. I and Agrover Gen. II [39] were designed to be research

platforms. Both Agrovers had four-wheel drive and steering, the difference being that Agrover Gen. I had pneumatically adjustable Ground clearance, and the wheel width could be changed depending on where it is used. The Pneumatic levelling feature was removed from Agrover Gen. II due to it being sluggish and hampering Agrovers agility. A multipurpose robot has been designed at Queensland University of technology. It was designed for tasks related to weed management, fertiliser application and seeding. The dimensions and shape of the robot were realised by finding a balance between the requirements needed to carry implements, payloads and drive autonomously in-crops, farm roads and in fallow fields [40].

There is only one field robot intended for use in livestock herding called Swagbot (Fig. 4). It is an omnidirectional robot that can navigate undulating and hilly terrain. It is currently being used for research in pasture and livestock monitoring [22].



Fig. 4. The cattle-herding robot 'Swagbot' [23].

The robot “BoniRob” (Fig. 5) has been designed to change its ground clearance and track width [41]. Although it has so far only been used to do phenotyping, it is not designed to do this for any single type of plant. Its ability to change its height comes from four legs with wheels attached to them. However, the legs do not have enough degrees of freedom to allow walking. The ability to change its ground clearance and track width is used so that it can optimise itself to whatever plant it is phenotyping. It is developed by Deepfield Robots, part of Robert Bosch start-up GmbH and BoniRob platforms are available for purchase [42].



Fig. 5. The Robot 'BoniRob' [41].

Recently, two different modular agricultural robots have been designed and built. These robots are interesting because they can be specialised for one task, and then they can be reconfigured using the same components to be specialised for another task. This reduces development costs of specialised robots and thus increasing the viability of automation of other tasks.

The first robot designed with modularity in mind was Armadillo [43] (Fig. 6 a). The robot has two track modules between which custom implements can be attached. The design of the implement determines the robots trackwidth and ground clearance. In addition to being modular and reconfigurable, other requirements were that it had to be low-cost and have good driving ability in rugged and cultivated terrain. Tracks were used instead of wheels because similar manoeuvrability to four individually turning and controlled wheels could be achieved with only two tracks, thus reducing complexity and likely increasing reliability. Tracks are also more capable in unstructured terrain but are harder on the soil when turning. The cost of Armadillo is \$50k and is made available to interested research groups. So far it has been used to collect images of weeds in maize fields, for data collection and tree mapping in orchards, mapping areas contaminated with land mines, and a version is being prepared that can remove weeds mechanically.

The other robot is Thorvad II [44] (Fig. 6 b), which takes “modularity” a step further. The robot has many different modules that can connect in different configurations. To realise these configurations custom “Robot Frame” modules can be made for specific tasks to which one or multiple steering, suspension, drive, battery enclosure, passive wheel, sensor interface, or sensor mounting modules can be clamped. The drive modules are wheels unlike the tracks on Armadillo but can be coupled to steering and suspension modules to customise the drive configuration to the intended task. The resulting robots from combining these modules can have varying trackwidths, number

of wheels, types of sensors, and implements. The robot is currently being used by the Norwegian University of Life Sciences in Norway and the University of Lincoln in the UK. Tasks it is being used for are phenotyping, tilling, farm logistics, and UV light treatment in greenhouses.

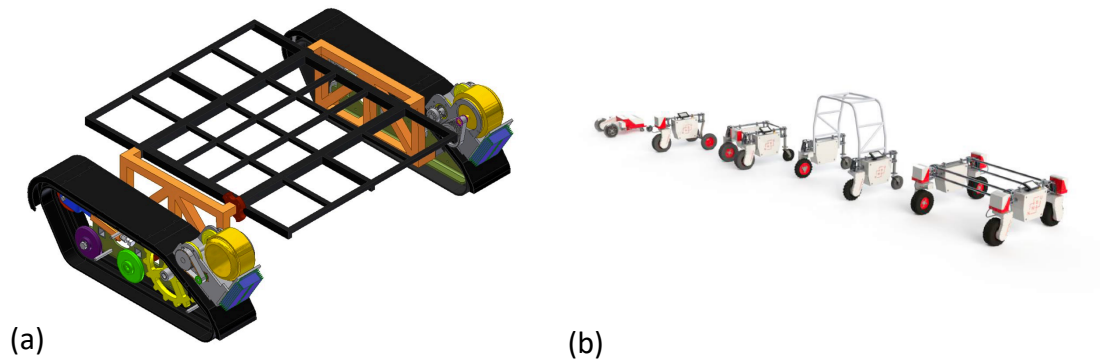


Fig. 6. a) The robot 'Aramdillo' [43]. b) The different configuration of the robot 'Thorvald II' [44].

The usefulness of a modular walking robot "Mero" (Fig. 7) in agriculture has been investigated [45]. Each "module" consists of two legs and a body. The modules can be joined together in different ways so that different implements and payloads can be carried. The authors say the benefit of a walking robot in agriculture is its ability to decreased impact on the environment. The robots contact area to the ground is discrete since the contact forces can be controlled. This allows the robot to pass directly over vegetation such as young trees without damaging them.



Fig. 7. The robot 'Mero' [45].

2.4 Robot locomotion

There are three main categories of locomotion (wheeled, tracked and legged) and four hybrid configurations (leg-wheels, leg-tracks, wheels-tracks, and legs-wheels-tracks) made from a combination of the main three. Fig. 8 shows the three main locomotion types and how the hybrid types are derived from them. An extensive review by Bruzzone, et al. [24] explains the different types and evaluates their capabilities.

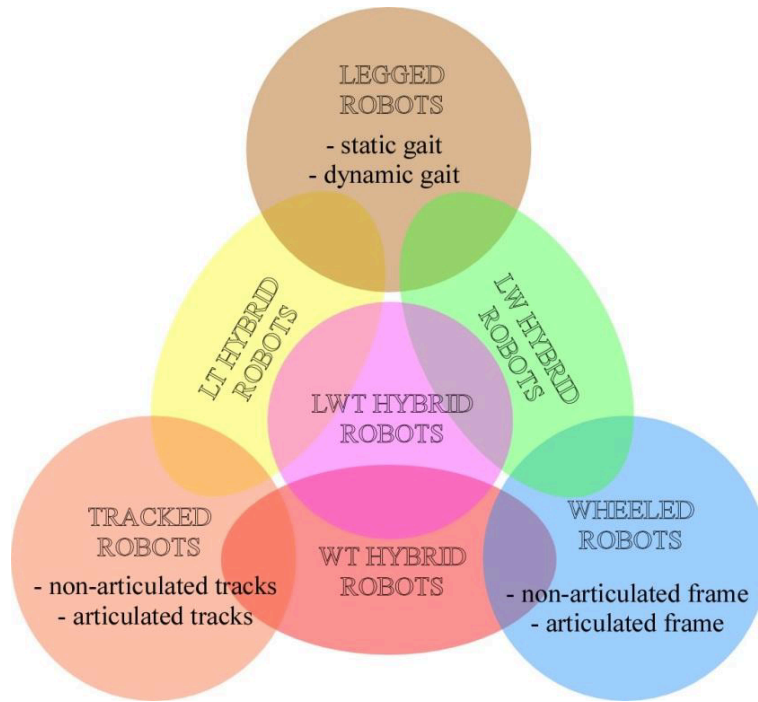


Fig. 8. Locomotion types and how they are related [24].

2.4.1 Wheeled locomotion

Wheeled locomotion is the most common type of locomotion for any moving vehicle. Mobile robots can have a varying number of wheels, but robots that are meant for rough terrain usually have 4, 6, or 8 wheels. Examples of wheeled robots for rough terrain are Shrimp [46] (Fig. 9 a) and Scarab [47] (Fig. 9 b). A robot with four or more wheels is inherently hyperstatic; therefore, it is best to use articulated frames or suspensions so the wheels can stay in contact with the ground over rough terrain [24]. Wheels that can have their position relative to the robot controlled are considered leg wheel hybrids [24] and are talked about later in section 2.4.6. The reason wheeled locomotion is popular is because it is efficient, cheap, easy to install on a robot, and allows a robot to travel at high speed. However, even with articulated suspension, wheels in unstructured environments can quickly lose contact with the ground, encounter a surface that has an insufficient friction coefficient or arrive at an obstacle that it is unable to pass over. Even though outdoor agriculture is considered an unstructured environment, wheels are by far the most common locomotion type currently used by agricultural machinery and

recently agricultural robots. These agricultural robots succeed by using wheels because they have been designed to do tasks revolving around crops which are planted by wheeled machinery therefor the terrain in which crops are planted is already suited to wheeled locomotion.



Fig. 9. a) The robot 'shrimp'[46]. b) The robot 'Scarab' [47].

2.4.2 Tracked locomotion

Tracked locomotion gives a vehicle excellent unstructured terrain capabilities, due to their large contact area with the ground and can be classified by the number of tracks they have [24]. The large contact area is also the only way that large, heavy machinery or robots can achieve contact pressure comparable to a human, which can help prevent damage to tree and plant roots [48]. Examples of tracked mobile robots for rough terrain are ROBHAZ-DT3 [49] (Fig. 10 a) and NanoKhod [50] (Fig. 10 b). The tracks can be articulated (relative passive track movement) or non-articulated, however, if the relative movement of the tracks is due to actuation, then it is considered a leg track hybrid [24] (see section 2.4.5). The most common and simple configuration is two non-articulated parallel tracks with differential steering [24]. This configuration is more capable than a four-wheel-drive articulated wheeled robot in soft terrains such as sand or mud thanks to the large track-ground contact area. When more than two articulated tracks are used, uneven terrain capability can be further improved [24].

Because tracked robots have excellent uneven terrain capabilities, there have been tracked robots developed for agriculture such as Armadillo [43] and Fitorobot [30]. They excel in operations such as tilling, seeding and spraying where the extra traction and decreased contact pressure with the ground is useful, especially in wetter conditions. None of the commercially available agricultural robots use tracks, probably because as

mentioned in [24] tracked locomotion, compared with wheeled locomotion is sluggish, uses more energy, and the tracks cause vibrations. These vibrations could fatigue parts, affect measurements and damage measurement equipment, especially when travelling on hard surfaces.

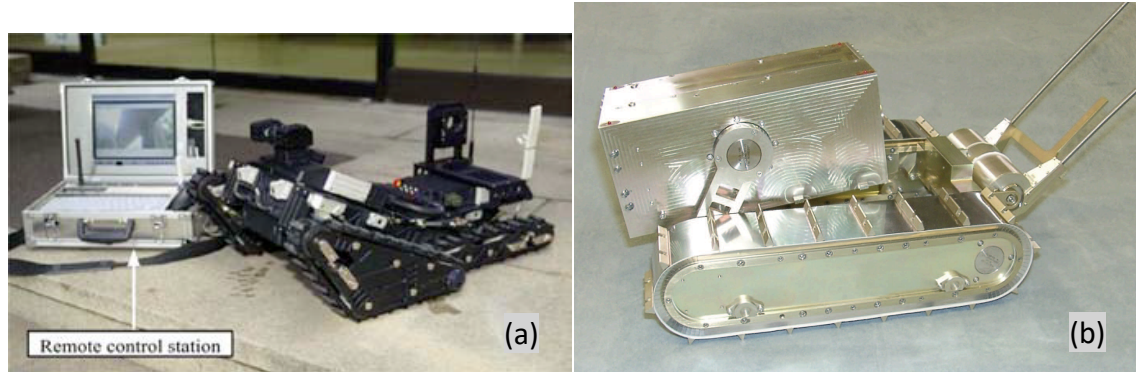


Fig. 10. a) The robot 'ROBHAZ-DT3' [49]. b) The robot 'Nnokhod' [50].

2.4.3 Legged locomotion

Legged robots are extremely versatile, competent in unstructured terrain, and commonly have 2 or 4 legs (but can have more). Current wheeled and tracked vehicles can only access half of the world's landmass, but the legs of humans and animals allow access to almost anywhere [51]. Examples of legged robots are Bigdog [51] (Fig. 11 a), hrp-4-humanoid [52] (Fig. 11 b) and COMET-I [53] (Fig. 11 c). Unlike wheeled or tracked robots, the pressure exerted by each legs contact point can be controlled, and selective contact points can be used depending on the terrain [54]. A legged robot can have a static gait or dynamic gait. With a static gait, the robot is naturally balanced similar to slow insects, whereas with a dynamic gait it is not naturally balanced, similar to fast walking, running, trotting or galloping animals and therefore relies on a sophisticated control system to keep it balanced [24]. The complex mechanical design required by legged robots has many moving parts [55], resulting in many potential points of failure.

Additionally, legged robots use two orders of magnitude more energy than wheeled robots on flat surfaces, and are not able to travel as fast as wheeled robots [55]. This has meant that legged locomotion is not currently considered as a viable locomotion choice in agriculture. However, due to its excellent unstructured terrain capabilities, it is a common locomotion type researched for remote location exploration and hostile or dangerous environments [54].



Fig. 11. a) The robot 'Bigdog' [51]. b) The robot 'HRP-4-humanoid' [52]. c) The robot 'COMET-I' [53].

2.4.4 Wheel-track hybrid locomotion

Wheel track hybrids combine the abilities of tracked and legged robots. This means they can easily navigate soft or unstructured terrain but can also efficiently and quickly move on flat, hard surfaces[24]. There are two ways these robots are configured: 1) The position of the wheels and tracks relative to each other can be changed to engage one or the other with the ground or 2) the shape of the track can be changed to resemble a wheel [24]. An example of a wheel tracked hybrid robot that changes the relative position of the track and wheel is NEZA-I [56] (Fig. 12 a) and an example of a robot that changes the shape of the track is RHMBot [57] (Fig. 12 b). Wheel track hybrid locomotion has been used in urban areas to give mobile robots the ability to climb stairs while still having the ability to move efficiently on flat ground. Because the wheeled options of these robots are non-articulated and simple, they are not very capable in unstructured terrain. Therefore, when used in an agricultural environment, the robots would have to almost exclusively remain in tracked mode, which means the extra wheels and transformation mechanism adds to the design complexity while not adding any benefits.

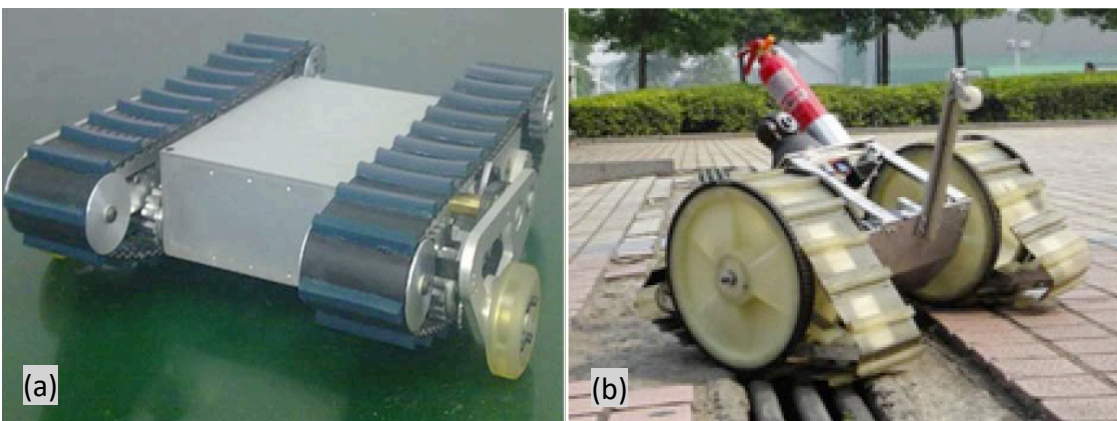


Fig. 12. a) The wheel-track hybrid robot 'NEZA' [56]. b) The wheel-track hybrid robot 'RHMBot' [57].

2.4.5 Leg-track hybrid

Leg-track locomotion combines the abilities of legged and tracked robots. They are well suited for rough terrain, but should only be used if speed and energy efficiency is not a concern [24]. They have been configured as: 1) a tracked robot with two parallel tracks,

and four separate legs attached to the robot body or 2) with the tracks integrated into the legs of a legged robot. An example of a robot two parallel tracks and four separate legs is [58] (Fig. 13 a), and examples of robots with tracks integrated with the legs are [59] (Fig. 13 b) and TITAN X [60] (Fig. 13 c). Although tracked leg robots are capable of operating in rough terrain, they have more of an advantage in urban disaster scenarios or on soft terrains such as sand and mud. This is because the legs can be used to climb onto or step over raised obstacles, while the tracks allow for easier and more efficient stair climbing or traversing soft terrain than with legs. The ability to climb onto or over raised objects with its legs is useful in an agricultural setting, but since farms can be large, the inefficiency of tracks negatively affects the range and possible working hours of a robots.

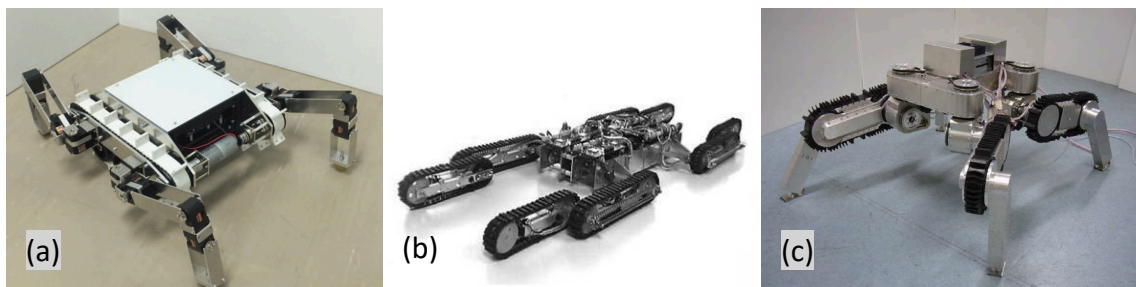


Fig. 13. a) A leg-track hybrid robot developed by Fujita et al. [58]. b) A leg-track hybrid robot developed by Yokota, et al. [59]. c) The leg-track hybrid robot 'TITAN X' [60].

2.4.6 Leg-wheel hybrid

Leg-wheeled robots combine the versatility of legs with the energy efficiency and speed of wheels [24]. There are three common ways in which legs and wheels can be configured: 1) legs with wheels attached at their ends, 2) fitting legs to the body of a wheeled robot or 3) having legs that double as wheels [61]. An example of a robot with wheels at its ends is ATHLETE [62] (Fig. 14 a), with legs fitted to the body of a wheeled robot, or wheels fitted to the body of a legged robot is HyTRo-I [63] (Fig. 14 b) and legs that double as wheels [61] (Fig. 14 c). Leg-wheeled robots have not been used in agriculture. However, in an agricultural setting, the legs can be used to climb onto surfaces, step over obstacles or get unstuck and walk through soft terrain. The wheels can be used to quickly and efficiently move to or from tasks over vast distances. On a farm, the most useful configuration would be (3) as it would allow for the wheels and legs to be used simultaneously, or if either fails, the remaining functional locomotion type can be used to get home. On top of the excellent unstructured terrain abilities explained above configuration (3) would allow the robot to change its ride height, track width, and centre of gravity on the move, and the legs can be used as a form of active suspension. Additionally, if either wheeled or legged locomotion fails, the remaining functional locomotion type could be used exclusively to return home.

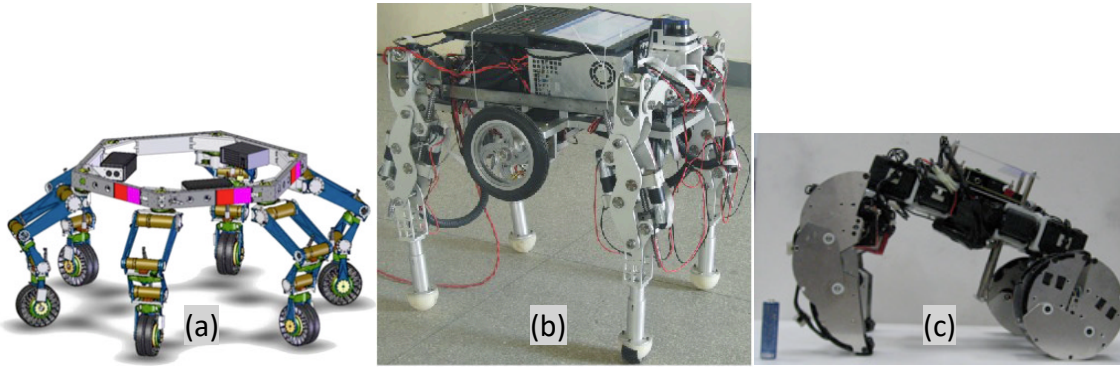


Fig. 14. a) The wheeled leg hybrid robot 'ATHLETE' [62]. b) The leg wheel hybrid robot 'HyTRo-I' [63]. c) A leg-wheel hybrid robot developed by Tadakuma et al. [61].

A robot that uses the wheel on leg design is Momaro [64] (Fig. 15). It was designed to compete in the DARPA challenge where it came fourth. Four out of the top five robots combined legged and wheel locomotion; the authors suggest this might indicate that leg-wheel locomotion is superior to other types of locomotion in unstructured environments. Momaro would be an appropriate platform for use as a multipurpose agricultural robot as, but it is unable to change its track width because its legs cannot rotate where they attach to the frame. However, it does not appear to be difficult nor impossible to modify Momaro to have this feature.

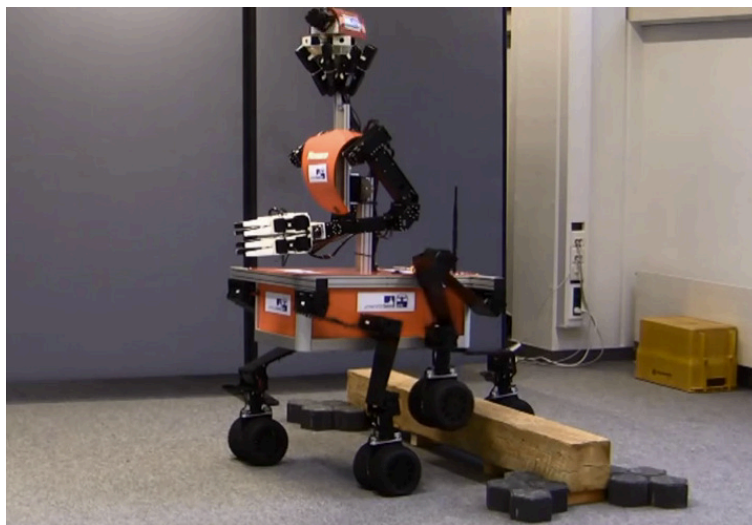


Fig. 15. The leg wheel hybrid robot 'Momaro' [64].

2.4.7 Leg –wheel-track hybrid

Leg wheel track robots use all three types of locomotion and have been designed in two different ways: 1) with four unequal obround shaped legs that can be oriented to mimic legs, wheels or tracks 2) with four transformable rims, each mounted to the frame that can transform from a round shape (wheel) to a diamond shape (tracked and legged) [65]. An example of a robot with unequal obround shaped legs is AZIMUT [66] (Fig. 16

a), and an example of a robot with transformable rims is [65] (Fig. 16 b). Both the configurations are well suited to urban environments as their tracked configuration give them the ability to climb stairs easily. Both have a simple leg configuration that will allow them to step onto obstacles or surfaces, but they cannot step over them since each leg does not have enough DOF (Degrees of freedom). The complexity of both wheel-track-leg hybrid designs and the fact that in legged mode they do not have sufficient DOF to step over objects does not give wheel-track-leg locomotion any clear advantage over the other hybrid locomotion types in terms of mobility in unstructured environments or speed and energy efficiency.

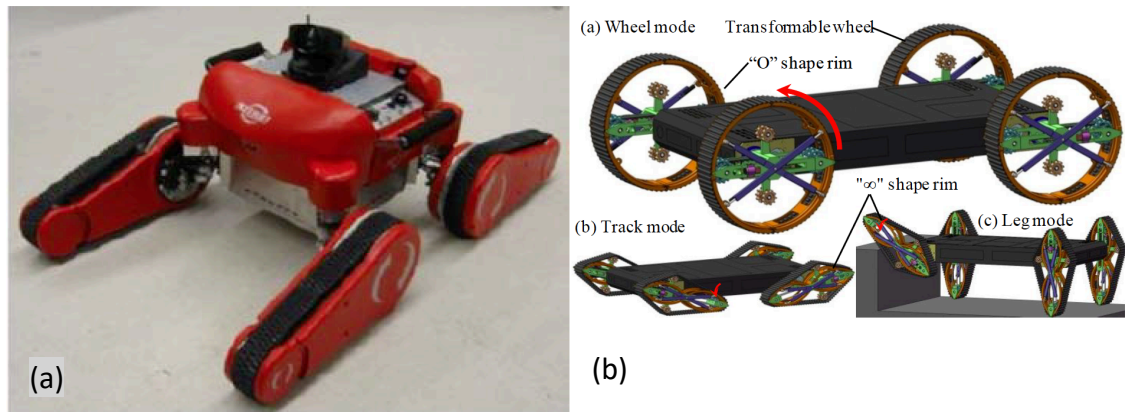


Fig. 16. a) The leg-wheel-track robot 'AZIMUT' [66]. b) A leg-wheel-track robot developed by Zhou et al. [65].

2.4.8 Locomotion selection

From the literature, it was decided that wheel-leg hybrid locomotion would be the best choice for a multipurpose agricultural robot due having the best combination of unstructured terrain abilities, and speed and efficacy on structured surfaces [24] as shown in Fig. 17.

The use of current robotic platforms was considered, but after evaluation, it was discovered they either were not available for purchase or were too expensive for the project budget. The project had a budget of 3000 NZD, but when enquiring to buy the available research robot ANYmal [67], we were quoted 250000 USD. Additionally, the two current wheel-leg hybrid robots that were not available for purchase but were deemed the most suited for use in agriculture (Momaro [64] and MAMMOTH [68]), lacked the key feature of being able to change their track width or lock the leg joints when they are not in use to save energy. Building a cheaper hybrid wheeled leg robot meant that a cheap low cost and powerful custom leg actuator also had to be developed (these are reviewed in section 2.5) as current viable options were also too expensive to fit the 3000 NZD budget. Developing both a leg and actuator is a massive undertaking; therefore, we focused on developing just the prototype hybrid wheeled leg to be used on an agricultural hybrid-wheel-legged robot.

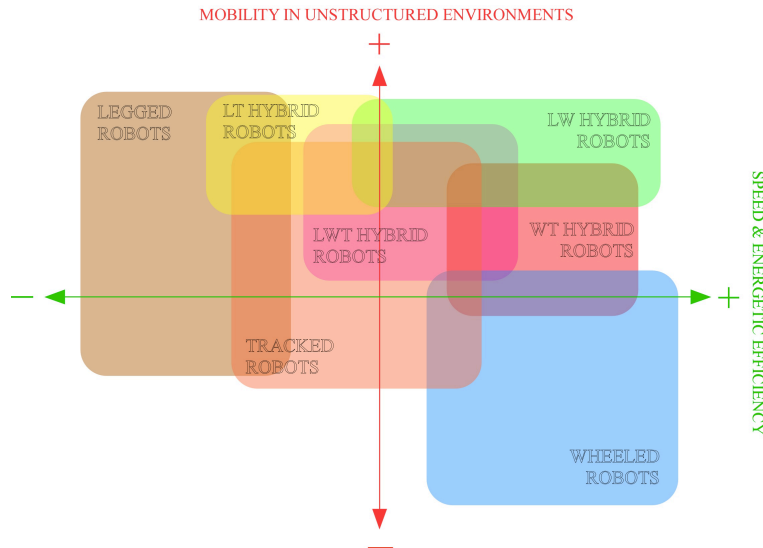


Fig. 17. Unstructured terrain, and speed and efficiency performance of all the locomotion types [24].

2.5 Leg actuators

Classical robots such as those used for pick and place applications use stiff actuators. A stiff actuator is an actuator that will follow a set path to a position and will not move from this position when an external force is applied until the force exceeds the limit of the actuator [69]. Stiff actuators are desired for robots because stiffness improves the precision, stability and bandwidth of position control [25]. The most common stiff actuator for mobile robots is the geared electric motor. The gear reduction is necessary to amplify the torque but keep the actuator small. However, the gears introduce friction and/or backlash, torque ripple, noise and an increase in the reflected inertia equal to the square of the reduction amount [25]. This means that any shock loads (common for a walking robot in unstructured terrain) cause significant stresses on the teeth of the output gear; additionally, damage to the robot or environment could occur [25].

For robots that must interact with humans or the natural environment, there is an area of research into compliant actuators. These actuators have the advantages of lowering peak output gear forces and turning force control into a position control problem, and those with an elastic element can store energy [25]. The first to design and use a compliant actuator was Pratt and Williamson, who presented a series elastic actuator SEA [70]. A SEA has a fixed compliance elastic element, which is only optimized for a specific environment/condition, however, in the case of leg wheeled hybrid robot in an unstructured environment, the exact stiffness that would be optimal is unknown.

A review by Van Ham, et al. [71] on compliant actuators with passive adjustable compliance found that the ability to change the compliance on walking robot actuators

can 1) optimise the amount of energy that can be stored during touchdown of the feet and then released during push-off 2) the natural frequency of the system can be regulated to increase or decrease the speed of walking. Additionally, the review identified four distinct designs, which are discussed below. Another review by Wolf, et al. [72] gives advice on design considerations for a variable stiffness actuator suited to your desired requirements.

2.6 Adjustable compliance actuator designs

2.6.1 Equilibrium-controlled Stiffness

Like a SEA, this actuator has a fixed compliance spring in series with a stiff actuator. Stiffness or output force is managed by actively controlling the equilibrium position of the spring [71]. Hollander, et al [73] has used this type of compliance control for powered ankle orthosis, as has Migliore, et al. [74] in addition with antagonistic-controlled stiffness (explained below in section 2.6.2) to produce a biologically inspired variable stiffness actuator. However, equilibrium controlled stiffness has the disadvantage that during hard knocks, if the controller bandwidth is too slow the controlled stiffness cannot be maintained, and energy is consumed to change the spring length [71].

2.6.2 Antagonistic-controlled stiffness

Antagonistic controlled stiffness requires two actuators working together to control a rotational joint in the same way the human biceps and triceps work together to control the arm [71]. Compliance comes from, and requires, a quadratic spring connected in series with both actuator and the joint as is shown in Fig. 18 b. To visualise how the compliance is controlled consider Fig. 18 b; if both actuators rotate in the opposite direction the stiffness of the joint increases or decreases but the position does not, and if both turn in the same direction the position changes but the stiffness remains constant. Koganezawa, et al. [75] designed an antagonistic actuator to mimic the human skeletomuscular system. However, the size of this design currently makes it unsuitable for use within a robotic leg. Tonietti, et al. [76] designed a compact antagonistic actuator using a belt and the compression of three springs, as shown in Fig. 18 b and c, this design is currently also too large for use in a robotic leg.

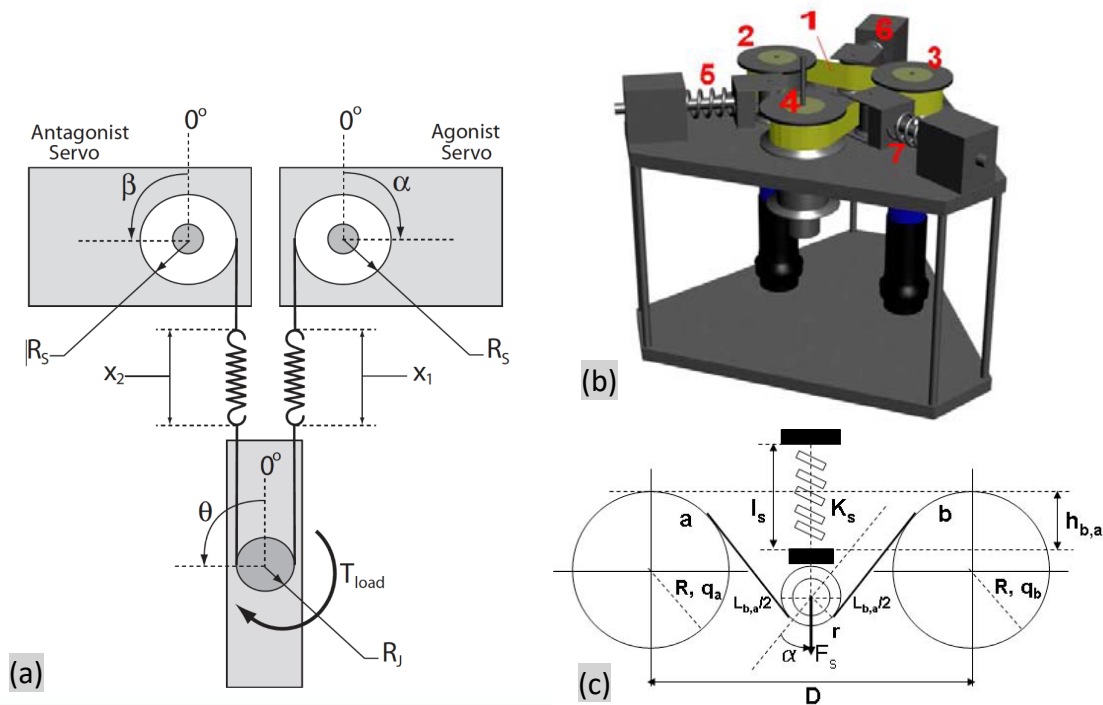


Fig. 18. a) Workings of an antagonistic joint with series elasticity [74]. b) Perspective view of the variable stiffness actuator developed by Toniatti, et al. [76]. c) Working principle of the antagonistic, variable stiffness actuator developed by Toniatti, et al. [76].

2.6.3 Structure-controlled stiffness

Structure controlled stiffness controls stiffness by physically changing the structure of the spring, for instance, the stiffness of a leaf spring depends on the modulus of the material, the moment of inertia, and the effective spring length [71]. The modulus can be changed slightly with heat, but not fast enough, therefore designs either change the inertia or the effective length.

A design changing the inertia by modulating the force pressing together layered steel sheets acting as a leaf spring is described by Kawamura, et al. [77]. When the sheets are pressed together the friction between the sheets increases the force required for the sheets to naturally slide over each other, enabling stiffness to vary until friction is high enough that the sheets stop sliding. This is a simple yet effective design, but it requires the inclusion of a vacuum system which adds complexity in control and weight to a mobile robot platform.

A design changing the effective length of two leaf springs called MeRIA is described by Liu, et al. [78]. The design can be seen in Fig. 19. The two bending bars (leaf springs) can be seen going between two cam followers at each side of the sliding block. When Motor 1 rotates by an angle θ_1 it causes the interaction force F , which drives the load. The deflection angle φ is a result of the coupling between the bending bars and the load. The compliance is varied by driving Motor 2 which rotates the lead screw, moving the sliding block up or down, and changing the distance along the bending bars where the

interaction force acts, which changes the effective length of the spring and the stiffness. The advantage of this design is that it is simple and easy to control, but it is quite large, making it a lousy option for use in a robotic leg, although the authors say they will make it smaller in the future by using high strength materials.

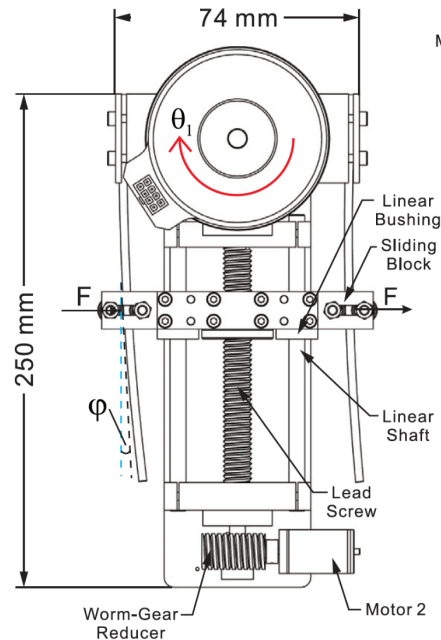


Fig. 19. The 'MerRIA' structure-controlled variable impedance actuator [78].

A design that changes the stiffness by changing the effective length of four leaf springs is proposed by Choi, et al. [79]. It uses two motors to move the load and change the stiffness. The mechanism allowing the joint elasticity is shown in Fig. 20 a. The two yellow disks at the top and bottom (linkage a) are each attached to one of the motors, and the load is attached to the "axis". For the motors to move the load, the torque has to act through linkage a, linkage b, the pivot and the spring to the "axis". The compliance of the joint is determined by where along the spring the "pivot" acts, which is determined by the angle between the two adjacent linkage a's. To understand how this works, consider Fig. 20 b, which shows the two adjacent linkage a's as a and c, the two adjacent linkage b's as b and d and r is the pivot's distance from the axis of rotation (pivots distance along spring). r can only be changed by changing the angle " 2α " (angle between the two adjacent linkage a's) since the lengths r1 and r2 are fixed. The advantage of this design is that both motors can be used to move the load, however, for the torque output the overall size of this design including the motor, makes it unsuitable for use in a robotic leg.

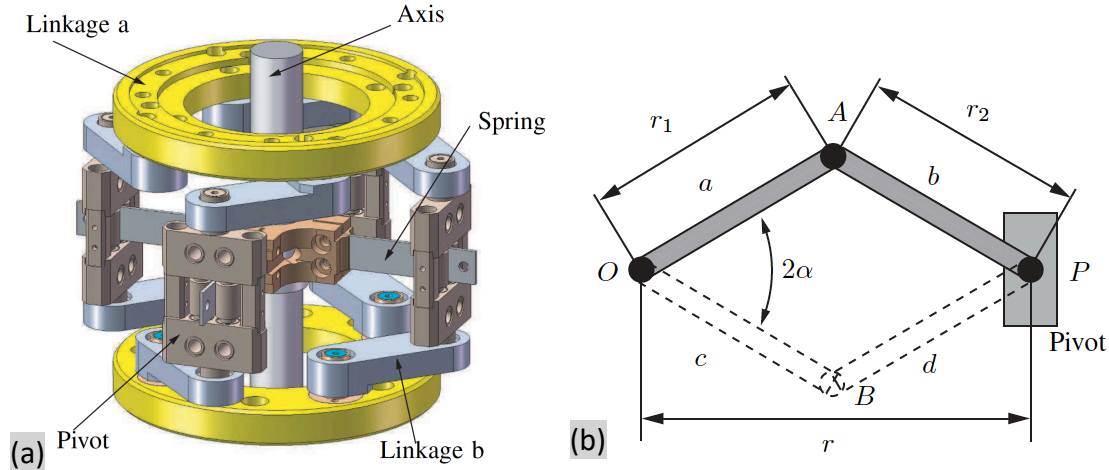


Fig. 20. a) The structure controlled variable stiffness mechanism developed by Choi et al. [79]. b) Diagram of the linkage used to change the effective length of the spring from the mechanism in a) [79].

2.6.4 Mechanically controlled stiffness

Mechanically controlled stiffness is like structure-controlled stiffness in that the stiffness is controlled mechanically. However, in mechanically controlled stiffness the length of the spring in use remains the same but the points where the spring attaches to the joint is moved, changing the pretension or preload of the spring [71]. Van Ham, et al. propose a mechanically controlled stiffness design called MACCEPA[80] shown in Fig. 21. It consists of a lever arm (small body in Fig. 21), a right body (rigid body), and a left body (moving body with the same axis of rotation as lever arm). Angle φ is set by a classical actuator, angle α determines the elongation of the spring, which causes a torque pulling the arm toward the rigid body when greater than zero. The angle determines the equilibrium position φ and is reached when angle α is zero. A second actuator is present at point b which determines the pretension of the spring by changing the length of the cable between point b and c, controlling the torque and stiffness at varying angle α . Advantages of the MACCEPA design are: 1) that it can be built with readily available parts, 2) the equilibrium position and compliance are controlled separately, and 3) the control signals are not influenced by the current position [71]. Disadvantages are that friction of the joint increases with increasing compliance, and the servos add to the space required within the design [71].

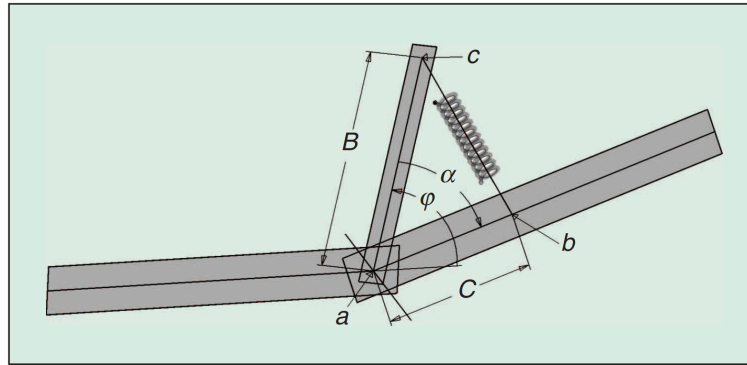


Fig. 21. Diagram showing the 'MACCEPA' working principle [71].

The literature showed that passive compliant actuators are commonly used in robots that have to interact with the real world such as the walking/running robot scarlETH [81] and COMAN [82], the hybrid wheeled-leg robot ANYmal [67], and robots working close to humans like the Unipi SofArm [83]. It would have been desirable to find a suitable off the shelf passive compliant actuator to save valuable development time and develop other parts of the hybrid agricultural robot. However, during the design of the leg, only one passive compliant actuator was available for purchase called ANYdrive [84] but cost it 12,000 NZD, which is more than the budget allowed for. Additionally, the passive compliant actuators found in the literature that met the torque requirements for the robot were 1) not accompanied with detailed component lists or mechanical design files, 2) were generally too large, or 3) used components that were also too expensive for the budget of this project. Therefore, it was decided to build a cheap, compact and powerful compliant actuator. Making a custom compliant actuator gives us the opportunity to 1) integrate self-locking which is desirable for a hybrid robot leg, but not available in ANYdrive or in the actuators from the literature, and 2) have the actuator and leg design supplement each other, to minimise the size of the actuator.

2.7 Robot control software/management software

It is easy to write the firmware for a microcontroller to control the position of an actuator. It is a little harder to write the firmware to control a whole robot arm/leg. Even harder still is writing the software to manage and coordinate an autonomous robot that has more than one robot arm/leg. This problem has led to the development of many robot middlewares. A review of available middleware by Elkady, et al. [85] says the purpose of middleware is to manage many different hardware devices and applications, encourage the use of new technologies, make software design easier, conceal the complexity of low-level communication and standardise the interaction with the countless available sensors, reuse software infrastructure between multiple research projects, and to lower development costs. Clearly then, to not reinvent the wheel it

would be beneficial to use a robot middleware specifically because it would: 1) make integration of hardware and software simpler and 2) make the step from hybrid leg to eventual autonomous agricultural hybrid wheeled-leg robot straightforward. However, not all middleware is equal; in this section, we aim to identify the middleware best suited for an autonomous agricultural robot.

Over the year, many robot middlewares have been developed these include Microsoft Robotics Developer Studio (MRDS) [86], Player [87], and Coupled Layer Architecture for Robotic Autonomy (CLARAty) [88]. However, they have not all remained actively supported. Using a middleware that is not actively supported can result in unreliable compatibility with current operating systems or hardware, and this problem only gets worse as time and technology advances. Having to spend time fixing compatibility issues negates some of the benefits of robot middleware. Therefore, it would be advantageous to use one that is actively supported. Currently, there is only three middleware still actively supported; they are ROS (Robot Operating System) [89], YARP (Yet Another Robot Platform) [90] and ROCK (Robot Construction Kit) [91].

Just because a robot middleware is actively supported does not mean it is appropriate for an agricultural robot. A key feature is the ability to reuse software infrastructure between multiple research projects [85]. An agricultural robot makes use of the same hardware components as other robots such as actuators, sensors, IMU, and drive motors. Therefore, the robot middleware that has the most available hardware interfacing drivers, and which provides an easy, well-documented way to write drivers for custom components would be the desired choice. Additionally, the navigation and object detection problem for an agricultural robot is different from that required by other robots, therefore, if algorithms to solve these problems are already implemented in a particular middleware, that middleware would be preferred, since it allows the existing research in the field to be utilised and furthered, and new research to be shared.

2.7.1 ROCK and YARP

ROCK (Robot construction kit) [91] and YARP (Yet Another Robot Platform) [90] are open source robot middleware developed by respectively the German Research Centre for Artificial Intelligence [92], and the Istituto Italiano di Tecnologia (IIT) [93] in collaboration with the RobotCub Consortium [94] and other contributors. They can be used free of charge for private and commercial use if appropriate accreditation is given. Both the ROCK and YARP websites provide well-written tutorials to guide you through using the middleware. There are no forums to ask questions or check for solutions to problems. Instead, one must join the ROCK- or YARP-users mailing list and mailing list archives for YARP can be found on SourceForge. If you want to report a bug, then this can be done through their respective GitHub repositories. There are interface drivers available for actuators and most types of sensors, but only one or two specific sensors are supported

for each sensor type. Therefore, you either must use the sensors that they provide drivers for or write your own drivers. ROCK or YARP have not yet been used in an agricultural robot. Therefore, there are no packages available specific to agriculture.

2.7.2 ROS

ROS (Robot operating system) [89] is an open-source robot middleware maintained by willow garage [95]. It can be used free of charge for private and commercial use if appropriate accreditation is given. Like the other actively supported middleware well-written tutorials to guide you through using the middleware are available on the ROS website. However, ROS is the most used robot middleware out there [96]. There is a forum on which to check for solutions to problems and ask questions of your own. Bugs can be reported through the GitHub repository. Because of the large user base of ROS, it is the middleware that actuator and sensor manufacturers generally provide an interface driver for, and if they do not provide one, then you can generally find one on GitHub that someone from the community has written. ROS even supplies libraries for Arduino and Mbed, making it easy to use custom actuators and sensors. ROCK and YARP both provide a way to interface with ROS, but this feature does not exist between ROCK and YARP themselves. ROS has been used in agriculture as the middleware of choice for the Field Robot Mind (FroboMind) platform [96]. The platform was developed to give developers of field robots for precision agriculture, a common, easy to use platform on which to develop and share software between different projects, in the hope that it will encourage the sharing of knowledge uses.

3 Requirements and Specifications of robot prototype

3.1 Overview

In this section, the requirements and specifications for the prototype hybrid wheeled leg are derived based on the legs intended use on a multipurpose wheeled-quadruped agricultural robot. Throughout this thesis, such a robot is called “hybrid robot”; however, it is not an actual robot as it is not in the scope of this project to design the final agricultural robot.

The specifications were identified by looking at 1) possible tasks the hybrid robot may need to perform, 2) the equipment required for these tasks, and 3) the features relating to the leg required for these tasks. The specific tasks mentioned below are chosen because the requirements of these tasks would make the robot versatile enough that it can adapt to a wide variety of other tasks not mentioned in this chapter. The specified tasks are identified from literature on current agricultural robots and by exploring new tasks made possible using hybrid wheel-leg locomotion in agriculture.

A mock-up frame design is also presented and is used as an indication for the weight of the frame. However, it was not considered where and how equipment and components would be attached, therefore the frame is not necessarily indicative of how a robot using this leg would look.

The derived specifications the best that can be attained without physically building the final hybrid robot and testing it on a farm.

3.2 Tasks and requirements

Before the prototype leg was designed, the potential tasks that a hybrid robot would be doing, the equipment it would carry, and the features it would require were identified.

3.2.1 Arable farming

By looking at literature on robots in arable farming, the following tasks were identified for the hybrid robot to do:

- Weed scouting
- Targeted weed spraying
- Mechanical weeding

- Vegetable picking
- Fruit picking
- Assisting with fruit picking
- Fertilising
- Seeding

Equipment required to complete these tasks:

- Spraying equipment
- Seeding equipment
- Robot manipulators
- Bottom view camera

Features required to complete these tasks:

- Mounting place for the different equipment
- Adapt to different crop row spacing
- Fit down fruit orchard lanes
- Ground clearance for several crops
- Tow a trailer

3.2.2 Livestock farming

By looking at literature on robots in livestock farming, and by identifying new potential tasks that could benefit from a highly capable uneven terrain robot, the following tasks were identified for the hybrid robot to do:

- Remove or place tread-in posts
- Temporary fence wire
- Monitor livestock
- Heard livestock

Equipment required to complete these tasks:

- Robot arm
- Standards holder
- Poly wire and reel

Features required to complete these tasks:

- Be able to support the weight of the different equipment
- Open gates
- Change ride height to pass under single wire temporary electric fences

3.2.3 Additional requirements and constraints

In both arable and livestock farming, the robot will need to carry autonomous navigation equipment, control computers, and batteries for power. Additionally, components should be selected, and designs derived that are as cheap as possible without compromising leg performance. There are two main reasons for this: 1) the budget for this project is only 3000 NZD, and 2) the literature states that for farmers to consider mobile farm robots, lower cost but yet high-performance solutions are required [33], [18], [38].

3.3 Load-carrying ability

A good estimate of the weight the leg will be supporting must be identified. The weight that needs to be supported will influence the structural design of the leg and the torque required from the actuators. To estimate the weight that one leg would need to support the weight of the hybrid robot's chassis, the parts housed within the chassis, and the weight of the equipment required for each potential task was estimated. The weight of the hybrid robot chassis and the parts housed within the chassis is estimated in section 3.3.1. The weight of the equipment needed for the potential tasks is estimated in sections 3.3.2 - 3.3.7

3.3.1 Frame and components

To get an understanding of the required sensors, computers, electronics, batteries and their respective weights as well as an idea of potential frame shape and size, two quadruped wheel-leg hybrid robots intended for unstructured terrain (Momaro [64] and Mammoth [68]) were analysed. These robots were identified as having a similar size, shape and configuration to what the final hybrid robot is expected to have. The specifications for Momaro were retrieved from [64], and the specifications for MAMMOTH were retrieved from [68]. The specifications for both robots stated their total mass and what components they used but did not state the individual component weights or the weight of their frame. However, the component weights were found online, and a mock-up frame was designed in SolidWorks to get a rough estimate of its weight.

Additionally, both robots did not mention information about generic components that were housed in the frame such as power regulation supplies, motor drivers and low-level computer. These are estimated for each robot based on the information available for them.

3.3.1.1 Momaro

Momaro [64] uses DYNAMIXEL Pro actuators which have an integrated controller and driver. Therefore, the only suspected extra components not specified are a power supply and a low-level computer. A laptop power supply was estimated as the weight for the power regulation electronics and a beagle bone black as the weight for the low-level computer. Additionally, only the processor and ram specifications are given for the main application computer; based on these specifications, an Intel NUC performance kit was chosen as the application computer. The weight of Momaros components is listed below in Table 1, and Momaros overall weight is 57kg

Table 1. Momaro component weights.

Component	Quantity	Type	Mass (kg)	Total mass (kg)
LIDAR system	1	Hokuyo UTM-30LX-EW + Dynamixel MX-64	0.336	0.336
RGB Camera	7	Not specified – estimated using Logitech c920	~0.480	~3.36
RGB-D Camera	N/A	Not used	N/A	N/A
Application Computer	1	Not specified – estimated using Intel NUC performance kit	1.500	1.500
Low-level computer	1	Not specified – estimated using a Beagle bone black	0.036	0.036
Router	1	NETGEAR Nighthawk AC1900	0.750	0.750
IMU	1	Pixhawk IMU	~0.090	~0.090
Battery	1	22v 16AH lithium ion	~2.063	~2.063
Power supply	1	Not specified – estimation based on a laptop power supply	~0.36	~0.36

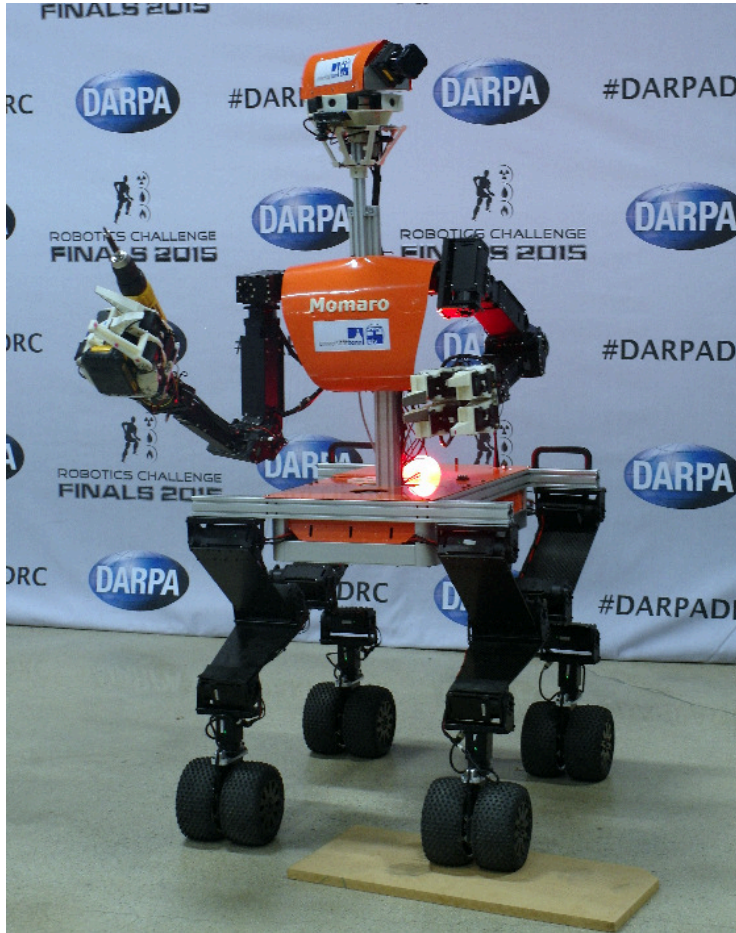


Fig. 22. The robot 'Momaro' [64].

3.3.1.2 MAMMOTH

MAMMOTH [68] uses linear and rotary actuators with a built-in motor controller and driver. Therefore, the only suspected extra components not specified are power regulation electronics, low-level computer, and a router. A laptop power supply is estimated as the weight for the power regulation electronics and a NETGEAR Nighthawk AC1900 as the weight of the wireless communication electronics. However, it will probably use a larger/heavier wireless communication device when on mars. Additionally, a beagle bone black was used to estimate the weight of the low-level computer and a base model intel NUC was used to estimate the weight of the more powerful application computer. The specifications of the Beagle bone black and the intel NUC closely matched the specification reported in [68]. The weight of MAMMOTHs components is listed below in Table 2, and MAMMOTHs overall weight is 80 kg.

Table 2. MAMMOTHs component weights.

Component	Quantity	Type	Mass (kg)	Total mass (kg)
LIDAR system	N/A	Not used	N/A	N/A
RGB Camera	N/A	Not used	N/A	N/A
RGB-D Camera	1	ASUS Xtion Pro Live	0.54	0.54
Application Computer	1	Not specified – estimated using Base Intel NUC	1.360	1.360
Low-level computer	1	Not specified – estimated using a Beagle bone black	0.036	0.036
Router	1	Not specified - estimated using a NETGEAR Nighthawk AC1900	0.750	0.750
IMU	1	VN-200	0.016	0.016
Battery	1	12x95wh lithium ion	~2.460	~2.460
Power supply	1	Not specified – estimated using a laptop power supply	~0.36	~0.36

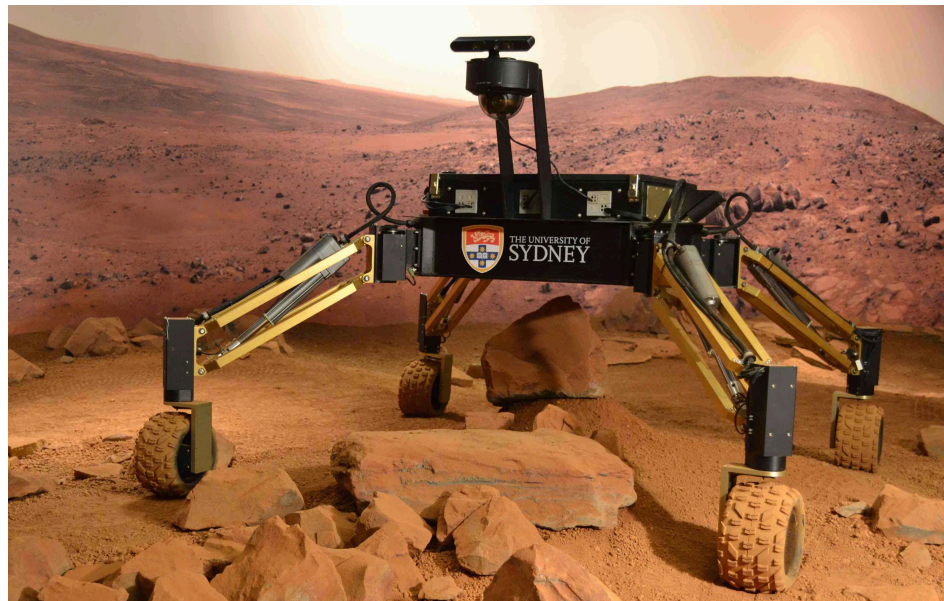


Fig. 23. The robot 'MAMMOTH' [68].

3.3.1.3 Additional components

Momaro and MAMMOTH are not intended for agricultural use, so are missing some additional components that would be useful for agricultural tasks and would need to be mounted in the frame. From the literature on current agricultural robots, an RTK-GPS and bottom facing cameras were identified as missing components for agricultural tasks.

An RTK-GPS can give positions that are accurate to 10 mm; this makes it beneficial for agricultural tasks where accuracy is essential such as seeding and weeding operations. The weight of a typical RTK-GPS is about 0.69 kg-1.31 kg.

Bottom facing cameras are useful for phenotyping and weeding tasks. These cameras are no different from the cameras used elsewhere in the frame, so they are assumed to have the same weight. It is predicted that 1-2 bottom facing camera would be needed.

3.3.1.4 Example Frame

A mock-up chassis/frame was modelled in SolidWorks 2018 (shown in Fig. 24) to determine what it would weigh. A rough idea of what it should look like was determined by looking at Momaro and MAMMOTH. The Mock-up model represents what an actual chassis might look like but lacks careful consideration of how electronics, sensors and batteries would mount or how it would interact with other equipment. The model has the following Specifications:

Width	0.6 m
Length	1.05 m
Height	0.18 m
Mass	18 kg
Material	6061-T6 Aluminium

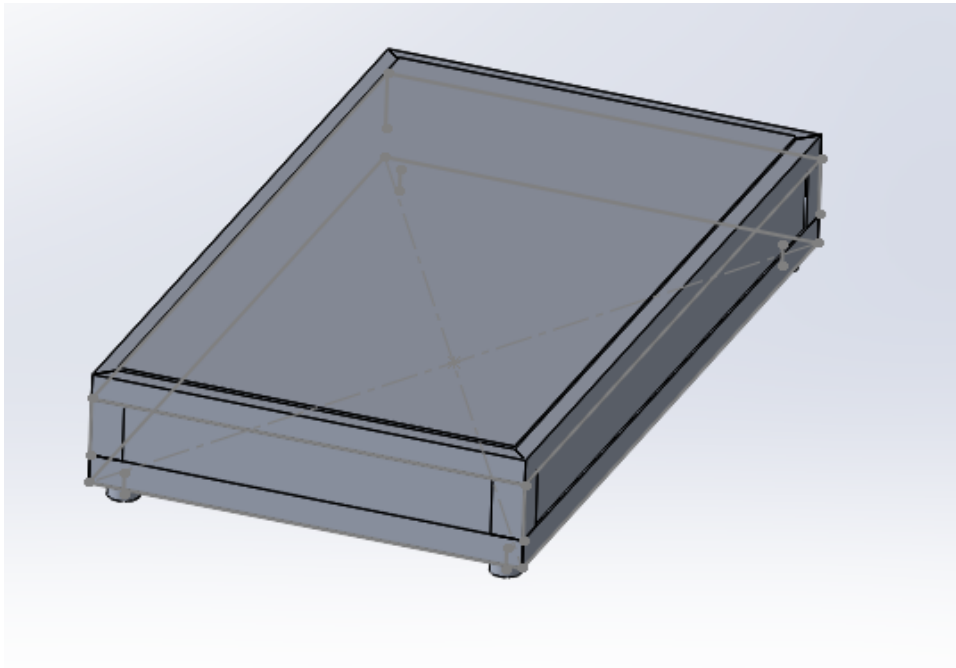


Fig. 24. Example frame for a final hybrid robot.

3.3.1.5 Final chassis weight

By looking at the robots Momaro and MAMMOTH (described above) it was derived which types of components, and the number of components, that an autonomous hybrid wheeled leg robot would require and how a potential frame may look. In addition to the identified components, it was concluded that an RTK-GPS and additional bottom facing cameras would be beneficial for the robot. These weights are best estimates as they are likely not the exact components that are going to be used; they are just representative of the type of components used.

Most of the components used in the two robots were of the same type, but they were not identical. They were either different models or a different brand altogether. In these situations, the heavier of the two components is chosen for the final specification to ensure a worst-case value is derived.

An additional 1 kg is added to the final result to account for variation and unforeseen components.

Table 3. Final frame and components weight.

Component	Quantity	Mass (kg)	Total Mass (kg)
Frame	1	~18	~18
Lidar system	1	~0.336	~0.336
RGB Camera	7	~0.480	~3.36
RGB-D Camera	1	~0.54	~0.54
Application Computer	1	~1.360 - 1.5	~1.5
Low level computer	1	~0.036	~0.036
Router	1	~0.750	~0.750
IMU	1	~0.016 - 0.090	~0.090
RTK-GPS	1	~0.69 - 1.31	~1.31
Battery	1	~2.063 - 2.460	~2.460
Power supply	1	~0.36	~0.36
Unforeseen components			
Total			28.742

3.3.2 Robot arm

Robot arms are required by many of the tasks identified in section 3.2. A vertically articulated arm can be mounted on top of the robot and would enable the robot to open gates, move tread-in posts, handle tools, pick fruit and spray large shrubs or weeds. A second Delta style robot arm could hang from the bottom of the robot and would allow

the robot to do tasks such as mechanical weeding, seeding, and precision spraying of small weeds.

Vertically articulated robot arms have been used extensively in car manufacturing because they can orient their end effector to approach an object along the vertical axis from many angles, like a human arm. This also makes them useful for real-world outdoor tasks such as those found in agriculture since most tasks require objects to be manipulated and oriented in free space. In agriculture, they have mainly been mounted to autonomous agricultural robots where they have been used for fruit picking and vegetable harvesting [97-100]. Away from agriculture, articulated robot arms have become the manipulator type of choice for mobile robots designed to interact with environments intended for humans [101]. This makes it an ideal manipulator type for a multipurpose agricultural robot which must interact with both human-made objects like gates and fences and natural objects like fruits and vegetables.

A Custom articulated robot arm intended for agriculture has been presented in the literature [102], and the commercially available UR5 articulated robot arm meant for manufacturing [103] has been used in agriculture [99]. The custom agriculture robot arm has been designed specifically for fruit picking and vegetable harvesting, spraying, and pruning; it is heavy at 64 kg. Its base is a vertical prismatic joint enabling it to pick fruit and vegetables from trees or plants of varying heights. However, its weight combined with its height would likely make the hybrid robot unstable and unable to pass under temporary fences easily. Stability and the ability to pass under temporary fences are features that would be extremely desirable for tasks on a livestock farm where terrain can be hilly and unpredictable. The commercially available UR5 robot weighs 35.6 kg. It is designed to manipulate tools and manufactured parts and is affective at picking sweet peppers. Due to the versatility and lighter weight of the UR5 weight was used to estimate the weight of an articulated robot arm suitable for the hybrid robot.

Delta robots are great for accurate high-speed pick and place type operations. Spraying weeds, manual weed killing, and seed planting based on the ground require the same movements as pick and place operations. Delta robots must be mounted to a surface directly above their working area, as opposed to a SCARA robot which has to be mounted to the side of its working area. This means Delta robots are ideally suited to be mounted to the underside of a robot. They have already been used in agriculture as seedling transplanting robots [104] and ecoRobotix Ltd. are about to commercialize an agricultural weed spraying robot using two delta robots mounted on its underside [17]. ecoRobotix Ltd. has not published the specifications of the Delta robot they are using. Therefore, it could not be considered for the weight estimation of the hybrid robot of this thesis; instead, the weight estimation had to be based on commercially available robots. From the commercially available robots, three robots are not too heavy and have

power requirements appropriate for the hybrid robot: the SIAX D3 500, the SIAX D4 500 [105] and the igus® drylin® delta robot [106]. Their weights ranged from 15-27 kg. The heaviest delta robot (27 kg) will be used as weight estimated for the hybrid robot.

Concluding, the estimated weight of the robot arms that the robot would use, and need to carry for various tasks is:

$$\begin{aligned} \text{Articulated robot arm weight} &= 35.6\text{kg} \\ \text{Delta robot weight} &= 27\text{kg} \end{aligned}$$

3.3.3 Temporary electric fences

Tread-in posts and poly wire are used to make temporary electric fences. Temporary electric fences are commonly used in the practice of break-feeding [107] where livestock are only given access to a small area of pasture to prevent trampling and damage of fresh pasture during the winter. The removal or placement of these temporary fences is a task that the robot may be able to do. Therefore, the weight of tread in posts, poly wire and the poly wire reel needs to be determined. The most common New Zealand paddock size also needs to be determined so that the number of temporary posts and amount of poly wire the robot has to carry to erect a temporary fence across most NZ paddocks, can be calculated.

According to Gallagher™, there are two types of tread-in posts. The first is pigtail posts which are popular on dairy and cattle farms, and the second is multiwire posts which are used for all other animals [108]. Pigtail posts commonly come in two different lengths: 720mm and 850mm, the latter weighing about 0.4kg. Multiwire tread-ins come in a range of different length from 845-1500 mm, the latter weighing about 0.6 kg.

The size and shape of NZ paddocks vary a lot, though most paddocks are around 4 ha in size [109]. Tread-in posts are usually erected across the width of the paddock, and although paddocks are usually longer than they are wide, it will be assumed they are square for the purposes of calculating the largest possible width. Gallagher suggests that on uneven ground pigtail posts should be planted every 20 m while multi wire posts should be planted every 10 – 12.5m [110]. Using the most common paddock size, largest width configuration, the smallest post spacing, and the heaviest post we can approximate the weight of posts the robot needs to carry if it needs to erect a temporary fence across the most common paddock size:

$$\begin{aligned}
Width &= \sqrt{40000} = 200 \text{ m} \\
No. of posts &= \frac{200}{10} = 20 \\
Weight &= 20 * 0.6 \text{ kg} = 12 \text{ kg}
\end{aligned}
\tag{1}$$

Also, the weight of the poly wire and reels needs to be added. A single-wire temporary electric fence will only require one reel filled with 500 m of poly wire weighing 4.24 kg, where a multi-wire fence requires three reels filled with 500 m poly wire weighing 12.72 kg. To ensure compatibility with both single-wire and multi-wire electric fences, 12.72 kg is used.

Erecting temporary electric fences may also require an articulated robot arm to place the tread in posts in the ground, a vision/Lidar system to find a suitable location to place the post and attach the wire to the post, and a GPS to determine where on the farm the post is being planted. The weight estimation of an articulated arm is done in section 3.3.2, and the weight estimation of the Vision/lidar system and GPS is done in the frame and components section (3.3.1).

Concluding, the total estimated weight of equipment the robot would need to carry for erecting temporary electric fences excluding the robot arm and additional equipment is:

$$Equipment \text{ weight} = 12 + 12.72 = 24.72 \text{ kg}$$

3.3.4 Targeted weed spraying

Site-specific, or targeted pesticide and herbicide spraying is a common area of research in precision farming. Targeted spraying can reduce the amount of pesticide applied to treat grapevines for disease by 65% to 85% [111] and across various crops it reduced herbicide application by up to 90% [17]. The reduced usage of pesticides and herbicide has both environmental and monetary benefits since there is little to no runoff of chemicals into the soil, and less pesticide or herbicide needs be purchased. Targeted spraying is a task that the final hybrid robot could be expected to do among crops and in pastures. Many robots have been designed for spraying among crops, but the only robot designed to do it in pastures is Ibex [112]. Due to the excellent uneven terrain abilities of wheel leg hybrid robots, the hybrid robot would be able to spray pastures in terrain that Ibex cannot go.

Thanks to the reduction in herbicide usage with targeted spraying, the herbicide tank size can be much smaller compared to conventional weed spraying. To estimate the weight of pesticide/herbicide and spraying equipment the robot may be carrying, weed

spraying robots in the literature were investigated [113, 114]. However, the literature did not state what volume of pesticide or herbicides the robots carried, or the weight of the spraying equipment they used. A recent commercially available smart weeding robot from ecoRobotix [17] carries 30 litres of herbicide, which ecoRobotix say is enough for a whole day worth of autonomous weeding spraying. Since neither the commercially available robot nor the robots from literature state what spraying equipment they use such as the pump and spraying nozzle, the weight of a 30 L all-terrain vehicle (ATV) sprayer was used to estimate the spraying equipment weight.

A 30 L ATV sprayer has a wet weight of 34.5 kg [115]. In addition, an articulated robot arm or a delta robot is needed to operate the spray nozzle, vision/LIDAR equipment is needed to identify the weeds, and an RTK-GPS is needed so the robot knows where on the farm it is and where it has already sprayed. The weight estimation of an articulated arm and delta robot is done in section 3.3.2, the weight estimation of the Vision/lidar system and RTK-GPS is done in the frame and components section (3.3.1).

Concluding, the total estimated weight of equipment the robot would need to carry to spray weeds, excluding the robot arm is:

$$\text{Equipment weight} = 34.5 \text{ kg}$$

3.3.5 Manual weeding

Manual weeding does not require the use of herbicides. Instead, the weeds are destroyed mechanically, usually with a robot arm. Either an articulated robot arm or a delta robot arm can be used for the weeding. Other equipment required for mechanical weeding is a vision/lidar system to identify the weeds, and a GPS, so the robot knows where on the farm it is and where it has already weeded. As described above, the weight estimation of an articulated arm and delta robot is done in section 3.3.2, the weight estimation of the Vision/lidar system and GPS is done in the frame and components section (3.3.1).

3.3.6 Seeding planting equipment

Seed planting is an area of interest for agricultural robot researchers because seeding accuracy can be improved compared to conventional seeding with tractors, and since agricultural robots are usually much smaller, soil compaction can be reduced [116]. Seeding is a task that the Hybrid robot would be able to do with the correct implements or robot arm.

To estimate the weight of seeding equipment required, the literature on seeding robots was investigated. However, information on what specific equipment was used and the volume of seeds carried was not stated. The traditional mechanical seed drills that attach to tractors use components and volumes of seeds that are too large to be considered for use on the final hybrid robot. However, a recent smart seeder made by Greentech robotics uses an electronically controlled seed dispenser called the SeedSpider Metering System [117] that would fit on the hybrid robot. Unfortunately, Greentech does not specify the weight of their dispenser or the seed outlets that it attaches to. Nevertheless, they do specify that the dispenser comes standard with a 7-litre capacity which, according to Greentech, is ideal for most situations. Seed density ranges from 400 to 850 g/L [118]. Using the 7 litres seed capacity, the most substantial weight of seeds the final robot will need to carry is 6 kg. This can be doubled to account for the weight of the empty seed dispenser.

Another way that seeding can be done is with a delta robot [104]. This Delta robot can be mounted to the bottom of the robot with a seeding end effector and dispenser attached. The weight of an appropriate delta robot is derived in section 3.3.2 with the heaviest delta robot being the SIAX D4 500 weighing 27 kg. This robot has a maximum payload of 2 kg, meaning 2 kg can be added for the weight of the seeding end effector. Even though the weight of a small-scale conventional seeding implement that can be used on the hybrid robot could not be identified, it is predicted that the weight of the delta robot seeding configuration is enough to account for a future custom conventional seeding implement.

Extra equipment needed for seeding is an RTK-GPS so that the hybrid robot can accurately determine its speed and plant the seeds accurately in rows. A vision/lidar system may be required to avoid possible obstacles present in the field. The weight estimation for the GPS and vision/LIDAR system can be found in the frame and components (3.3.1).

Concluding, the total estimated weight of equipment the robot would need to carry for planting seeds, excluding the robot arm and additional equipment is:

$$\text{Equipment weight} = 2 + (2 * 6) = 14 \text{ kg}$$

3.3.7 Livestock monitoring and herding

The hybrid robot may be required to monitor or herd livestock. There is already a livestock monitoring and herding robot called Swagbot [119]. Swagbot only appears to have a camera to monitor livestock and wireless communication equipment to communicate with UAV and the farmer. UAV's are used to give the robot a bird's eye

view of its surroundings. Therefore, the equipment required for livestock monitoring and herding is covered in the frame and components section (3.3.1) by the vision lidar system and the wireless router.

3.3.8 Final hybrid robot weight specification

The final weight that the legs will be required to carry will be equal to the task that requires the heaviest combination of components. The following tables show the required leg payload for each of the tasks it is expected to do.

Table 4. Weight of robot in different configurations.

Task	Task Equipment specific (kg)	Robot arm (kg)	Frame and components (kg)	Total (kg)
Temporary fence erection	24.7	35.6	28.7	89.1
Targeted weed spraying	34.5	27/35.6	28.7	88.3/98.8
Manual weeding	N/A	27	28.7	55.7
Seed planting	14	27	28.7	69.7
Livestock monitoring	N/A	0	28.7	28.7

3.4 Leg height range

While the leg is intended to give the robot the ability to walk, it also gives it the ability to change its ride height during wheeled locomotion. The height range affects the length of the leg links (higher average range means longer links), which in turn affects the torque required from the actuators (longer links demand more torque). Height range was determined by looking at what scenarios might demand a specific height and then calculating what the desired height is. Scenarios, where the height will need to change, are travelling with a delta robot below the robot, going under single wire temporary electrical fences and weed related tasks over crops (spraying, scouting and manual weeding).

3.4.1 Going under single wire temporary electric fences

Going under single wire temporary electric fences would reduce both the time required for the robot to travel around a livestock farm and the chance of livestock escaping from where they are temporarily fenced off. The legs need to be able to lower the height of the robot so that the highest point of the chassis and robot arm is lower than the electric

wire. Therefore, we need to determine at what height from the ground the wire is, roughly how thick the chassis will be and how thick the arm will be when folded down.

From section 3.3.3 we know the wire height of pigtail tread-in posts is 0.72-0.85 m. The chassis thickness is not known precisely, but we will base it on the mock-up chassis in section 3.3.1.4 which is 0.18 m thick. The thickness of the UR5 robot arm in its folded down position is 0.16 m. A clearance distance of 10 mm will be used. Therefore, to pass under a temporary electric fence, the maximum allowed height the legs could take the frame from the ground while still being able to use its wheeled locomotion is:

$$\text{Maximum allowed height} = 0.72 - 0.18 - 0.16 - 0.01 = 0.38 \text{ m}$$

3.4.2 Crop and pasture heights for weeding

Weeding operation requires the robot to drive over crops and pastures. Therefore, it is crucial to know the maximum height of commonly grown crops and pastures. The maximum height of commonly grown crops can be seen in Fig. 25 and that of commonly grown pastures in Fig. 26.

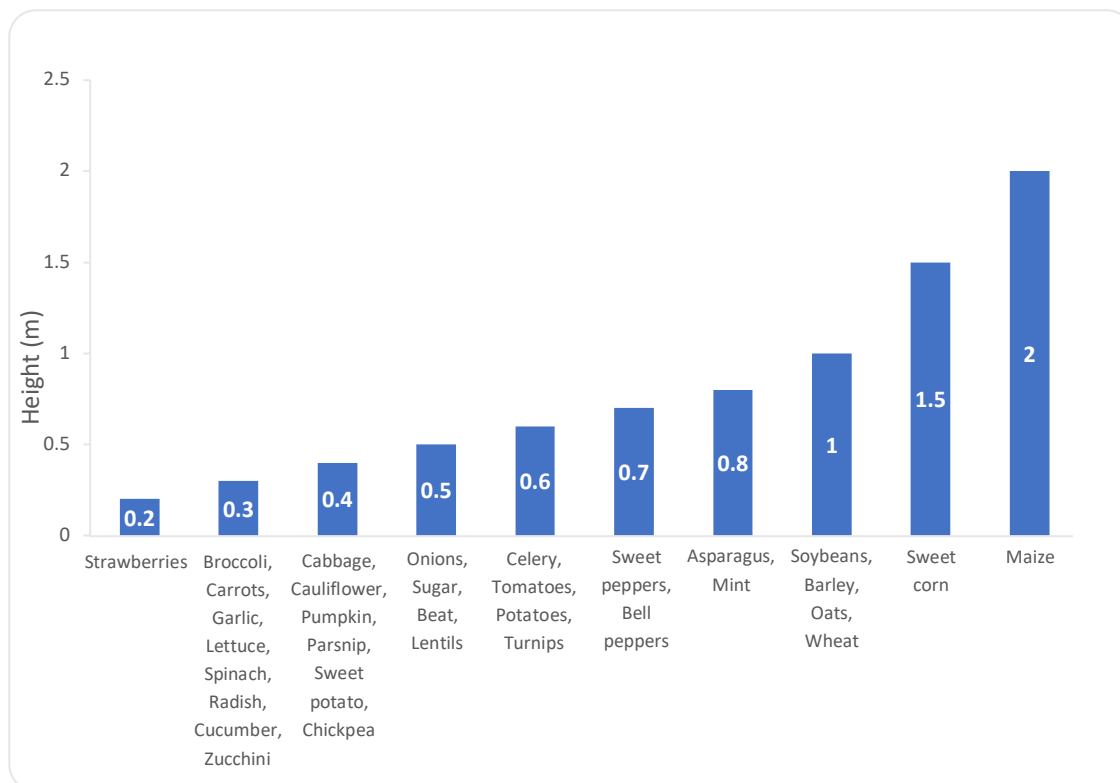


Fig. 25. Height of common crops. Data retrieved from [120].

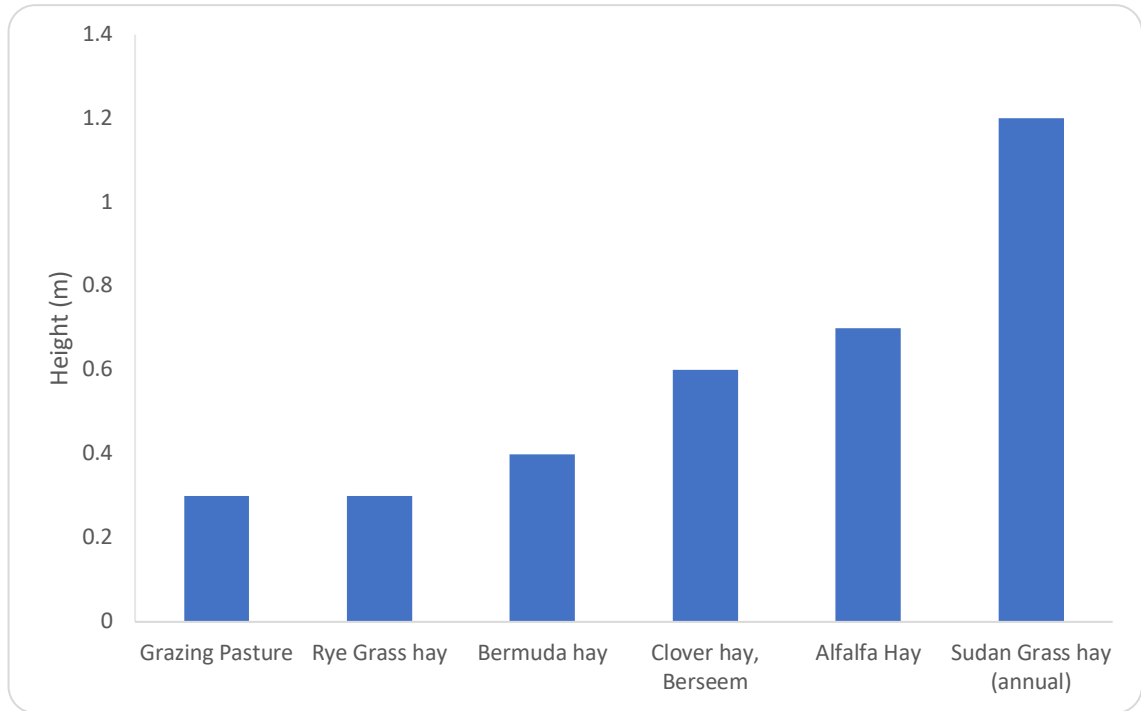


Fig. 26. Common pasture heights. Data retrieved from [120].

Looking at the two graphs above, a clearance height of 2.5 m will allow the robot clearance of all common crops. However, making the robot this tall would make it unstable (unless it were extremely wide) and would add cost and weight because larger actuators would be required. Therefore, a clearance height of 1 m is chosen since it gives a robot clearance to travel over most crops and pastures found in agriculture while not requiring the robot to be too big.

Crop clearance height = 1 m

3.4.3 Delta robot clearance

Since a delta robot will be hanging from the bottom of the robot, it will take up room below the robot. If the hybrid robots maximum ride is too low, the delta robot will not fit under the hybrid robot. However, if the hybrid robots ride height is too high, the delta robot cannot reach the ground to perform weeding or seeding operations. Therefore, the fully extended and fully contracted lengths of the two delta robots, identified in section 3.3.2, needs to be found.

The SIAX D4 500 delta robot has a fully contracted length of 600mm and a fully extended length of 800mm. The igus delta robot has a fully contracted length of 500mm and a fully extended length of 670mm. To find what clearance is needed when using a delta robot in crops, the only available weeding robot using a delta robot was looked at again: the ecoRobotix autonomous robot weeder [17]. Although the reach of its delta robots

is not specified, it is stated that it can only spray weeds in crops shorter than 0.25 m. However, it can weed in beetroot and rapeseed crops (“with more to come”), which have a maximum growing height of 0.4 m and 0.6 m, respectfully. This is likely because weeding is mostly done at the start of the crop growth cycle to stop competition from weeds while growing [121]. Pastures can also be weeded before they reach their 0.3 m height. Therefore, a delta robot clearance height ≥ 0.25 m at the neutral height of the SIAX D4 500 delta robot (0.7 m) is desirable to give the hybrid robot the ability to weed in crops and pastures. This means the legs of the hybrid robot needs to extend to a minimum length of:

$$\text{Minimum workable height} = 0.7 + 0.25 = 0.95 \text{ m}$$

3.4.4 Overall height specification

The leg length required for different scenarios is shown below in table blah. The leg can move to a minimum height of at least 0.37 m and a maximum height of at least 1 m.

Table 5. Leg height requirements.

Scenario	Height constraint (m)
Driving under a temporary electric fence	<0.37
Driving in crops	>1
Weeding with a delta robot	>0.95

4 Mechanical Design of Hybrid Leg

A prototype hybrid wheeled leg intended for use in a multipurpose agricultural robot was developed conforming to the specifications set out in Chapter 3. The leg has five degrees of freedom. The position axes (DOF 1-3) enables the leg to change a mobile robot's ride height and track width and give a mobile robot the ability to walk. The movement axes (DOF 4 and 5) allows the leg to orientate its wheel in the desired steering direction and then drive the wheel in that direction.

4.1 Concept designs

Since the basis of a robotic leg is its revolute joints, how these joints could be actuated was the focus of the concept generation stage. They were derived by hand and based on the two main actuation types: linear and rotary. The concepts consisted of possible ways an actuation type could actuate a joint. The chosen concept was determined by looking at how it would influence the overall leg design, what components were required, and how it would influence any future development of the prototype leg.

4.1.1 Linear actuation

Linear actuators differ by their source of actuation. There are three primary power sources for linear actuation: electromechanical, hydraulic, and pneumatic. When referring to an actuator as a "linear actuator", it is generally assumed you are talking about an electromechanical linear actuator. Hydraulic linear actuators are referred to as hydraulic rams or cylinders, and pneumatic linear actuators are referred to as pneumatic rams or cylinders.

From the concepts that were drawn and further investigation into available linear actuators, several downsides became apparent that resulted in a decision not to use a linear actuator on the hybrid robotic leg. The joints would only have a range of motion like that of a human knee or elbow joints, while this is enough for walking it may limit how the leg can actively change its configuration during wheeled locomotion. Another drawback is that linear actuators take up a lot of space, especially if compliance is added to their design.

The concept sketches that were conceived are shown in Fig. 27.

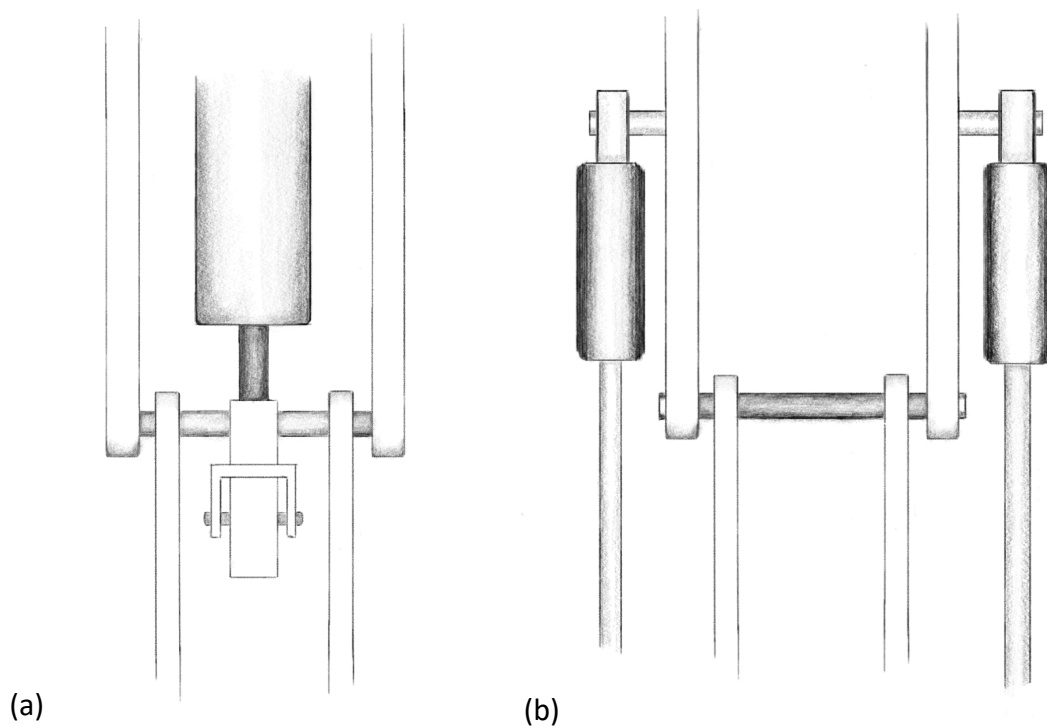


Fig. 27. a) Linear actuation concept using a single cylinder. b) Linear actuation concept using dual cylinders.

4.1.2 Rotary actuation

Rotary actuators have the same three power sources as linear actuators: electromechanical, hydraulic and pneumatic. However, they have the advantage over linear actuators of being able to (depending on the type) rotate a joint by 360° and they can easily be designed in a compact form factor. Additionally, rotary actuators can be configured in many ways because there are efficient and compact mechanisms available to change the direction and axis of rotational movement. This makes rotary actuators perfect for most applications. The concepts for legs using rotary actuators are shown in Fig. 28 in the next section.

Hydraulic rotary actuators output a large amount of torque for their size. However, for them to operate, they require a hydraulic pump, reservoir, hydraulic fluid, and a valve bank. This makes them less efficient than electromechanical actuators due to losses from the resistance of the fluid and leaks in the system [122]. Additionally, when used on a walking robot, the extra weight of these accompanying components means a large amount of the extra torque is used to carry them, which adds to the energy inefficiency of the system. This inefficiency can be compensated for with larger batteries. However, this means more weight and a larger robot chassis to carry both the components and batteries. However, when the leg is not in use hydraulic actuation can improve efficiency by making use of the fact that hydraulic fluid cannot be compressed: if you close the

appropriate valves, you can prevent the fluid from escaping the actuator, therefore locking it in place using little to no energy.

Pneumatic rotary actuators work on the same principle as hydraulic rotary actuators, but instead of using an incompressible hydraulic fluid, they use air. This means they have the same drawbacks as hydraulic actuators: they require a pump (compressor) and associated components, and they are inefficient because of friction and leakage. Where they differ from hydraulic actuators is their torque output and rigidity when locked. They have a lower output torque because they operate at much lower pressures, and they are less rigid when locked because air is compressible. The fact that they are less rigid could be beneficial to the leg as it will give it inherent compliance toward load impulses, which can save components from failure by absorbing and then releasing the energy of the knock more gradually.

Electromechanical rotary actuators work with electricity, and only require an additional electronic controller to operate, which is much lighter than the additional components required by both the hydraulic and pneumatic rotary actuators. Other benefits are they are easier to control, they can turn rotational movement back into electricity, and are more reliable because they have fewer points of failure. However, they do not have the same inherent ability to make themselves rigid without using energy unless a worm drive is used, which is not appropriate for all applications. Additionally, if they are used without a gear reduction, then larger motors and large voltages and/or currents are required, which means larger cables, controllers, and potentially batteries will be needed. This means for high torque applications, such as joint actuation, a gearbox is required to increase output torque through mechanical advantage.

The hydraulic and pneumatic actuators ability to stay rigid and use little to no energy is an attractive feature on a wheeled-leg robot that is not always walking. However, with an additional brake mechanism, an electromechanical actuator could have the same feature at a significantly lesser weight than the additional components required for a hydraulic or pneumatic system. Moreover, pneumatic and hydraulic systems are a lot more expensive than an electromechanical system and are more prone to failure. Therefore, it was decided to use an electromechanical rotary actuator on the leg since its drawbacks were small and the benefits were in line with the requirements of the leg: low cost and lightweight.

4.1.3 Concept selection

In Fig. 28, concept (a) has a single, solid body for both the upper and lower links. They are joined where they overlap through a bearing to form a revolute joint. The motor attaches to the side of one of the links and drives through the centre of the bearing to

actuate the other link. Benefits of this design are that the two links are offset, so the actuated link is free to rotate 360° about the joint. However, due to the offset, the joint bearing must endure moment loading since there is no room to space two bearings apart. Bearings that can support moment loading such as crossed roller and 4-point contact bearings are expensive.

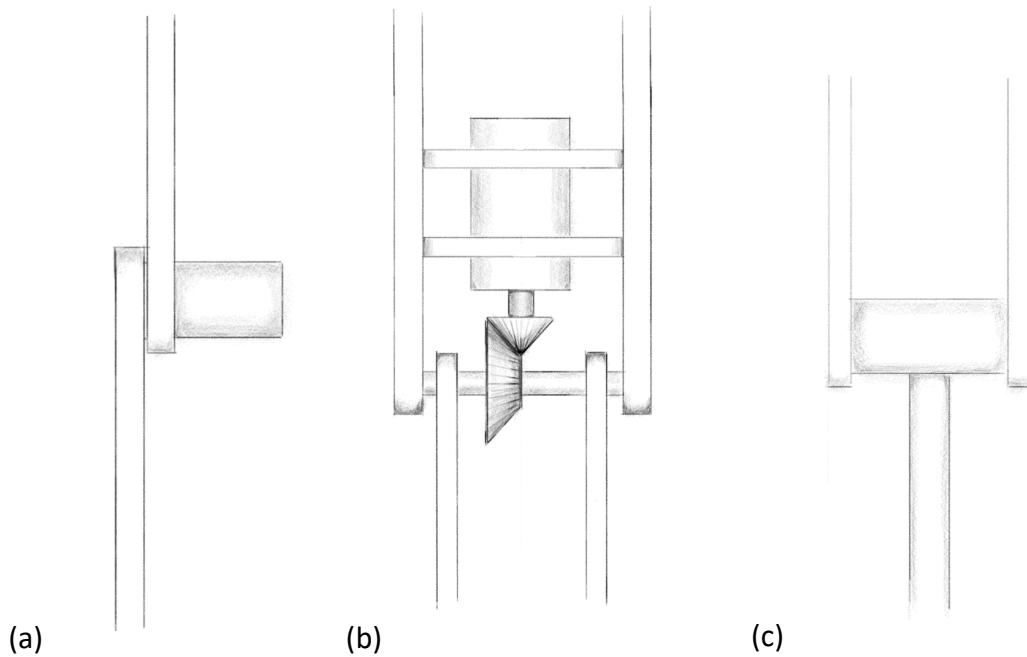


Fig. 28. a) Concept (a) single bearing joint with overlapping links. b) Concept (b) dual bearing joint with motor at a right angle to the axis of rotation. c) Concept (c) dual bearing joint with inline motor drive.

Concept (b) in Fig. 28 relies on a drive that is perpendicular to the axis of rotation, which requires the actuator motor for both the Hip joint and Knee joint to be within the Femur link. To achieve this, each actuator has to work differently: the Knee joint actuator motor and pinion needs to remain stationary and drive the bevel gear, whereas the Hip joint actuator motor and pinion have to move about a stationary bevel gear. This means two different actuator and compliance mechanisms need to be designed and implemented. The two-body upper link design in this concept allows the axis of rotation to be supported by bearings on each side of the link. Because the bearings are spaced relatively far apart, a moment load on the axis of rotation will be felt as radial loads by the two bearings, permitting the use of cheap deep groove ball bearings.

Concept (c) in Fig. 28 uses a multi-body design like concept (b), meaning cheaper deep groove ball bearings can be used. However, it differs from concept (b) because it has the actuator mounted inside the joint, in line with the axis of rotation, thus eliminating the need for bevel gears, and allowing for a link design that is less dependent on the design of the actuator, and therefore more modular. The potential downside of this design is that the joint width must be equal to or greater than the width of the actuator. However,

there is no foreseeable impact on the leg's performance by having a wider upper link. The round Tibia link design of this concept, which could also be implemented on concept (b), can be utilised for the wheel steering design like the head tube is used on a bicycle.

After considering all three concepts, it was decided to develop concept (c) further since it allows for a more modular leg, where a single actuator and compliance design can be used for both the Hip and Knee joints, saving cost and development time.

4.2 Mechanical design

This section describes the mechanical design of the prototype hybrid wheeled leg shown in Fig. 29. It specifically describes the design of the three links (Base link, Femur link, and Tibia link) and the components used. The actuator used in the Hip joint and the Knee joint is described in Chapter 5.

The prototype leg was designed to be:

- Low cost
- Lightweight
- Easy to manufacture
- Easy to assemble
- Strong

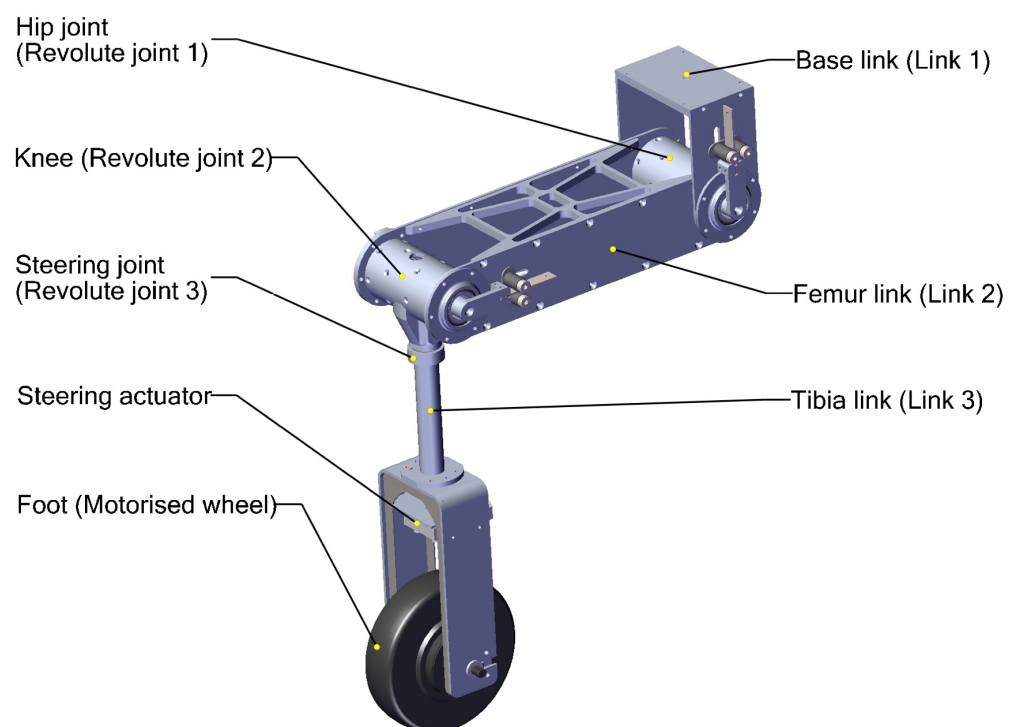


Fig. 29. Overview of the prototype hybrid wheeled leg. (Render from SolidWorks Composer).

4.2.1 Base link

The Base link described in this section (see Fig. 30) is not the final Base link that will be used on the final agricultural robot. Instead, it is designed to mount the prototype leg to a bench or other flat surface for testing, and it may be used as a reference design for the eventual Base link. It lacks the rotate degree of freedom (DOF) that will be present on the eventual Base link, for example, to give the eventual agricultural robot the ability to change its track width. It was decided not to add the rotate DOF to this prototype because there was not enough time, and the rest of the leg's functionality can still be tested without it. Additionally, the Base link cannot be properly designed until the final robot's chassis is designed, which is not within the scope of this thesis.

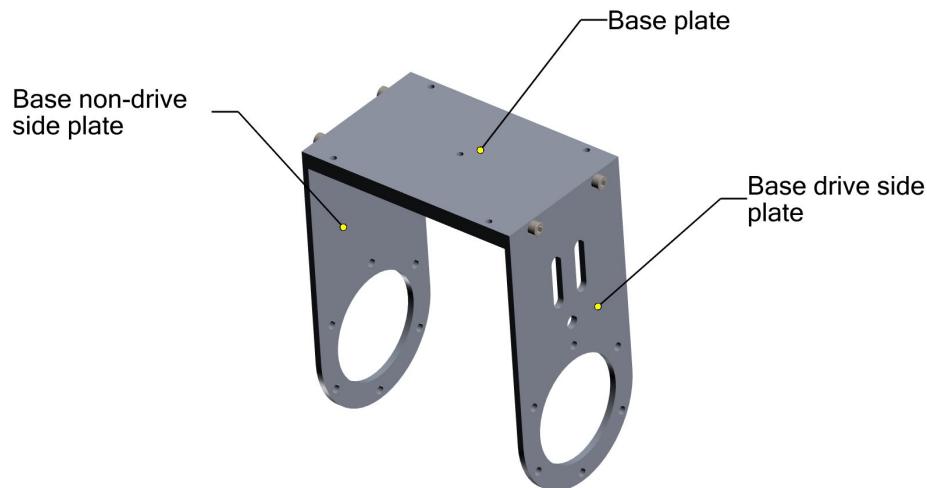


Fig. 30. Parts of the base link intended for testing. (Render from SolidWorks Composer).

Function:

The Base link is what joins the leg to a robot platform or a bench for testing. The Base link described in this section, and as shown in Fig. 30, is intended to be mounted to a bench or similar flat surface. On the one end, it has a Base plate for clamping or bolting it to a bench or flat surface, and on the other end, it has 66.5 mm(\varnothing) holes to mount it to the Femur link through one of the custom compliant actuators.

Dimensions:

Base link: 190 mm(L) X 149 mm(W) X 96 mm(H).

Materials:

All the parts in the Base link are made from 6061-T6 aluminium plate.

Fabrication method:

Both side plates were entirely water jet cut. The Base plate was cut to size on a water jet cutter, then the two M5 holes on the side of the Base plate to which the two side plates mount were manually drilled and tapped on a milling machine.

4.2.2 Femur link

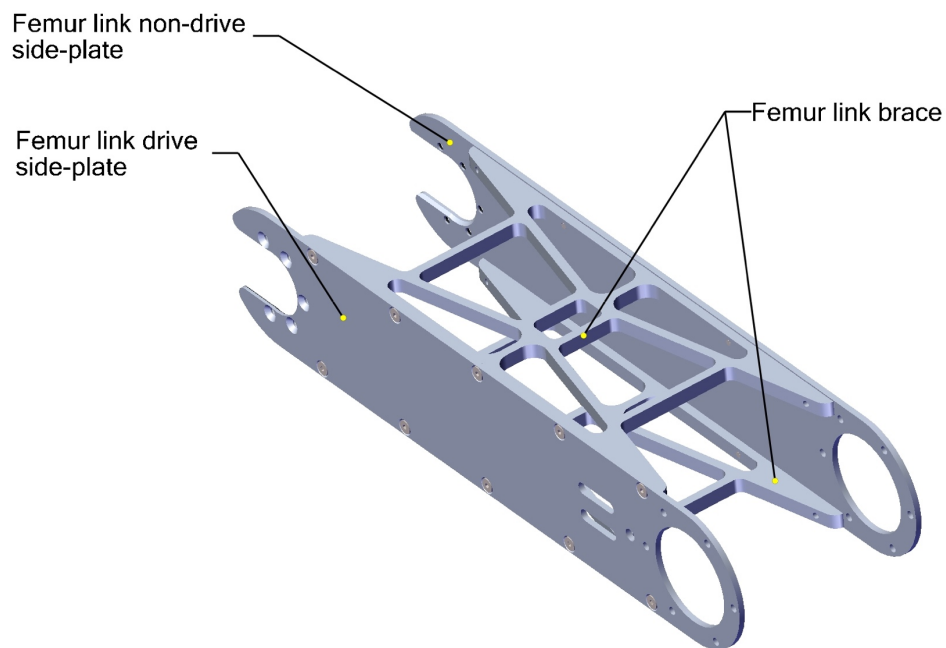


Fig. 31. Parts of the Femur link. (Render from SolidWorks Composer).

Function:

The Femur link joins the Base link to the Tibia link through the custom compliant actuator at each of its ends, see Fig. 31.

Dimensions:

Femur link: 490 mm(L) X 139 mm(W) X 96 mm(H).

Materials:

All the manufactured parts of the Femur link are made from 6061-T6 aluminium.

Fabrication method:

All parts are first cut out with a water jet cutter. The 5.5 mm(\varnothing) holes on both side-plates are then countersunk by hand, and the M5 holes on the edge of both Femur link braces are then accurately drilled on a milling machine before being tapped. The assembly is then bolted together with M5 CSK socket screws.

4.2.3 Tibia link

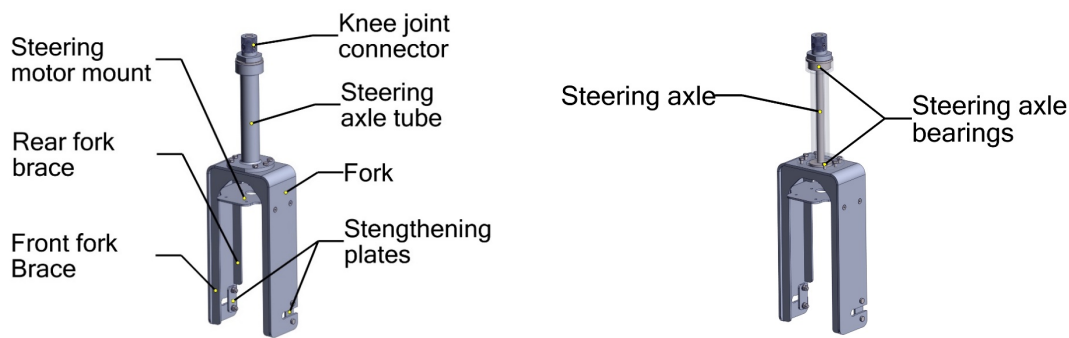


Fig. 32. Parts of the Tibia link. (Render from SolidWorks Composer).

Function:

The Tibia link assembly (Fig. 32) is the last link of the leg. It contacts the ground through the wheel at one end and connects to the Knee joint at the other end. It can also rotate 360 degrees (depending on the Steering servo) just below the Knee joint so that the wheel can be steered in the desired direction. Although only 180 degrees is needed as the wheel motor can be driven in both directions.

Dimensions:

Tibia link: 452 mm(L) X 126 mm(W) X 70 mm(H).

Materials:

The Fork is made from 3 mm and 4 mm 6061 -T6 aluminium plate.

The Steering motor mount is made from 3mm 6061 -T6 aluminium plate.

The Steering axle is machined from a 12 mm(\varnothing) 316 stainless steel rod, and the Knee joint connector is machined from 40 mm(\varnothing) 6061-T6 solid aluminium round bar.

The Steering axle tube with integrated bearing housings is machined out of 76.2 mm(\varnothing) 6061-T6 solid aluminium round bar.

Fabrication method:

The Fork, Steering motor mount, both Fork braces, and the Strengthening plates are water jet cut. The Fork is then folded to form a u-shape and the Fork bracing is then welded to the inside of the Fork to increase its stiffness. The Steering motor mount is also folded to its final shape.

The Steering axle and Knee joint connector are both machined to size on a lathe. The Steering axle is then pressed into the Knee joint connector and secured by two grub screws spaced 90° apart.




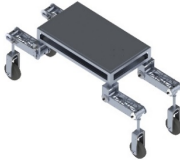

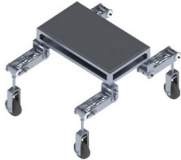



The Steering axle tube with integrated bearing housings is machined from a 6061-T6 solid round bar. The 6301-2RSH bearings are then pressed into the bearing housings at either end of the Steering axle tube.

4.3 Design analysis

4.3.1 Possible configurations

The prototype hybrid wheeled leg is designed to give an agricultural robot the ability to change its track width and ride height. Table 6 shows the possible common configurations. Even though only three different configurations of track width and ride height are shown in the table below, it should be noted that the track width and ride height can be varied to any position in the range of narrow and wide, and low and high respectively.

Table 6. Possible leg configurations on the final agricultural robot.

	Narrow	In-between	Wide
Low			
Neutral			
High			

4.3.2 Possible Loading

The leg will experience a load due to the weight of the robot and from potential collisions with objects. The worst-case collisions are expected to be head-on and can happen when the robot is in any configuration. To get an understanding of the stresses and deformation on the leg caused by the robot weight and object collision forces, a

static finite element analysis (FEA) simulation was conducted in SolidWorks 2018 using a simplified model of the leg, on each configuration. Four different loading scenarios were simulated: 1) Pure weight loading (Fig. 33), 2) weight and head-on collision loading in a narrow configuration (Fig. 34), 3) weight and head-on collision loading in an in-between configuration (Fig. 35), and 4) weight and head-on collision loading in a wide configuration (Fig. 36). In each of the four scenarios, the leg was configured to be tall (a), neutral (b) or short (c). The deformations that occurred under the specific loadings and in the specific configurations are shown in the figures below.

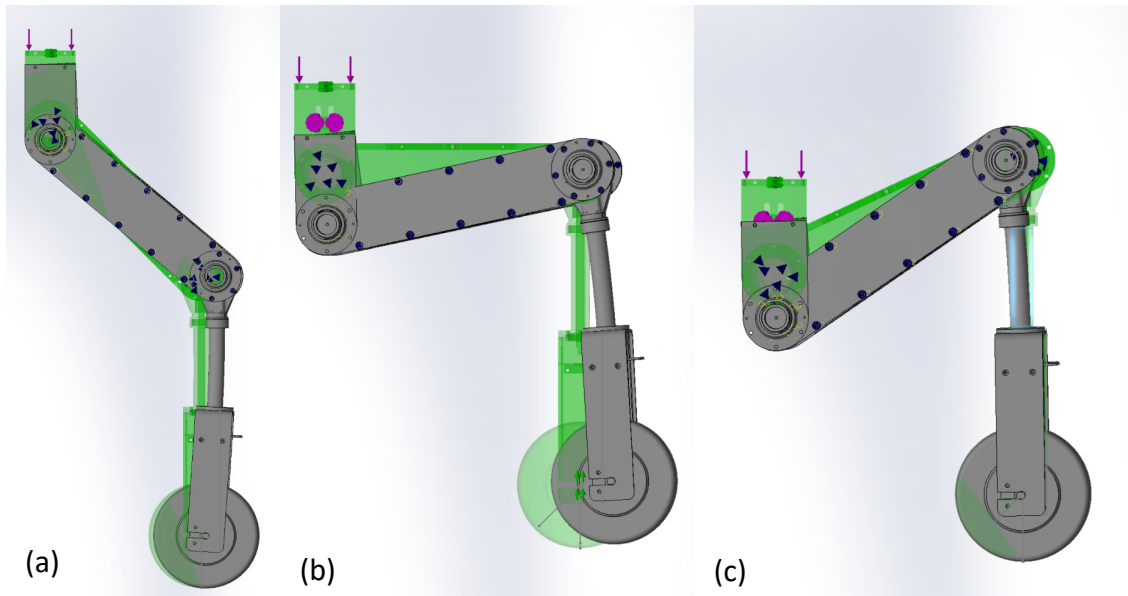


Fig. 33. Exaggerated leg deformation from a pure weight loading with a) tall height configuration, b) neutral height configuration and c) short height configuration.

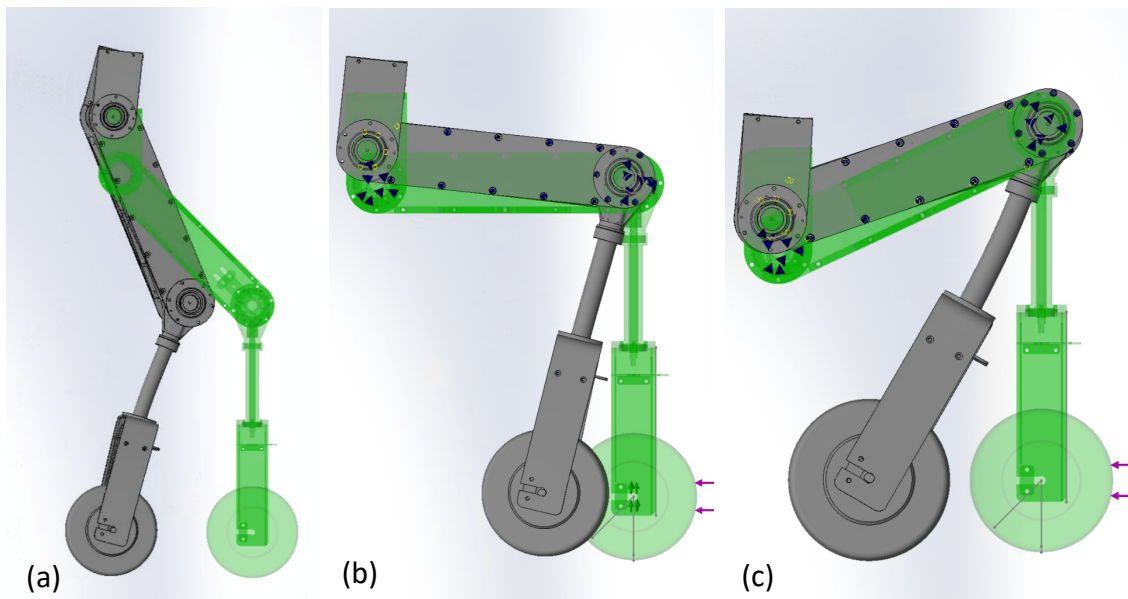


Fig. 34. Exaggerated leg deformation from weight and head-on collision loading in a narrow stance with a) tall height configuration, b) neutral height configuration and c) short height configuration.

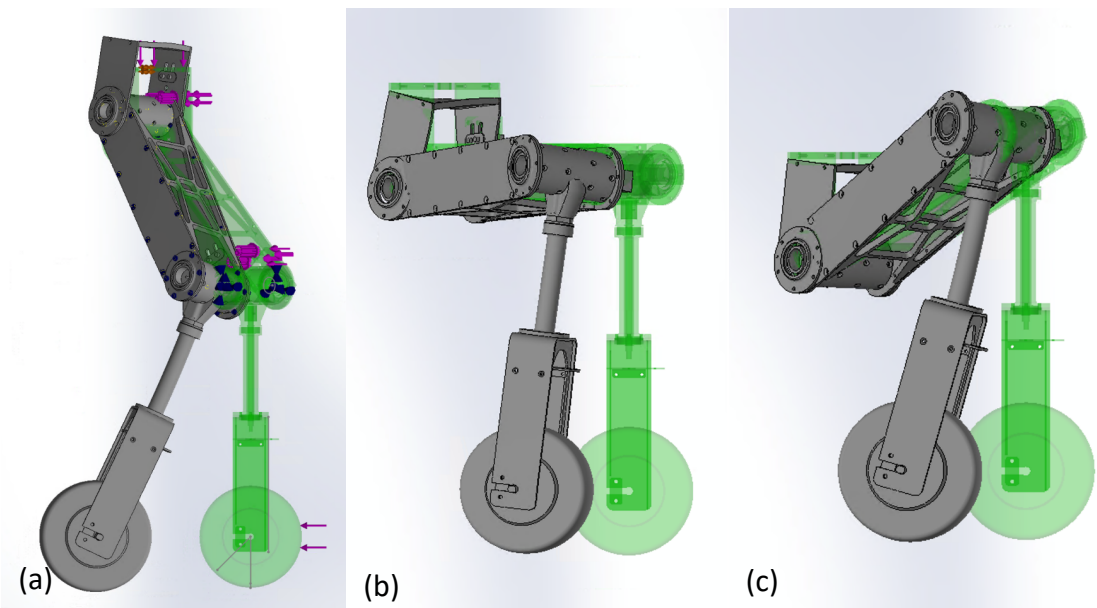


Fig. 35. Exaggerated leg deformation from weight and head-on collision loading in an in-between stance with a) tall height configuration, b) neutral height configuration and c) short height configuration.

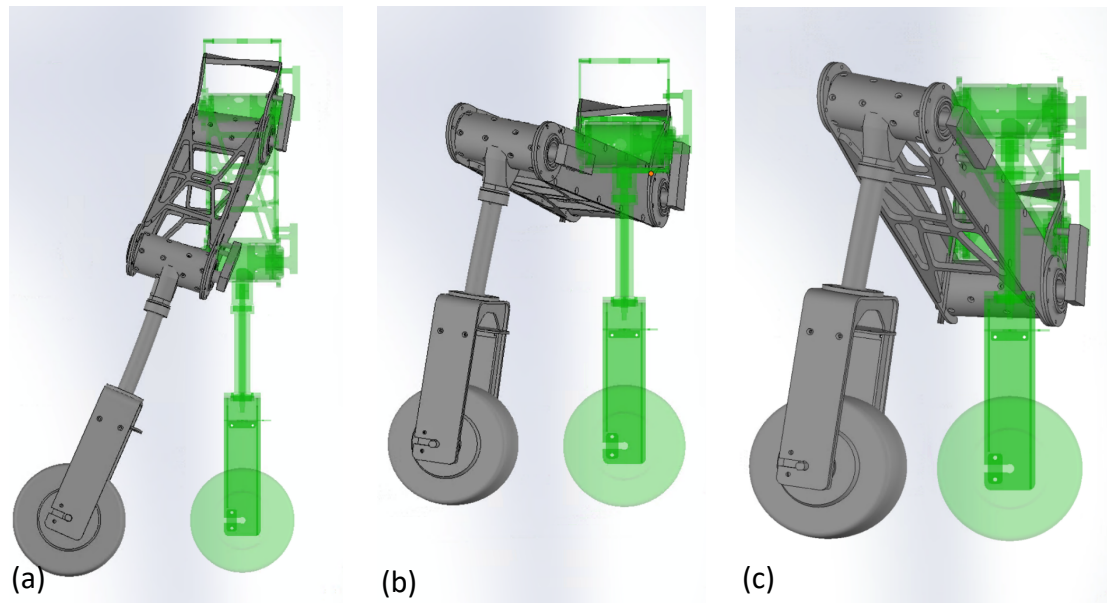


Fig. 36. Exaggerated leg deformation from weight and head-on collision loading in a wide stance with a) tall height configuration, b) neutral height configuration and c) short height configuration.

4.3.3 Finite Element Analysis

During the design phase, finite element analysis (FEA) in SolidWorks 2018 was used to ensure the leg can tolerate the expected forces acting on it. The leg model was simplified (Fig. 37) to only focus on the structural components of the leg by removing motors and defining bearing connectors instead of using a model of the actual bearings. This allowed bolt connectors and surface contacts to be precisely defined for each link while keeping the simulation times short for an iterative design process. The bolted surfaces were defined with no penetration contacts and appropriate friction values. The bolt connector preload torques were set to values from the NASA installation torque tables for non-critical Applications [123].

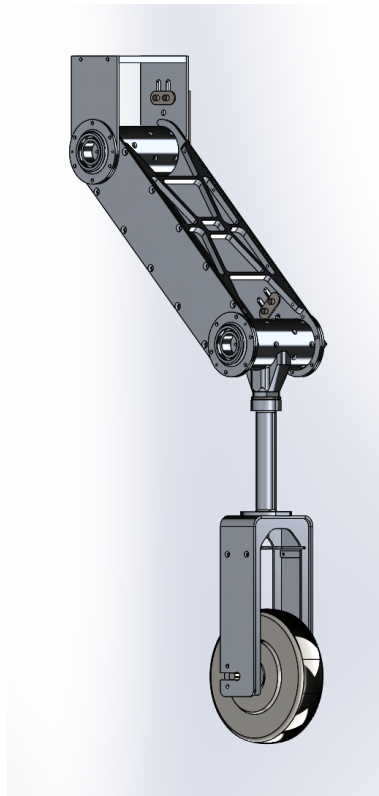


Fig. 37. Simplified leg model used in the leg analysis simulations. (Same model used in section 4.3.2 above).

4.3.3.1 Weight loading

In the specifications chapter (Chapter 3), the maximum weight that the robot will have to carry was identified to be 98.8 kg, and since the robot has four legs, each leg would be expected to carry 24.7 kg (242 N). To account for some uncertainty and ensure that the leg can withstand a weight loading above this anticipated load, while not increasing the weight of the leg extensively, a safety factor of 1.5 was used. Therefore, a weight of 37.05 kg (363 N) was applied to the leg during the simulations.

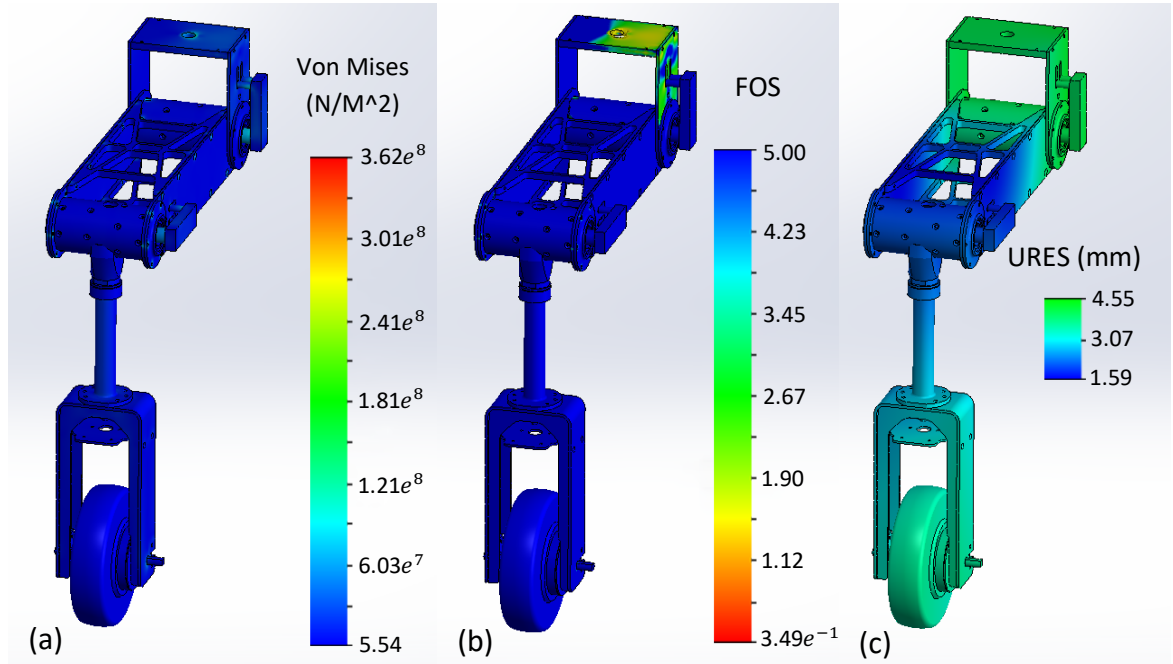


Fig. 38. Weight loading simulation results of the leg in a neutral height configuration: a) stress results, b) factor of safety results, and c) displacement results.

Fig. 38 shows the simulation results of the leg in the neutral configuration, the configuration in which it experienced the highest stress from just the weight force. Since the safety factor was already applied to the simulation load, a FOS greater than one is desired.

The results show that the Tibia link, Femur link and Custom actuator can confidently support the weight of the robot, with safety factors above 5. The chassis mounting hole on the Base link Base plate is the only location that does not meet the desired FOS. However, as mentioned in section 4.2.1, the Base link is not the final version with the final mounting mechanism. Therefore, the failed result on the Base plate is ignored, but it should be considered when designing the final Base link. For the simulation in the sections below the Base link material was changed to Titanium Ti-8Al-1Mo-1V, to increase its rigidity and perform closer to how the final Base link should.

4.3.3.2 Impact loading

The impact the leg may have to endure will be from a collision with an object. It is difficult to model precisely what happens to the leg during a collision, but it can be done with a dynamic study. Running a dynamic study in SolidWorks 2018, such as a drop test takes around two days on the computers available at Massey University, this makes it impractical to use as part of an iterative design process for the prototype design. An alternative way to simulate a collision is to use a static study and calculate the collisions equivalent static force F_e [124, 125]. For a horizontal collision, the equivalent static force is calculated as follows,

$$\begin{aligned}
U &= \frac{1}{2}mv^2 \\
k &= \frac{F_{st}}{\delta_{st}} \\
F_e &= \sqrt{2Uk}
\end{aligned} \tag{2}$$

where U is the kinetic energy of the leg at the time of the collision, m is the mass of the robot, v is the velocity of the robot at the time of the collision, k is the stiffness of the leg, F_{st} is the applied static force, δ_{st} is the deflection of the leg due to this applied force.

To calculate the stiffness k of the leg, a static simulation was run in SolidWorks to determine the static deflection δ_{st} of the leg in all configurations when a known force (200 N) is applied in the direction of the collision. The calculated stiffnesses are shown in Table 7.

Table 7. Leg collision stiffness (N/m) in various stances without added compliance.

	Leg trackwidth		
Ride Height	Narrow	In-between	Wide
Low	71942.45 N/m	35273.40 N/m	355096.42 N/m
Neutral	162601.63 N/m	60422.97 N/m	43956.04 N/m
High	224719.10 N/m	155038.76 N/m	19801.98 N/m

The results showed that all configurations have a large stiffness. If the robot was to have a collision at the average human walking speed of 5 km/h while in one of these configurations, the equivalent static force would range from 1859 – 6261 N. This is 5.1-17.2 times larger than the 363 N maximum expected weight loading. To lower these high collision forces, adjustable compliance was added to the custom actuators. This allows the stiffness of the leg to be set to a predictable, desired value. However, the actuator compliance does not add compliance to the leg in wide configurations and only adds some compliance in the in-between configurations. To add compliance in wide and in-between configurations, compliance needs to be added to the joint between the Base link and chassis when the final Base link and chassis are developed.

By looking at the FOS data from the deflection calculation simulations in Fig. 38 above, the force at which critical components started to yield can be roughly calculated and are shown in Table 8. These force values are used to determine a maximum allowable leg stiffness in each leg configuration to withstand a collision at 5 km/h and are shown in Table 9. The compliance of the custom actuator will be designed around these calculated stiffness values.

Table 8. Estimated maximum allowable leg collision force.

	Leg trackwidth		
Ride Height	Narrow	In-between	Wide
Low	~2000 N	~1900 N	~1900 N
Neutral	~3400 N	~3000 N	~1900 N
High	~4000 N	~3000 N	~1300 N

Table 9. Approximate maximum allowable leg stiffness to withstand a 5 km/h head-on collision.

	Leg trackwidth		
Ride Height	Narrow	In-between	Wide
Low	20987 N/m	18942 N/m	18942 N/m
Neutral	60655 N/m	47223 N/m	18942 N/m
High	83951 N/m	47223 N/m	8867 N/m

Since the stiffness of the leg without compliance (Table 7) exceeds the required stiffness to withstand a head-on collision at 5 km/h (Table 9) it is evident that compliance is needed to lower the leg stiffness and collision forces.

Even with the ability to tolerate a collision, the best way for the robot to protect itself is to avoid collisions altogether. Since the final robot is expected to drive autonomously, collision avoidance is expected to be part of that algorithm. However, the robot may identify a collision scenario too late to avoid it, but it is expected to have attempted to stop; lowering the collision speed. Therefore, if a collision were to happen, it is likely to happen at a low speed.

Impact/shock loading in the vertical direction from driving over rough terrain will also be lowered due to the compliance in the actuators. Therefore, with the weight loading safety factor above 5, vertical impact/shock loading is not expected to cause leg failure.

4.4 Components

4.4.1 Joint actuator

The search for an off-the-shelf joint actuator that met the performance and, most importantly, budget requirements, returned no results. Some met the performance requirements, and some met the budget requirements, but not both. The only way that both the performance and budget requirements could be met was through the development of a custom actuator. Detailed information on the design of the custom actuator can be found in Chapter 5.

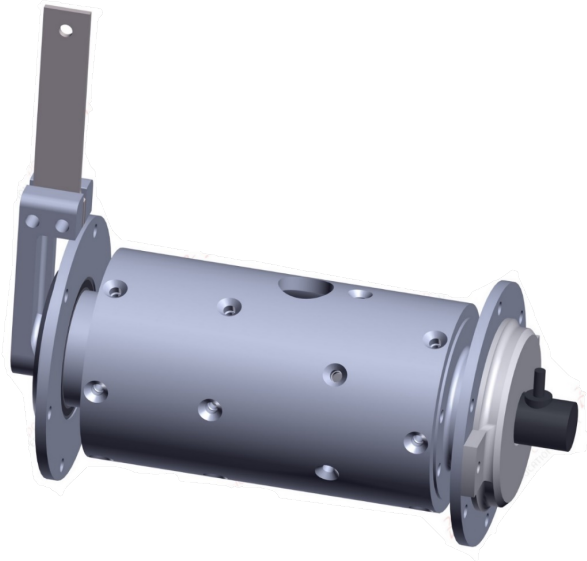


Fig. 39. Custom prototype joint actuator.

4.4.2 Motorised wheel

A 24 V, 350 W hub motor and tire was used as the wheel and motor for the leg [126], see Fig. 40. It was chosen because of its durable and simple all-in-one design. This design is used on electric scooters where it has proven to be durable. The wheel is capable of 28 km/h and can carry at least 100 kg. The specifications can be found in Table 10.



Fig. 40. Wheel with integrated hub motor used on the hybrid wheeled leg [126].

Table 10. Motorised wheel specifications.

Voltage	24 V
Power	350 W
Rim size	8 inch
Top speed	28 km/h
Diameter	200 mm

4.4.3 Turning servo

Actual steering torque is commonly calculated empirically [127]. However, a safe estimate of the required steering torque can be calculated. First, the worst-case ground tire friction force needs to be identified; for this, the largest friction coefficient μ the tire will encounter needs to be identified. This will be when the tire is in contact with concrete or asphalt, which produces a friction coefficient μ as high as 0.9 [128].

Taking the normal force F to be 363 N, calculated from the maximum weight expected to be on the robot as identified in Chapter 3, dividing it by the four legs, and then adding a 1.5 safety factor to account for errors. From this, it follows that the worst-case ground tire friction force F_{fric} is:

$$F_{fric} = \mu F = 363 * 0.9 = 326.7 \text{ N} \quad (3)$$

From here it is not straight forward to calculate the torque needed to steer the wheel when the robot is fully loaded hence why it is generally done empirically. In order to calculate the torque, we need to know the radius r from the steering axis at which the ground tire friction force restricts rotation. This will be within the area that the tire contacts the ground, known as the contact patch. The contact patch is difficult to calculate as it depends on characteristics of the tire which are not known for the chosen tire. Therefore, the contact patch for the chosen wheel is intentionally overestimated to be around 50x20 mm to ensure the required torque is not underestimated. The radius r at which the tire ground friction force restricts rotation is also difficult to calculate and again depends on characteristics of the tire that are not known for the chosen tire. However, the radius will not be outside the contact patch; therefore the worst-case radius can be taken as 25 mm (half the 50 mm of the longest side of the contact patch). However, this was multiplied by a 1.5 safety factor to 37.5 mm to account for errors and ensure that the chosen servo has more than enough torque. The torque required to steer the wheel t_{st} is:

$$t_{st} = r F_{fric} = 326.7 * 0.0375 = 12.3 \text{ Nm} \quad (4)$$

This led to the selection of the low cost ASMC-04B 12-24 V servo with 17.7 Nm of torque as Steering servo [129]. Its specifications are shown in Table 11.

Table 11. Steering servo specifications.

Voltage	11-24 V
No-load Current	<400 mA
Max current	3 A
Stall Torque	17.7 Nm
Weight	550 g



Fig. 41. ASMC-04B 12-24V servo used for steering [129].

4.4.4 Bearings

There were two types of bearings used in the leg. Two KML 6808 2RS bearings used in the joint actuator and two SKF 6301-2RS bearings are used in the wheel turning mechanism. This section focusses on the two 6301-2RS bearings for the wheel turning mechanism. Information on the two KML 6808 bearings can be found in chapter 5.

The 6301-2RS bearings will have to endure both axial and radial loading. A deep groove ball bearing is primarily designed to handle radial loading. However, it is rated to carry an axial load half that of its rated radial load. The 6301-2RS bearing's static radial load rating is 4.15 kN, and therefore its static axial load rating is 2.08 kN.

The two 6301-2RS bearings will primarily be under an axial load due to the weight of the robot but will experience radial loading when there is a collision, or the Tibia link is actuated past vertical. Due to the robot's weight, the maximum expected axial load on one leg (including a 1.5 safety factor), would be 363N. This means that even a single

6301-2RS bearing can support the axial load with an overall safety factor of 5.7. This ensures that the bearings will be able to withstand any shock loading caused by driving on rough terrain.

The calculation for the radial load on each bearing from the non-axial component of any force acting on the wheel is:

$$\begin{aligned} F_{ra} &= \frac{L}{L_{AB}} F = \frac{402}{170} F \\ F_{rb} &= \frac{L_A}{L_{AB}} F = \frac{232}{170} F \end{aligned} \quad (5)$$

where F is the non-axial component force, L is the distance from the wheels axis of rotation to bearing B, L_A is the distance from the wheels axis of rotation to bearing A, and L_{AB} is the length from bearing A to bearing B.

In section 4.3.3.2 Table 8 it was found that the maximum force that the leg can tolerate in a collision is 4000 N. Using equation (5) this collision force results in a 9459 N load on bearing A and a 5459 N load on bearing B. Both bearing loads are larger than what the 6301-2RS bearing can withstand. Taking the most loaded bearing (bearing A) and rearranging equation (5) for F , the 4150 N rating of 6301-2RS bearing means the bearings in their current configuration can only withstand a 1755 N collision force. By rearranging equation (2) for k , the 1755 N collision force limit means the leg stiffness cannot exceed 16161 N/m if the bearings are to withstand a head on collision at 5 km/h.

For any load on the wheel that has both an axial and a radial component, the equivalent bearing load needs to be calculated [130]. The equivalent radial load is calculated differently for dynamic and static loading conditions. The bearings in the wheel turning mechanism are considered statically loaded. Therefore, according to SKF, the following equation can be used to calculate the equivalent static bearing load [131]:

$$\begin{aligned} \text{For } P_0 < Fr, \quad P_0 &= Fr \\ \text{For } P_0 > Fr, \quad P_0 &= 0.6 Fr + 0.5 Fa \end{aligned} \quad (6)$$

where P_0 is the equivalent static bearing load, Fr is the radial force, and Fa is the axial force.

4.5 Findings and recommendations

The finite element analysis (FEA) studies in the above sections highlighted two areas of potential weakness in the leg: the Base link and the Femur link brace. To increase the strength of these parts, one can change the material, change the design to better deal with the loads acting on it, or both.

4.5.1 Base link

The weight loading FEA study in section 4.3.3.1 shows that the Base link cannot satisfactorily cope with the maximum expected loading on the leg. The Base link used in the study is not intended to be the same link used on the final robot; it is only meant for bench testing the leg. The final Base link will not be designed until the overall robot is realised. Therefore, to increase the bench testing Base links strength for the FEA studies without wasting time on changing its design, its material was changed to Titanium Ti-8Al-1Mo-1V. For all further studies, including the impact loading studies, the Titanium Base link did not fail. However, this will not be a viable solution for the final Base link since Titanium is very expensive and hard to work with; instead, a new design is the better option.

4.5.2 Femur link brace

After the Base link failure, the next weakest component was the Femur link brace. It showed weakness in the wide configuration during the impact loading simulations in section 4.3.3.2. This is because an impact in the wide configuration causes a twisting torque along the Femur link, which causes high stresses in the centre of the Femur link brace, as shown in Fig. 42 (a). If a solid 10 mm thick plate is used as the Femur link brace, these high stresses do not occur, and the Femur link brace does not yield, as shown in Fig. 42 (b). However, the solid Femur link brace weighs 1.22 kg; four times more than the current Femur link brace used in the prototype hybrid wheeled leg. The leg with the current Femur link braces but excluding components (actuators, wheel, encoders and bearings) weighs 5.26 kg. Therefore, swapping both Femur link braces out with solid ones (1.22 kg) would increase the weight of the leg by 35 %. Clearly, a lot of weight can be saved in the Femur link braces alone.

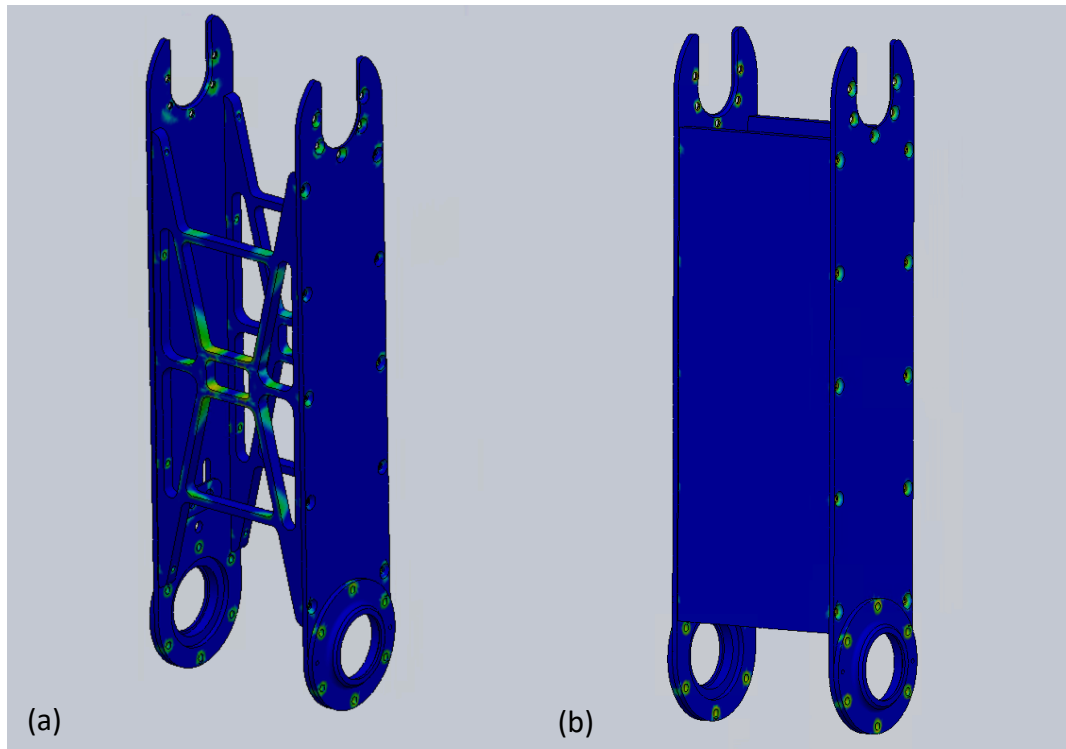


Fig. 42. a) current Femur link brace showing points of high stress in the centre during a wide stance, head-on collision simulation. b) Solid Femur link brace showing no points of high stress during a wide stance, head-on collision simulation.

The effectiveness of changing the material to increase the part strength is mentioned in section 4.5.1. However, due to cost, availability, and machining issues that more exotic materials such as titanium bring, they are not always the answer. A lot of the time, a part can use the same material but be redesigned better to achieve similar weight reduction as the original design. The leg was initially designed in SolidWorks 2017. However, it was later transitioned to SolidWorks 2018. A new feature introduced with SolidWorks 2018 simulation was topology optimisation.

To investigate how topology optimisation could be used to reduce the weight of the leg with little to no strength reduction, a SolidWorks topology optimisation was run to determine an optimal shape for the Femur link brace that weighs within 50 g of the original Femur link brace. The resulting Femur link brace shape can be seen in Fig. 43 (a). The resulting part is organic looking and is not suitable for traditional manufacturing techniques such as milling or water jet cutting. To make a manufacturable part, the optimised Femur link brace was used as a guide to indicate where material could be removed for designing a new Femur link brace. The resulting practical optimised Femur link brace can be seen in Fig. 43 (b).

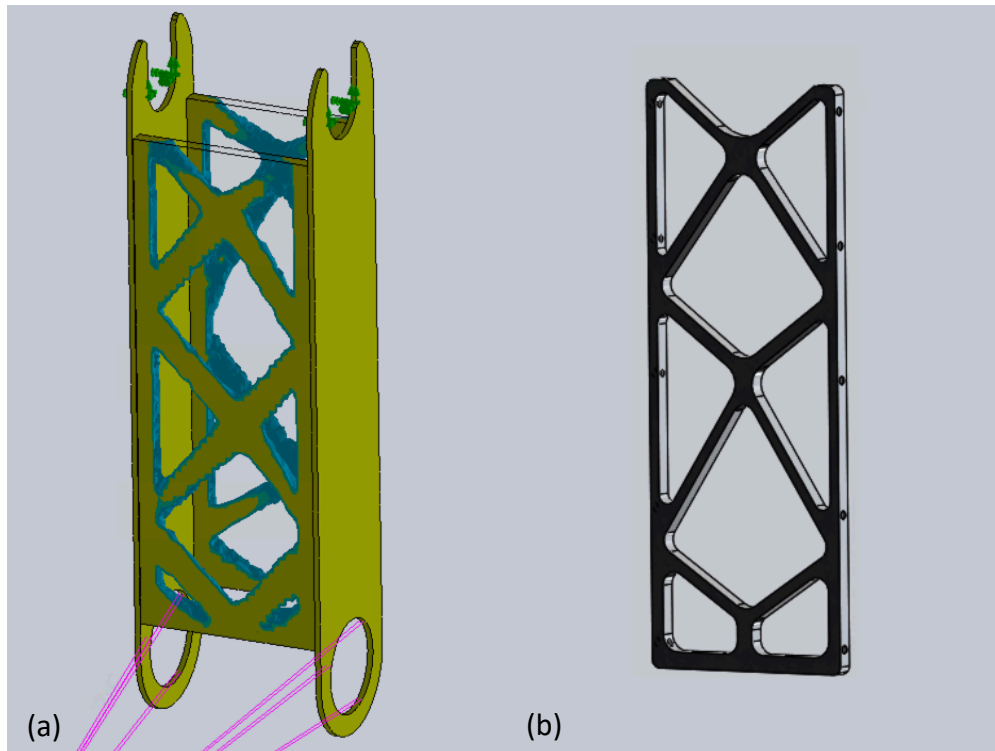


Fig. 43. a) Topology optimisation result. b) Femur link brace design based on the topology optimisation result.

When using the topology optimised Femur link brace to re-run the wide stance impact simulations from section 4.3.3.2 that highlighted the weakness in the original Femur link brace, there are no more stress concentrations in the centre of the topology optimised Femur link brace, see Fig. 44. This increased the safety factor of the Femur link brace for a 200 N wide stance impact from ~ 6.5 to ~ 18 , while only weighing 20 g more than the original Femur link brace.

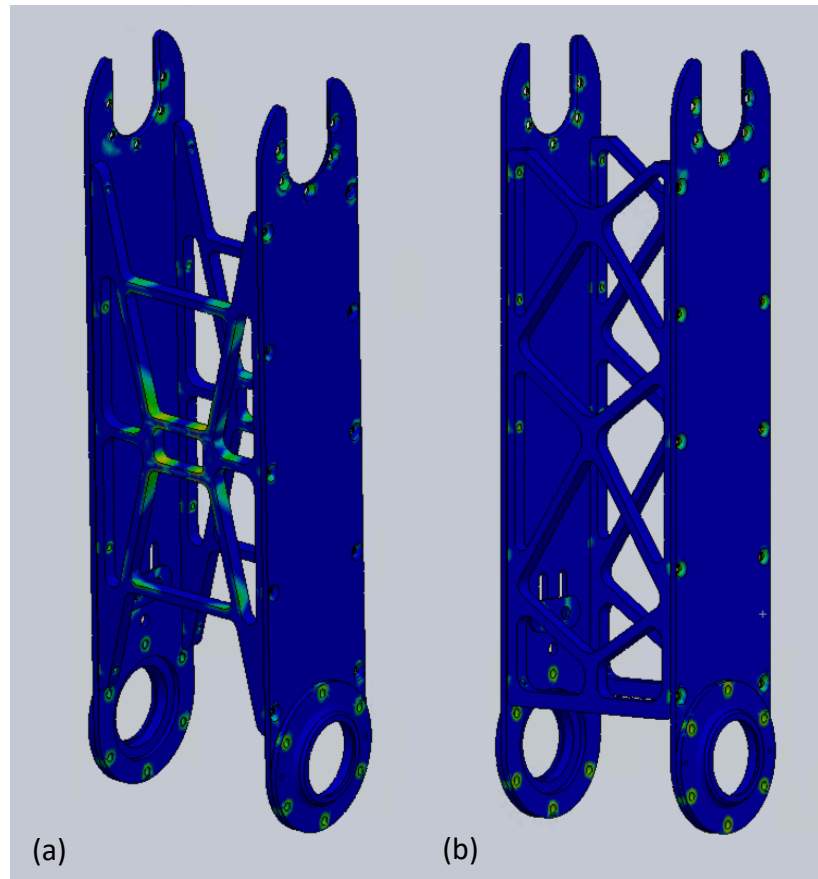


Fig. 44. Femur link before (a) and after (b) topology optimisation. Green and yellow areas indicate stress concentrations.

5 Actuator Design and Control

A custom modular prototype leg actuator was developed for the prototype hybrid wheeled leg described in chapter 3. In chapter 4, requirements for an actuator were established, which are:

- Electromechanical actuation.
- Low power consumption when not being used.
- Able to withstand shocks from walking or driving over rough terrain.
- Low cost (must fit within the 3,000 NZD budget).
- Can be mounted directly on the axis of rotation.

Additionally, in section 3.3.8, the expected weight of the final fully loaded robot was identified. The actuator will need to output enough torque to operate the joints when the leg is supporting the maximum anticipated weight.

Actuators are available that meet many of the requirements listed above. However, finding a specific actuator that met all these requirements was impossible. Since the joint actuator heavily influences the leg's abilities, the only option was to develop a custom actuator for the leg that met the hardware and cost requirements.

It was decided to design and build a custom compliant actuator because it was impossible to find a prebuilt compliant actuator that cost less than our budget of 3,000 NZD. However, this decision meant a substantial amount of time was dedicated to its design, build, and control system development, and not towards the design of the overall leg. On the other hand, it did mean that the leg and actuator could be designed to work optimally with each other and incorporate the exact features that are required for a hybrid wheeled-leg.

5.1 Requirements

5.1.1 Cost

The cost is the biggest reason a prototype custom actuator was designed and built instead of purchasing one off-the-shelf. The overall budget to design, build and test the prototype leg is 3,000 NZD. To put that into context, an actuator found that meets nearly all the performance requirements, except for output torque, was called ANYdrive (see Fig. 45) and is currently used on the quadruped robot ANYmal [67] and costs 12,855 NZD.

The 3,000 NZD budget is not just for the building of one leg; it also has to cover any design changes and replacement parts that fail during testing and prototyping. Therefore, the prototype actuator is designed to use the cheapest components where possible, but still allow the actuator to have enough performance to test the intended functions of the actuator and leg.

ANYdrive an integrated series elastic actuator

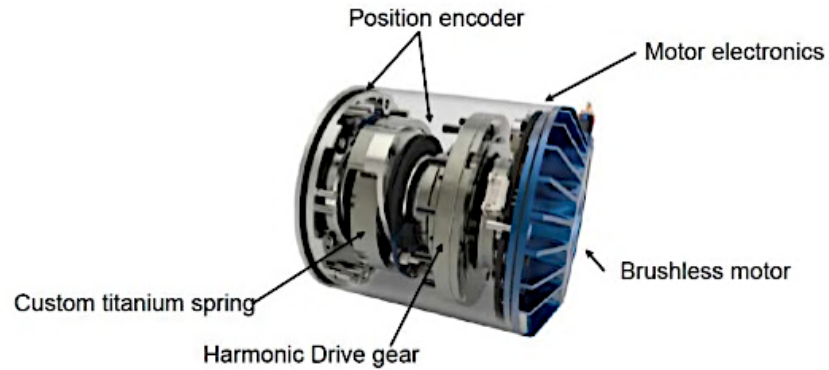


Fig. 45. The ANYdrive actuator [84, 132].

5.1.2 Torque

The joint that will experience the most torque is the Hip joint. Therefore, the calculation can focus on this joint and the rest of the leg can be treated as rigid, simplifying the calculation. To calculate the torque that the Hip joint experiences, first the wheel ground reaction force N and the distance x from the wheel to Hip joint needs to be calculated. The distance x is calculated as follows:

$$x = r_1 \sin \theta_1 + r_2 \sin \theta_2 \quad (7)$$

where r_1 is the Tibia link length, θ_1 is Tibia link's angle from vertical, r_2 is the length of the Femur link, and θ_2 is the Femur link's angle from vertical. See Fig. 46.

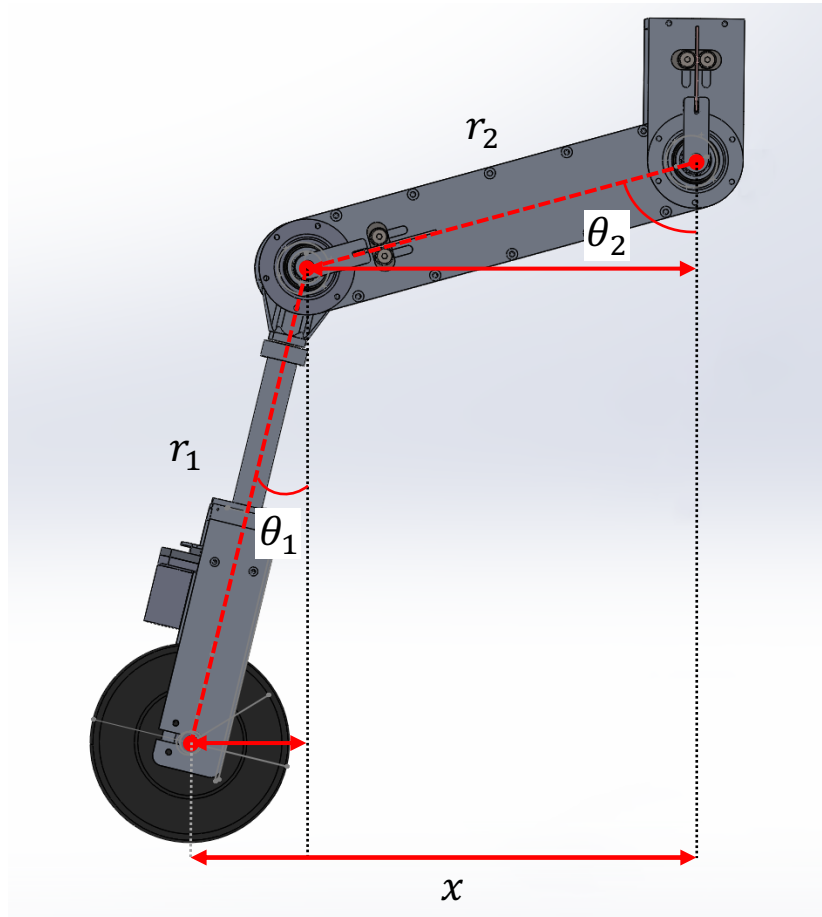


Fig. 46. Calculation of distance x using equation (7).

Torque t on the joint is calculated according to:

$$t = xF \quad (8)$$

The wheel ground reaction force F is equal to the maximum expected load on one leg (363N), including a 1.5 safety factor.

Equation(8) highlights that the larger the distance x , the larger the torque on the Hip joint. Where x will be the longest is when the final agricultural robot is travelling with its legs set to neutral height, as shown in Fig. 47. It is possible for x to be longer if the Tibia link moves outward from vertical. However, this is not expected to happen during wheeled locomotion as the robot would be more difficult to steer, and situations where it may be needed during walking, are predicted to be rare. For situations where the Tibia link goes outward past vertical, the 1.5 safety factor should cover the extra torque that would be induced on the Hip joint.

Using (7) and equation(8), in the neutral height configuration, the maximum torque on the Hip joint is:

$$(r_1 \sin \theta_1 + r_2 \sin \theta_2)F = 363 * 0.404 = 147 \text{ Nm} \quad (9)$$

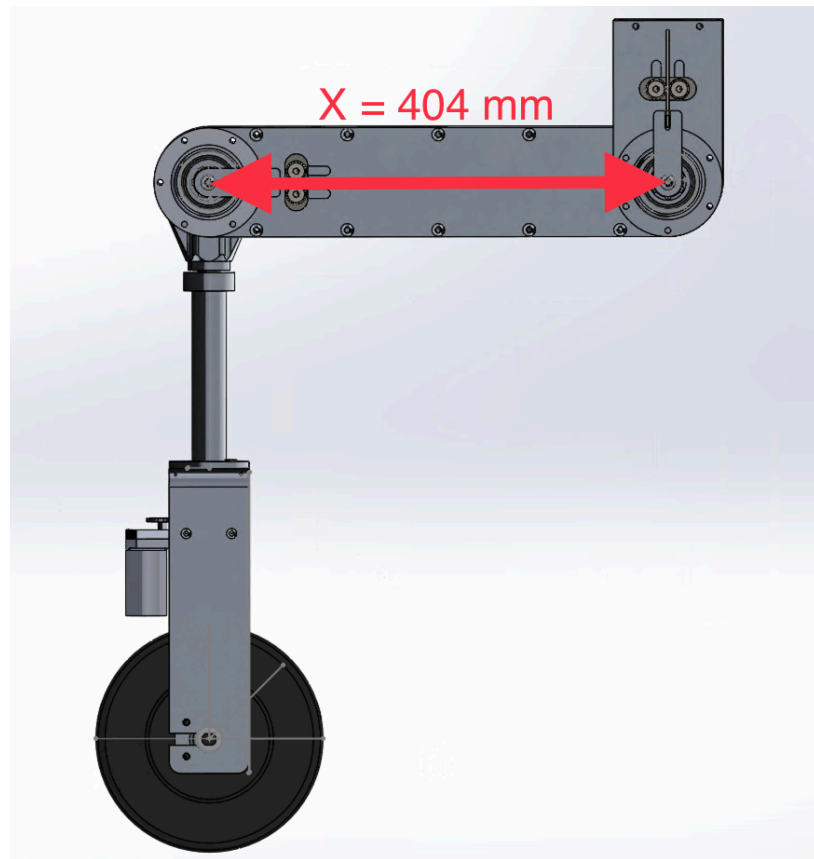


Fig. 47. Leg configuration that has the largest x value.

5.1.3 Compliance

Compliance was added to the actuator so that it could withstand the shocks from walking and driving over rough terrain. Additionally, as shown in section 4.3.3.2, it is not just the actuator that gets protected by the compliance, it also lowers the forces exerted on the leg in a collision or when driving over rough terrain.

5.1.4 Modularity

Due to the low-cost requirements, the most powerful and subsequently most expensive motors were not used. Instead, the actuator is designed in such a manner that it is modular and that the structure of the actuator does not change when motors from different manufacturers are used

5.1.5 Low power consumption

Hybrid wheeled leg locomotion was chosen because the robot will not always be on unstructured terrain in which case it can use efficient wheeled locomotion. However, to maintain a constant joint angle, the leg actuators use energy and create heat to oppose the torque created by the weight of the robot trying to move the joint away from its angle set point. To prevent the joints from expending energy while remaining stationary, the actuators need to be mechanically non-back driveable.

5.2 Mechanical design

This section describes the mechanical design of the prototype custom adjustable compliant actuator. An overview of its design is shown in Fig. 48. The componentry used in the actuator is described in section 5.4.

The custom prototype actuator was designed to be:

- Cheap
- Light
- Strong
- Easy to adapt to a different drill motor and gearbox (modular).

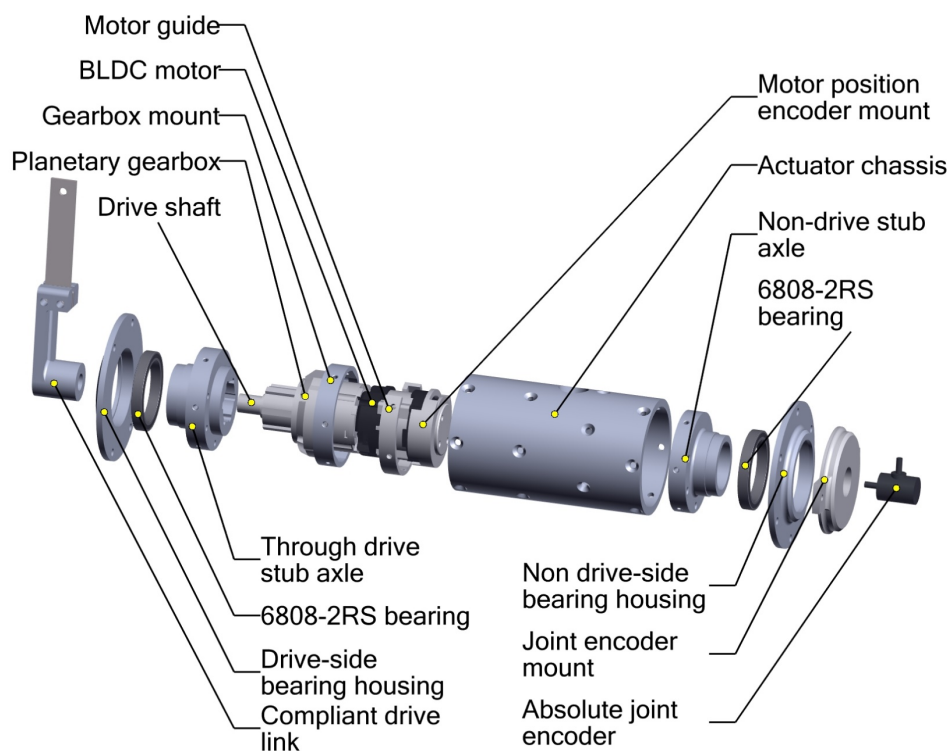


Fig. 48. Overview of the prototype custom complaint actuator.

5.2.1 Compliant drive link

The Compliant drive link (Fig. 49) is what gives the actuator its compliance. The Motor-drive-to-spring adapter screws onto the motor shaft on one end and then clamps onto the Leaf spring at the other end. The leaf spring is where the compliance of the drive link comes from. The Adjustable spring pivot point can slide up and down the Leaf spring to change the properties of the Leaf spring by changing its effective length.

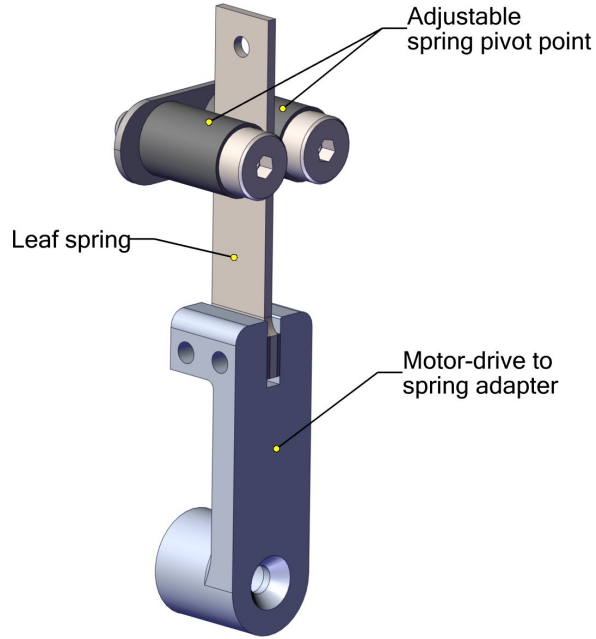


Fig. 49. Parts of the Compliant drive link.

The torsional stiffness of a Leaf spring as a function of its length can be modelled using the following equation:

$$S = (r + l)^2 \frac{Ewt^3}{4l^3} \quad (10)$$

where r is the length from the motor axis to the Leaf spring, l is the effective length of the leaf spring, E is the Youngs modulus of the Leaf spring, w is the width of the Leaf spring, and t is the thickness of the Leaf spring.

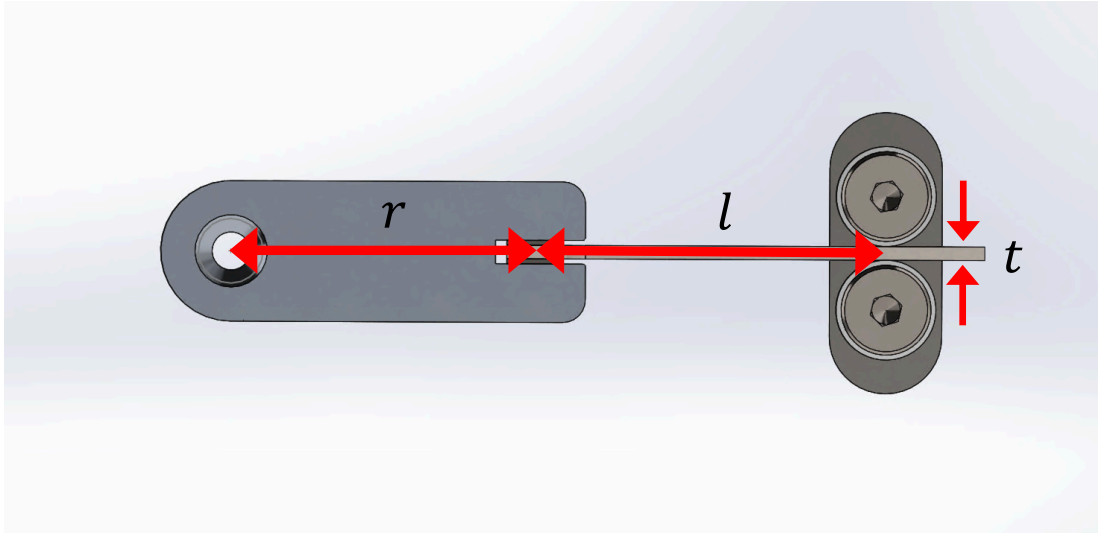


Fig. 50. Parameters of the Compliant drive link used in equation (10).

Dimensions:

Motor-drive-to-spring adapter: 75.5 mm(L) x 25 mm(W) x 25 mm(H).

Leaf spring: 85 mm(L) x 17 mm(W) x 2.4 mm(H).

Adjustable spring pivot point rollers: 24.9 mm(L) x 17.75 mm(\emptyset).

Materials:

The Motor-drive-to-spring adapter is made from 6061-T6 aluminium, the Leaf spring is made from spring steel, and the Adjustable spring pivot point rollers are made from nylon.

Fabrication method:

The Motor-drive to spring adapter is machined with a CNC milling machine, the Leaf spring is cut to the desired shape on a laser cutter, and the Adjustable spring pivot point rollers are machined on a lathe.

5.2.2 Actuator chassis

The Actuator chassis is the primary structural member of the custom compliant actuator. There are two versions of the Actuator chassis, one for the Hip joint and one for the Knee joint (Fig. 51). They both share the same basic design with four sets of six 4.5 mm countersunk holes spaced around the circumference, where the two stub axles, the Gearbox mount, and motor guide attach. The only difference is that the Knee joint version has a welded-on adapter into which the Tibia link is secured, which is absent with the shoulder joint.

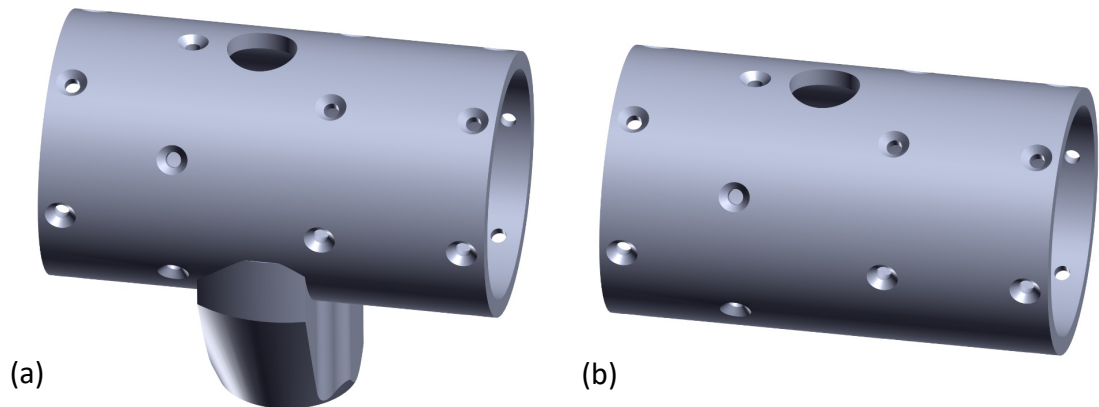


Fig. 51. a) Knee joint Actuator chassis. b) Hip joint Actuator chassis.

Dimensions:

Knee joint: 126 mm(L) x 108 mm(\varnothing).

Shoulder joint: 129 mm(L) x 76 mm(\varnothing).

Materials:

Both chassis versions are made from 6061-T6 aluminium.

Fabrication method:

The cylinders of both shoulder joints were initially machined on a lathe to the correct inner diameter (ID) and outer diameter (OD). Then the holes around the circumference were drilled and countersunk on a milling machine using an indexing head and then finally the Knee joint to Tibia link adapter was welded onto the Knee joint chassis cylinder.

5.2.3 Actuator stub axles

There are two matching pairs of stub axles, one pair for the shoulder joint actuator and one pair for the Knee joint actuator (Fig. 52). Each stub axle in both pairs mount to the Actuator chassis and provide a surface onto which the bearings that allow joint rotation can be pressed. The Non-drive side stub axle of both actuators has a nipple from which the Joint encoder gets its drive. The Through drive side stub axle of both actuators has a central hole to allow the actuator motor's drive to pass through. The difference between the two pairs is that the shoulder joint actuator has extra mounting holes so that the Femur link can attach to it. The Knee joint does not have these mounting holes as the attachment of the Tibia link is done through the Actuator chassis.

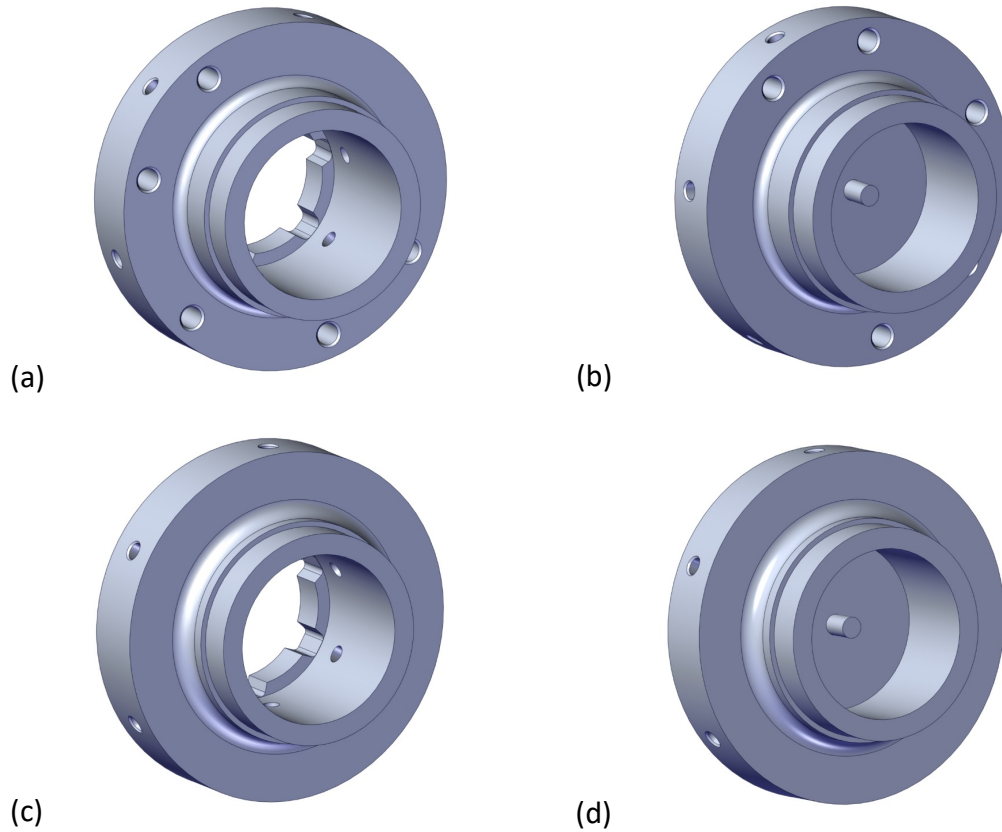


Fig. 52. a) Shoulder joint actuator through drive-side stub axle. b) Shoulder joint actuator non-drive-side stub axle. c) Knee joint actuator through drive-side stub axle. d) Knee joint actuator non-drive-side stub axle.

Dimensions:

Both through drive side stub axles: 32.5 mm(L) x 66 mm(\varnothing)

Both non-drive side stub axles: 24 mm(L) x 66 mm(\varnothing)

Materials:

All stub axle variants are made from 6061-T6 aluminium.

Fabrication method:

Both Non-drive side stub axles were first machined to the correct OD and ID on a lathe. The Femur link mounting holes on the shoulder joint Non-drive side stub axle were drilled and tapped on a milling machine using a dividing head. The Actuator chassis mounting holes on both Non-drive side stub axles were also drilled on a milling machine using a dividing head.

Both through drive side stub axles were first machined on a lathe to the correct OD and ID. The internal splines were then machined on a CNC milling machine. The Femur link mounting holes on the shoulder joint through drive side stub axle were drilled and tapped on a milling machine using a dividing head. The Actuator chassis mounting holes

on both through drive side stub axles were also drilled on a milling machine using a dividing head.

5.2.4 Bearing housings

Each joint actuator has two bearing housings (Fig. 53). The shoulder joint actuator bearing housings bolt to the Base link and the Knee joint actuator bearing housings bolt to the Femur link. The same bearings that are pressed onto the stub axles are then pressed into the bearing housings, creating the joint axis of rotation. On both joint actuators, the Non-drive side bearing housing has two holes to which the Joint encoder mount bolts to.

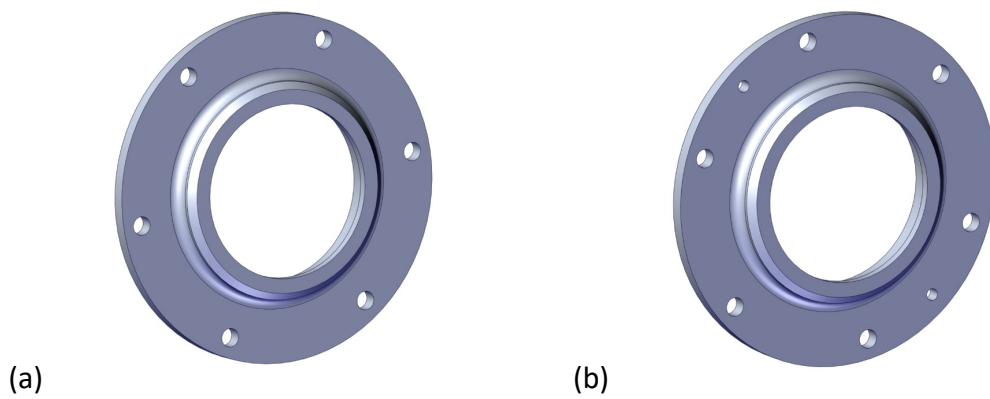


Fig. 53. a) Drive side bearing housing. b) Non-drive side bearing housing.

Dimensions:

Both bearing housings: 10 mm(L) x 96 mm(\varnothing).

Materials:

Both bearing housings are made from 6061-T6 aluminium.

Fabrication method:

Both bearing housings are first turned on a lathe, and then the mounting holes get drilled on a mill using an indexing head.

5.2.5 Gearbox mount and motor guide

Both the Gearbox mount (Fig. 54.a) and Motor guide (Fig. 54.b) bolt to the inside of the Actuator chassis, but have different functions. The Gearbox mount provides a mounting place for the actuator motor's gearbox to mount. The motor guide is needed because the motor is not solidly mounted to the planetary gearbox and therefore it can unclip itself due to high torques under load; therefore the motor guide prevents the motor from rotating.

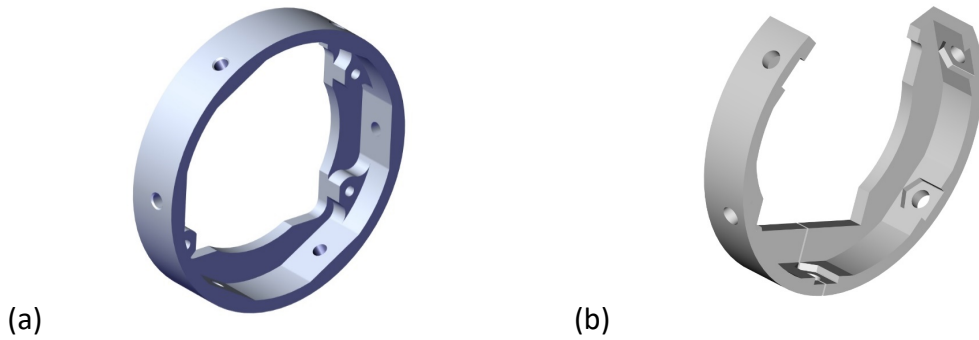


Fig. 54. a) Gearbox mount. b) Motor guide.

Dimensions:

Gearbox mount: 13 mm(L) x 66 mm(\emptyset).

Motor guide: 11 mm(L) x 96 mm(\emptyset).

Materials:

The Gearbox mount is made from 6061-T6 aluminium, and the Motor guide is made from 3D printed ABS plastic.

Fabrication method:

The Gearbox mount is machined on a CNC milling machine, and the Motor guide is printed on a 3D printer.

5.2.6 Encoder mounts

The Motor position encoder mount (Fig. 55.a) attaches to the back of the drive motor and aligns the custom-made encoder with the motor axis of rotation so that the motor angle can be read. The Joint position encoder mount (Fig. 55.b) provides a mounting place for the Joint encoder in line with the joint's axis of rotation.

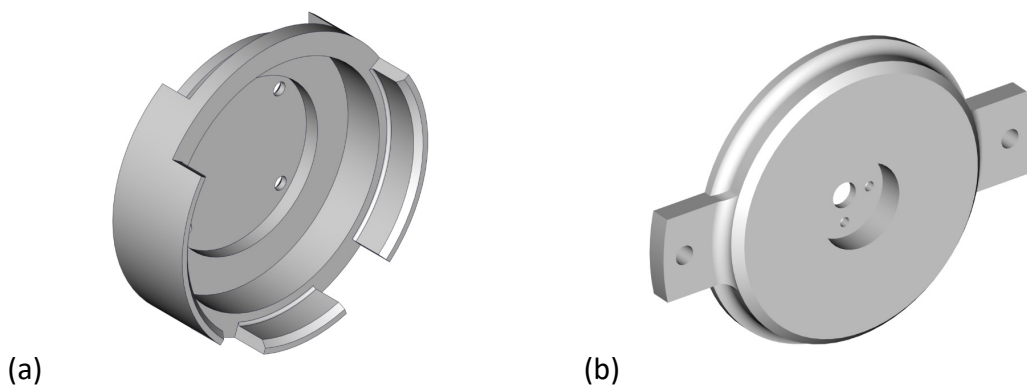


Fig. 55. a) Motor position encoder mount. b) Joint position encoder mount.

Dimensions:

Motor position encoder mount: 18 mm(L) x 50.5 mm(\emptyset).

Joint position encoder mount: 10 mm(L) x 50.5 mm(\emptyset).

Materials:

Both the encoder mounts are made from 3D printed ABS plastic.

Fabrication method:

Both encoder mounts are 3D printed.

5.3 Analysis

5.3.1 Torsional stiffness

The analysis of the Compliant drive link confirmed that by adjusting the spring pivot point, the torsional stiffness of the actuator could be controlled. The Compliant drive link was simulated in SolidWorks using FEA. It was fixed where it screws onto the motor, and then a 50 Nm equivalent force was applied to the Leaf spring at equivalent lengths ($r + l$) ranging from 78 mm to 115 mm (red arrows in Fig. 56). The stiffness was also calculated for the same effective lengths using equation(10), and the results were compared. The torsional stiffness calculated using SolidWorks FEA simulation, and the torsional stiffness calculated using equation (10) can be seen in Fig. 57. The torsional stiffness calculated using a SolidWorks FEA simulation and equation (10) is slightly different, which is to be expected as the SolidWorks FEA simulation takes into account the interactions and material differences between the Motor-drive to spring adapter and Leaf spring, whereas equation (10) does not take into account the interactions and material differences. However, the SolidWorks simulation and equation (10) results are so similar that, if the compliance was made to be actively controlled, the actuator controller could use equation (10) to calculate where the pivot point should be (length l) during operation, to achieve the desired compliance.

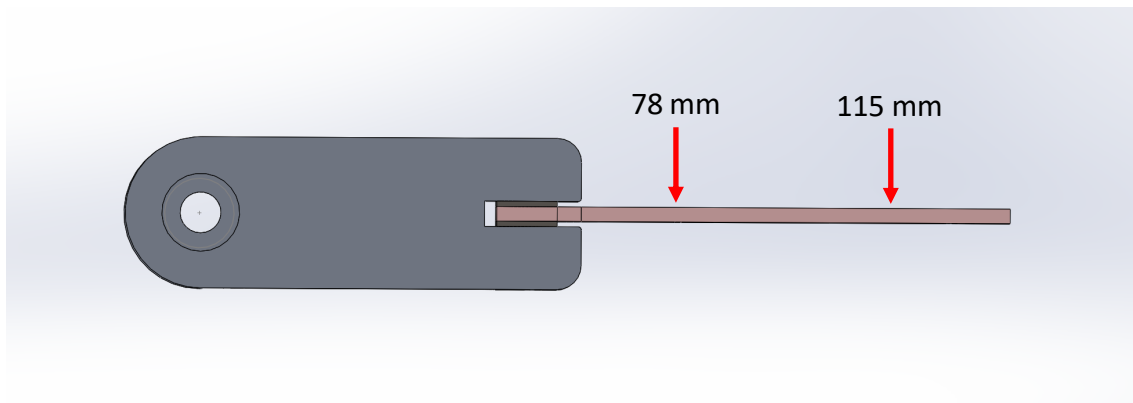


Fig. 56. Compliant drive link simulation displacement result.

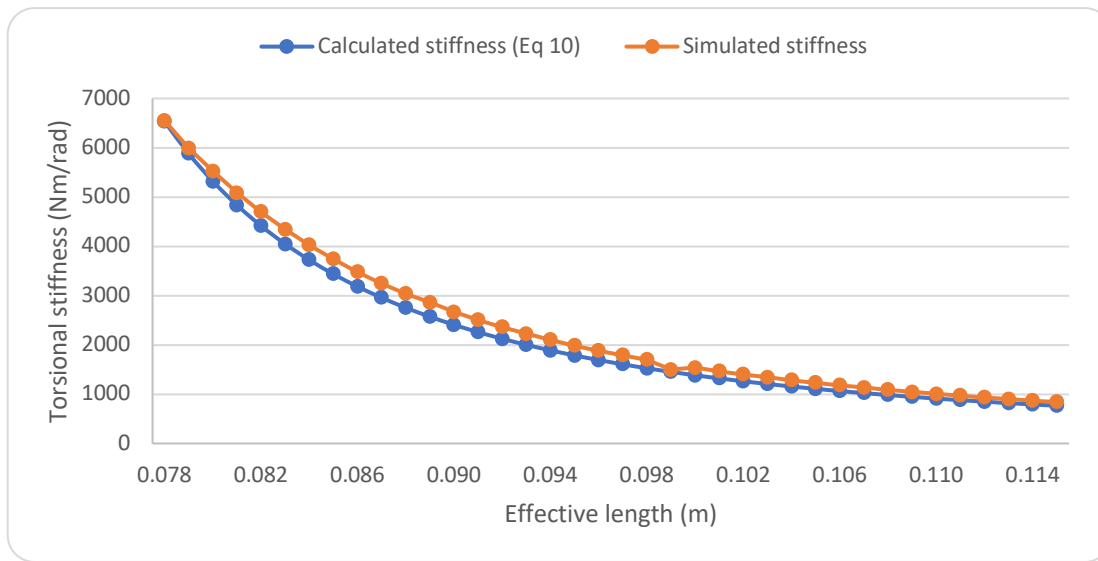


Fig. 57. Torsional stiffness of Compliant drive link calculated using SolidWorks simulation and equation (10).

5.3.2 Strength

The custom Actuator chassis, Stub axles, and Bearing housings were included in the leg analysis simulations done in section 4.3.3. These components did not show early signs of failure. Additionally, the Motor guide, Motor position Encoder mount and Joint position encoder mount were not tested because they are not structural components. The motor guide will have barely any torque on it as it is just ensuring the motor does not unclip itself from the gearbox; the motor torque is transmitted to the joint through the gearbox which is secured to the actuator housing through the Gearbox mount. Both encoder mounts were not tested since they will have no torque on them during leg operation. Two components that will have loading on them during operation are the Compliant drive link and the Gearbox mount, which are discussed below.

5.3.2.1 Compliant drive link

The maximum required torque from the actuator is 147 Nm as calculated in section 5.1.2. A force equivalent to 147 Nm was applied to the Leaf spring at the location of the purple arrows in Fig. 58. The Motor-drive-to-spring adapter can handle this torque with a minimum FOS of 2.5, as shown in Fig. 58. However, the Leaf spring is not able to handle this torque. The Leaf spring is not a permanent component of the Compliant drive link; it is designed to be easily replaced by a Leaf spring with properties (thickness, material, and width) that suit the conditions in which it will be used. To handle the maximum 147 Nm torque, a Leaf spring with different properties will need to be used. However, for testing, the current spring is fine as the motor used for the prototype actuator can only output 50 Nm of torque (more details on the motor can be found in section 5.4.2).

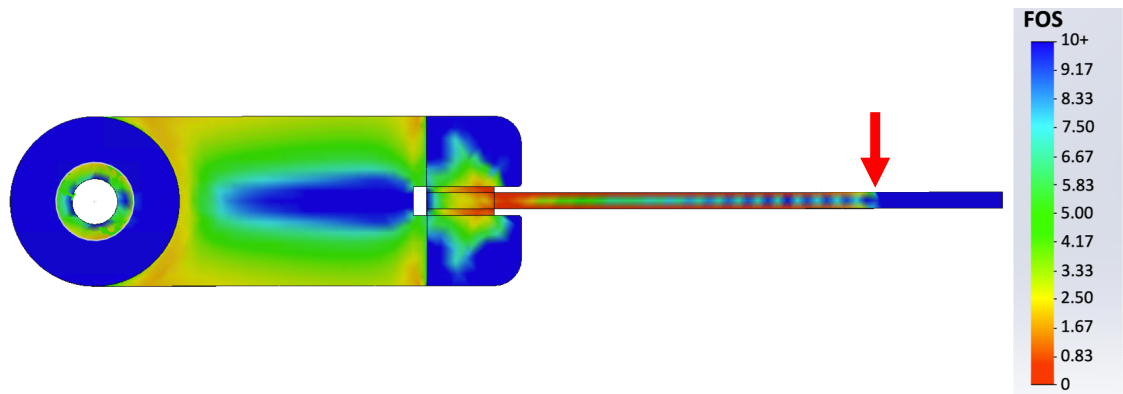


Fig. 58. Compliant drive link FOS results with 147 Nm torque applied.

5.3.2.2 Gearbox mount

To test the strength of the Gearbox mount, the maximum 147 Nm torque calculated in section 4.3.3 was applied to the Gearbox mount in a SolidWorks simulation. The simulation result can be seen in Fig. 59. The Gearbox mount can tolerate this torque but only with a FOS of one. This is acceptable because the motor and gearbox that the gearbox mount is made for only has an output torque of 50 Nm; the motor and gearbox was used during the development of the custom compliant actuator because of its form factor and price, as explained in section 5.4.2. When a high-output torque motor and gearbox is used in the Actuator chassis, the accompanying Gearbox mount will need to be designed to handle the higher torque.

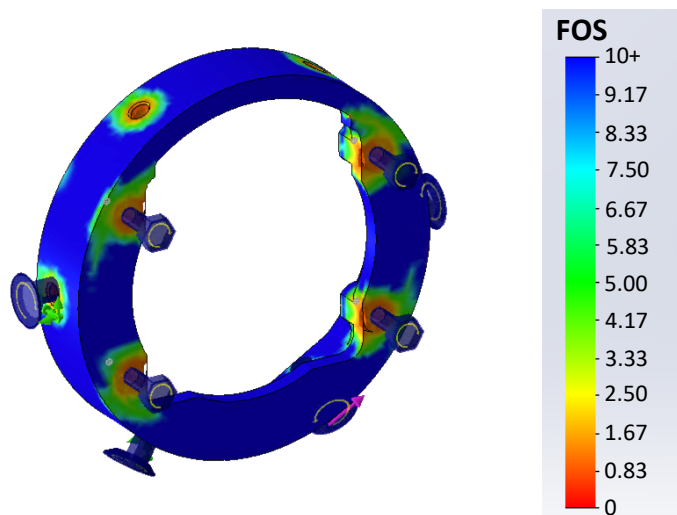


Fig. 59. Gearbox mount FOS with a 147 Nm torque applied.

5.4 Componentry

5.4.1 Bearings

Two KML 6808-2RS bearings are used in the custom compliant actuator. When the leg is only supporting the weight of the robot, the loading is directly radial. However, during head-on collisions, while travelling in the in-between and wide configurations, the actuators will have to support a bending moment. However, KML 6808-2RS bearings are single row deep groove ball bearings which are excellent at supporting radial loads but not bending moments, but they are cheap compared to crossed roller and four-point contact bearings that are capable of supporting moment loads. Therefore, two KML 6808-2RS bearings were used and spaced apart on the axis of rotation. This converts the bending moment into equal but opposite reaction loads for each bearing to support, as shown in Fig. 60. Demonstration of how a moment causing load F is converted into two equal but opposite radial loads F_r .

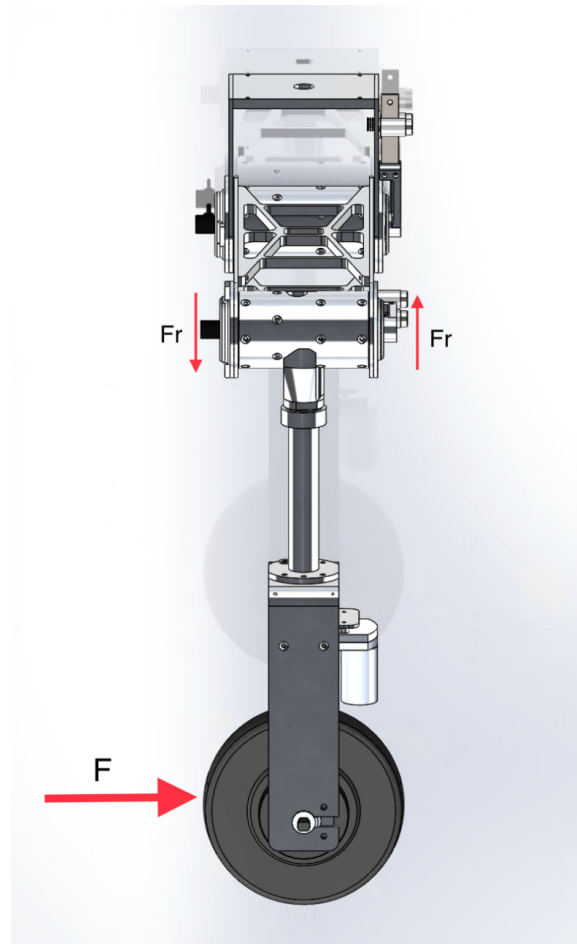


Fig. 60. Demonstration of how a moment causing load F is converted into two equal but opposite radial loads F_r .

During the analysis of the leg design (section 4.3.3), the joint bearings were defined as bearing connectors. This makes SolidWorks calculate the loads that would be on a bearing instead of just showing the stresses within a model of a bearing. This makes it

easy to determine if a bearing can withstand the forces present during a loading condition.

From the weight loading simulation run in section 4.3.3.1, when the leg is loaded with 363 N, the maximum actuator bearing load is 930 N. The KML 6808-2RS bearing can withstand a 4.4 kN load, which results in a FOS during operation of 4.7. This FOS will account for any shock loading that may occur while travelling over rough terrain.

A new collision simulation was run using the 1755 N force identified in section 4.4.4 as the maximum force the steering axis bearings can handle in a collision. The simulation results are not a clear pass or fail. The actuator bearings can withstand 1755 N collisions in the in-between neutral, wide neutral, wide low, and all narrow configurations. However, in-between high, in-between low, and wide high configurations produce axial bearing forces greater than 9800 kN.

Ball bearings that can withstand axial loads greater than 9800 kN are substantially larger than the KML 6808-2RS bearings currently used. Therefore, the actuator would have to be redesigned to be slightly larger, which in turn means the leg would have to be redesigned to be larger in order to accommodate it. Roller bearings able to withstand 9800 kN can be sourced that are thinner than KML 6808-2RS bearings, but are inherently much wider, especially if axially rigid variants are used. The increased width would only require the stub axles and bearing housings to be redesigned. Therefore, if different bearings are to be used, roller bearings would be the better option.

5.4.2 Motor

Finding a motor able to provide enough torque in a small and light package, without costing more than the 3,000 NZD budget was challenging. Motors that met these requirements were found in cordless drills. Modern cordless drills combine a brushless DC motor with a planetary gearbox. They can provide up to 138 Nm (made by Hitachi) of torque [133] and are available with spindle lock mechanisms, which is useful in a leg to lock it in position without using energy. From section 5.1.2 it was calculated that the actuator needs to have 147 Nm of torque, while there is no drill motor available with this much torque at the moment, cordless drill manufactures are in a “specs” competition to see whose drill can output the most torque. Therefore, a drill with 147 Nm or more torque is likely in the near future. Additionally, the 147 Nm rating is calculated as the expected maximum weight loading including a 1.5 FOS; when using the 138 Nm motor the actuator would still be able to support the actual expected weight, it would just be operating with a slightly lower FOS of 1.41.

For the prototype, a motor from a Certa PowerPlus 18 V Brushless DC Drill [134] was chosen for the prototype actuator, see Fig. 61. Its specifications are listed in Table 12.

Certa motor and gearbox specifications.. The Certa PowerPlus 18 V Brushless DC Drill motor only provides 50 Nm of torque, although this is quite a bit less than the required torque and will not be used in the final actuator. However, it is sufficient torque to test the functionality of the prototype leg and only costs 79 NZD. The extremely low cost of this motor while sharing the same features and form factor as the higher torque cordless drill motors available was the reason it was used during prototyping. It allowed the actuator communication and control firmware to be tested and tuned without the possibility that if something went wrong and the motor burnt out, there would not be enough budget left to purchase a replacement motor.



Fig. 61. Certa 18V cordless drill motor and gearbox.

Table 12. Certa motor and gearbox specifications.

Weight	526 g
Gear ratio	60:1
Spindle locking mechanism	Mechanical
Stall torque 18V	50 Nm
Stall Current	100 A

The actuator's mechanical design and surrounding control hardware was designed so that only the Gearbox mount, Motor guide, and Motor encoder mount would have to change if a more powerful motor was used. These mounts are not structural; swapping them out does not affect the rigidity of the actuator.

5.4.3 Joint encoder

A Calt HAE18U5V12 synchronous serial interface (SSI), 12-bit, non-contact hall effect, absolute rotary encoder (see Fig. 62) was used to directly measure the actuator angle to a resolution of 0.09 degrees. A C library was written for Arduino to read and format the SSI data coming from the sensor and publish it as a ROS message over UART to a computer running ROS. The SSI data format and timing is depicted in Fig. 63, and the encoders specifications are listed in Table 13.

The distance between the shoulder joint and Knee joint is 404 mm, and the distance between the Knee joint and wheel is 492 mm, giving a movement accuracy between the shoulder and Knee of 0.62 mm and between the Knee and Wheel of 0.75 mm. Therefore, the overall system movement accuracy between the shoulder joint and wheel is 1.37 mm.



Fig. 62. Calt HAE18U5V12 SSI absolute encoder [135].

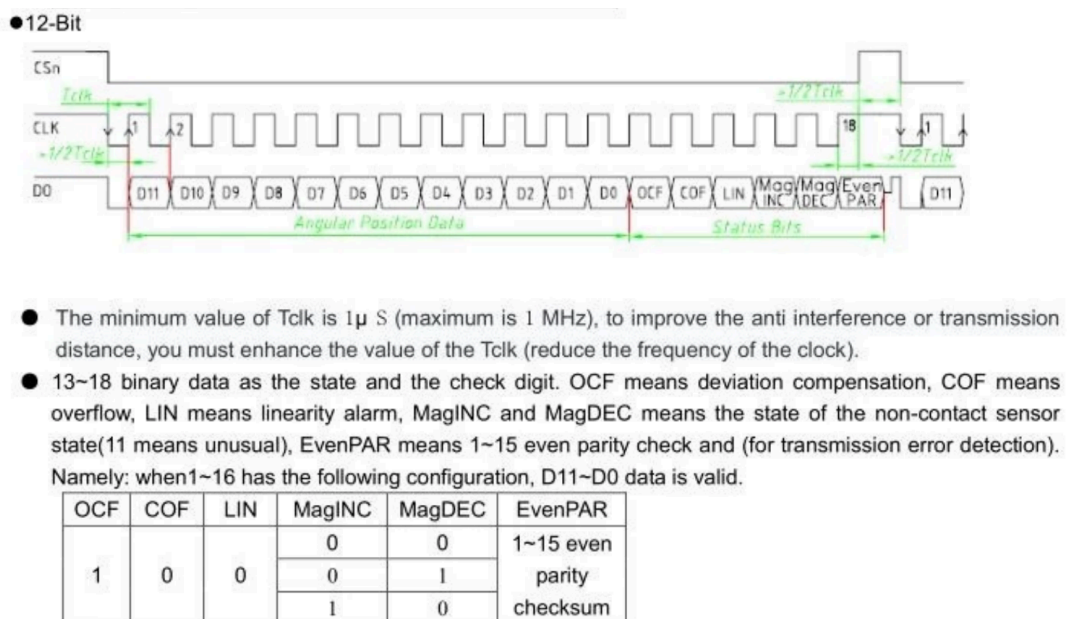


Fig. 63. Calt HAE18U5v12 encoder SSI data format and timing [135].

Table 13. Calt HAE18U5v12 encoder specifications.

Resolution	4096 positions per revolution
Operating voltage	3.3 V or 5.5 V
Typical current usage	<20 mA
Sampling Rate	≤1 MHz

5.4.1 Motor encoder

The Motor encoder is an AS5047P 14-bit On-Axis Magnetic Rotary Position Sensor with 12-Bit Decimal and Binary Increment Pulse Count (see Table 14 for specifications). It is used to measure the angle of the actuator motor before the planetary gearbox and was connected to and read by the VESC open source brushless DC motor controller over the Serial Peripheral Interface (SPI). The AS5047P SPI data timing characteristics are shown in Fig. 64. This encoder is used in place of the UVW commutation hall sensors fitted as standard to the Certa brushless DC drill motor.

The standard UVW hall sensors only inform the brushless DC motor controller (ESC) when a phase should be energised. For the 4-pole BLDC motor used in the actuator, it means the UVW hall sensors only output six positions per revolution (60 degrees). This gives the controller only enough information for basic trapezoidal control, even at low RPM. Yet, the 60-degree resolution is not enough if the motor is to be for position control. Additionally, the basic trapezoidal control produces a torque ripple which becomes a problem when a large load is rotated at low RPM. This torque ripple inherently has an adverse effect on position control.

Replacing the UVW hall sensors with an AS5047P encoder provides 14-bit position resolution (16384 PPR) and enables the use of the Field Oriented Control (FOC). FOC utilises the precise rotor position information to control the stator currents through PWM so that a 90-degree angle is maintained between the stator magnetic field and rotor magnetic field, continually maintaining maximum torque. Additionally, FOC eliminates torque ripple, which consequently improves motor efficiency and makes significantly more accurate position control possible.

Table 14. AS5047P encoder specifications.

Resolution	16384 positions per revolution
Operating voltage	3.3V or 5. 5V
Typical current usage	15 mA
Max sampling Rate	4.5 MHz

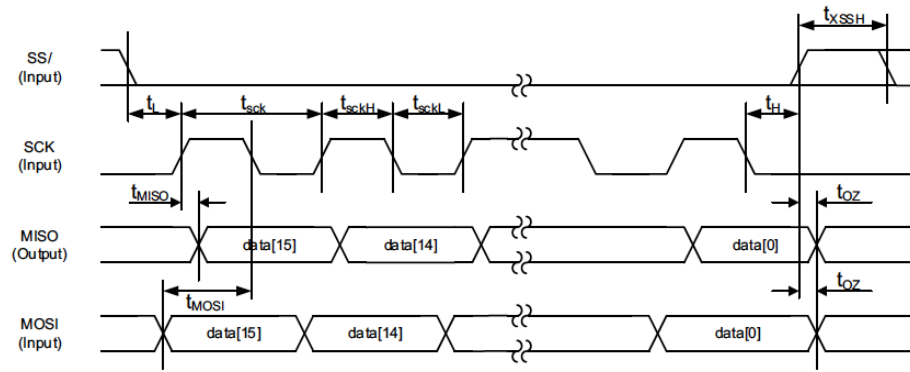


Fig. 64. AS5047P encoder SPI data timing [136].

5.4.1.1 PCB

To use the AS5047P Integrated circuit (IC), a custom PCB needed to be developed (Fig. 65) along with the Motor encoder mount detailed in section 5.2.6. The custom PCB was designed around the sample schematic provided in the AS5047P Adapter Board manual [137]. The AS5047P IC (Q1 in Fig. 65) is soldered to the centre of the PCB, and the PCB is designed to attach in the centre of the Motor encoder mount. This ensures that the AS5047 IC is aligned concentrically to the rotor shaft of the motor.

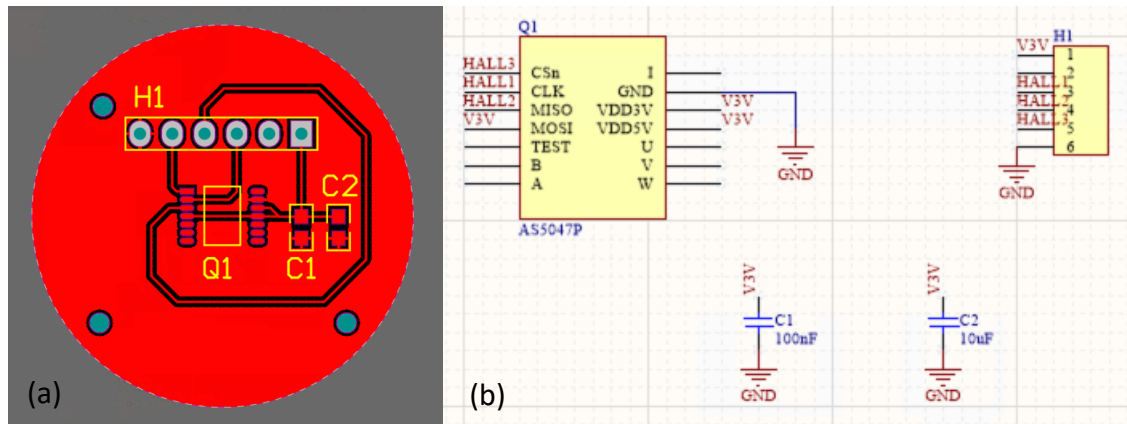


Fig. 65. a) Custom AS5047P encoder PCB layout. b) Custom AS5047P encoder PCB schematic.

5.4.2 Motor Driver

The VESC Hardware version 4.12 (Fig. 67) was used to drive the Joint actuator motor and the leg Wheel motor. This driver was chosen for its low price, high current output, large feature set, versatility, and open-source hardware and software. Its specifications are listed in Table 15. The VESC tool is the VESC's accompanying application that communicates to a computer running Windows, Linux or macOS over USB. With the VESC tool, the VESC can be set up for a specific control type, calibrated for a specific motor and encoder, and the PID for both speed and position can be tuned. Once set up,

calibrated and tuned the motor can be controlled from the VESC tool, and sensory information such as motor encoder position and output currents can be monitored and graphed in real-time. Being fully open source, the formatting of the data sent over USB is known and can be used to control and read data from the VESC for various robotic applications without the need for an intermediate microcontroller. There is also a CAN bus interface which has the same control and data formatting as the USB interface.

A firmware modified by Robin Fröjd [138] was compiled and flashed to the VESC. This firmware allowed for position control and tracking of more than one rotation of the brushless motor. In addition to the modification of the firmware, the configuration header file was configured so the AS5047 can be connected to the I2C/UART/ADC header and not the default encoder header. There are two reasons the new I2C/UART/ADC header was used over the default encoder header: 1) Although not implemented in the VESC firmware, it is capable of HW SPI, 2) there is no hall sensor filters that must be removed before SPI can be used.

It was originally planned to communicate to the VESC over CAN bus so that each leg would only have a single CAN network cable that branches off to the two actuators and wheel. To develop the CAN bus - to - ROS driver was going to take a considerable amount of time. Therefore, to speed up the development process, an existing VESC to ROS USB driver [139] developed by MIT for the MIT Racercar project [140] was used and slightly modified to be compatible with the updated VESC firmware currently used. To translate the raw VESC data from the VESC driver into ROS messages and translate the ROS messages into VESC commands that can be sent by the driver, a ROS hardware interface developed by Robin Fröjd [141] was used and modified. It was modified to interface with the joint position microcontroller, interface with the default ROS joint position interface and controller instead of only the velocity interface and connect to more than two VESCs. Once the system is fully realised over USB, it will be much easier to write the VESC to CAN bus driver since the VESC CAN and USB data formatting are the same. A Flow diagram demonstrating how the VESC communication and control works can be seen in Fig. 66.

To simplify the leg control further, it is planned to modify the VESC firmware so that the Calt HAE18U5V12 joint angle encoder can be directly read by the VESC instead of the microcontroller as explained in section 5.4.3 below. There was not enough time to implement this feature for the prototype actuator, but due to the use of ROS, the functionality of the leg could still be realised by using a separate microcontroller.

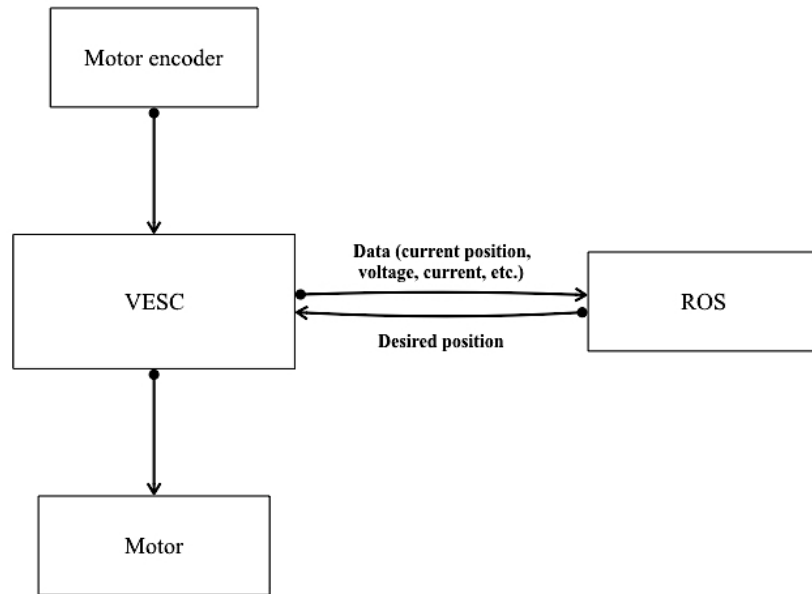


Fig. 66. VESC communication and control flow diagram.

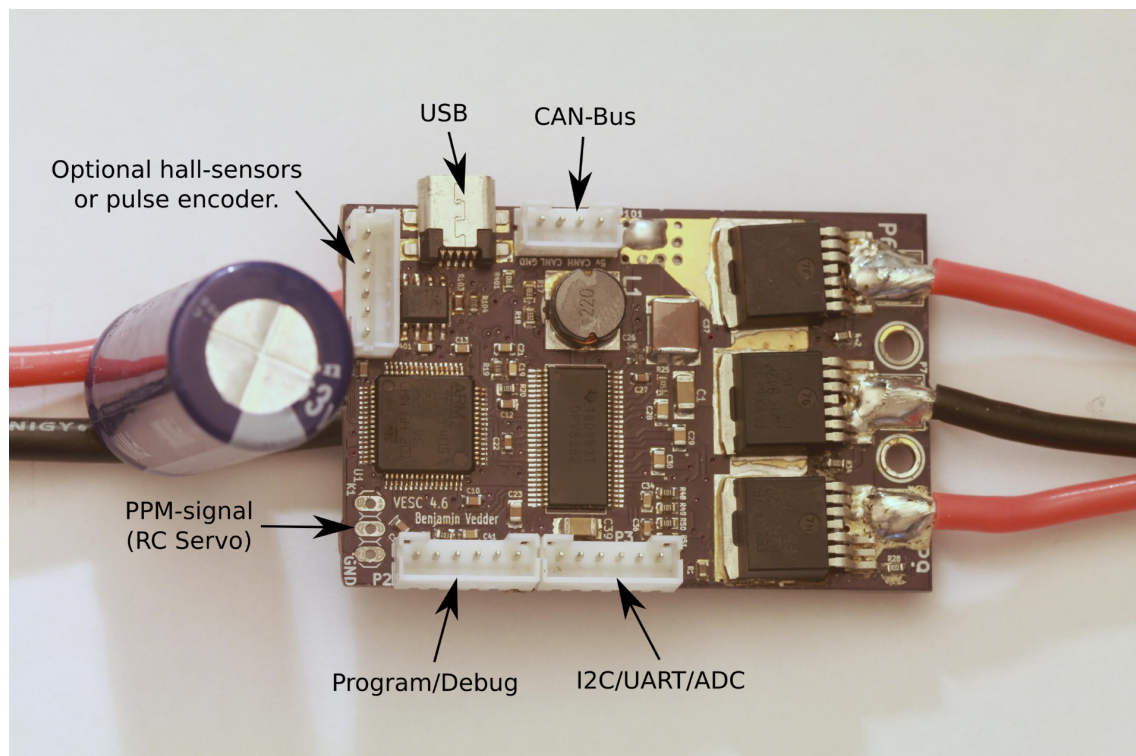


Fig. 67. VESC HW version 4.12 I/O [142].

Table 15. VESC specifications.

Weight	85 g
Operating voltage	8 V – 60 V
Continuous output current	50 A
Peak output current	240 A
Control types	Position, velocity, duty cycle, current

5.4.3 Micro-controller

An Arduino Uno, as shown in Fig. 69, was used to read the two joint encoders, control the leg Steering servo and send and receive data to and from ROS. It was used because it is cheap, the ATmega328p chip is more than powerful enough (specifications are listed in Table 16), and with the Arduino “wiring” framework, it is quick and easy to read a sensor, control a servo motor, and communicate with ROS using the Arduino ROS message libraries. The plan is to get rid of the micro-controller eventually, and instead, the joint VESCs will read the joint encoder, and the wheel VESC will control the Steering servo. With Arduino, it was possible to realise an intermediate solution within a day. Additionally, the C-library that was developed on Arduino to read the joint encoders can easily be ported to work on the VESC. A Flow diagram demonstrating how the Arduino communication and control is implemented can be seen in Fig. 68.

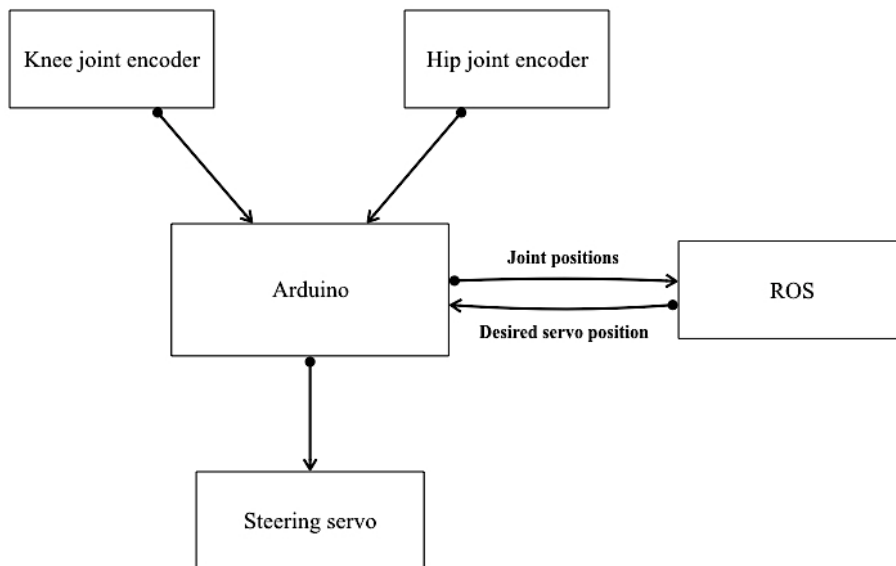
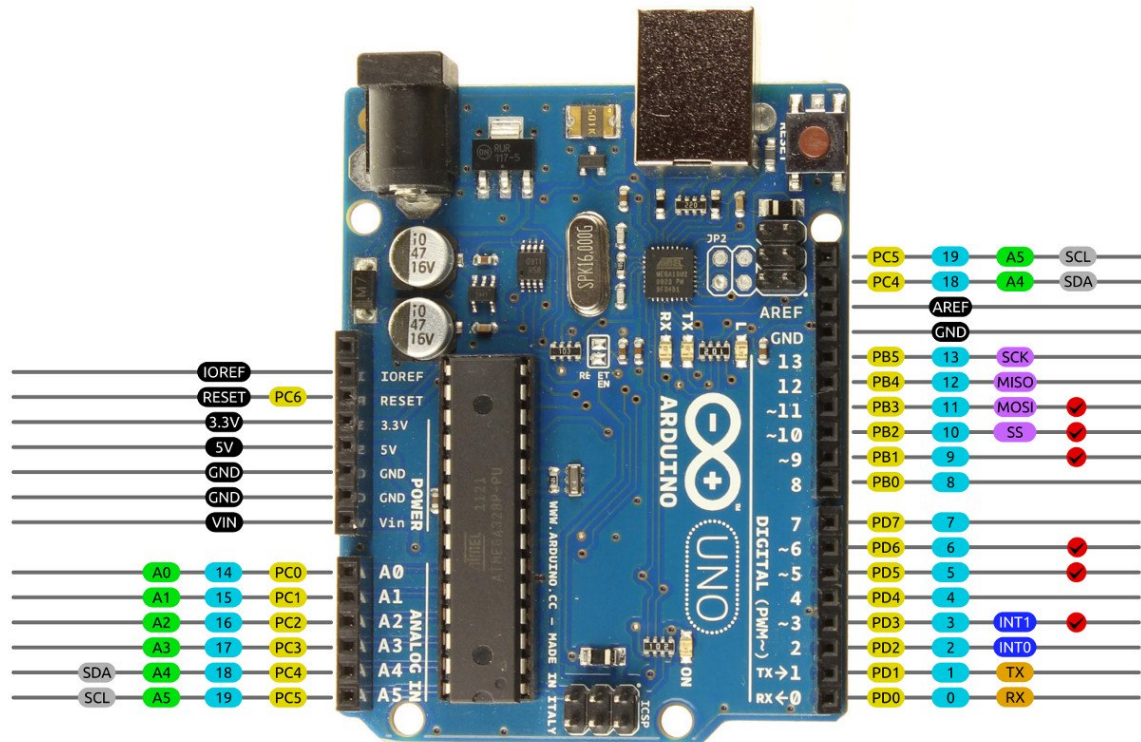


Fig. 68. Arduino communication and control flow diagram.

Arduino Uno R3 Pinout



AVR DIGITAL ANALOG POWER SERIAL SPI I2C PWM INTERRUPT

CC BY SA 2014 by Bouni
Photo by Arduino.cc

Fig. 69. Available I/O on the Arduino Uno microcontroller.

Table 16. Arduino Uno specifications.

Weight	25 g
Microcontroller	ATmega328P
Operating voltage	5 V
Input voltage	7 V – 12 V
Digital I/O pins	14
Analogue input pins	6
Clock speed	16 MHz

6 Testing and Results

From the design described in the previous chapters, a prototype hybrid wheeled leg was built, as shown in Fig. 70. The Knee actuator and Bench testing Base link were manufactured first and used for bench testing, and control and communication development. To simulate the Tibia link and provide a way to apply a torque to the actuator, a 30 mm OD x 26 mm ID x 580 mm pipe was screwed into the Knee joint actuator. The bench testing rig with pipe can be seen in Fig. 71 a) and the bench testing rig with Tibia link attached can be seen in Fig. 71 b). The bench testing rig allowed the leg performance to be tested without the risk of damaging the whole leg if something went wrong.



Fig. 70. Final prototype hybrid wheeled leg.

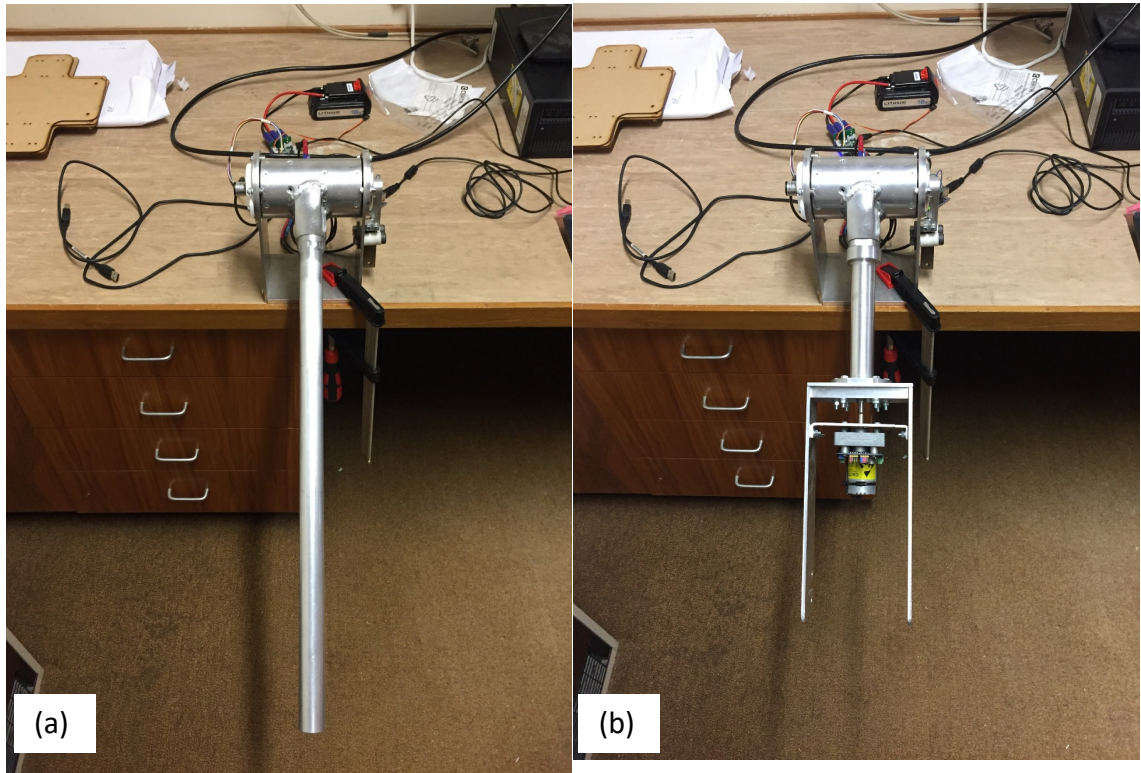


Fig. 71. a) Bench testing rig with test pipe connected. b) Bench testing with Tibia link attached.

6.1 Compliance

To validate that the actuator's adjustable compliance mechanism described in section 5.2.1 works, an Instron 5967 universal testing system was used. The bench testing rig with the test pipe attached was placed inside the Instron, and a force applied halfway down the length of the pipe until the ram moved 42 mm. This was repeated for hard (shortest effective length) medium (intermediate effective length) and soft (longest effective length) compliance settings, the results are shown in Fig. 72. The results show that the compliance is indeed adjustable, with a 58% change in compliance between the softest and stiffest settings.

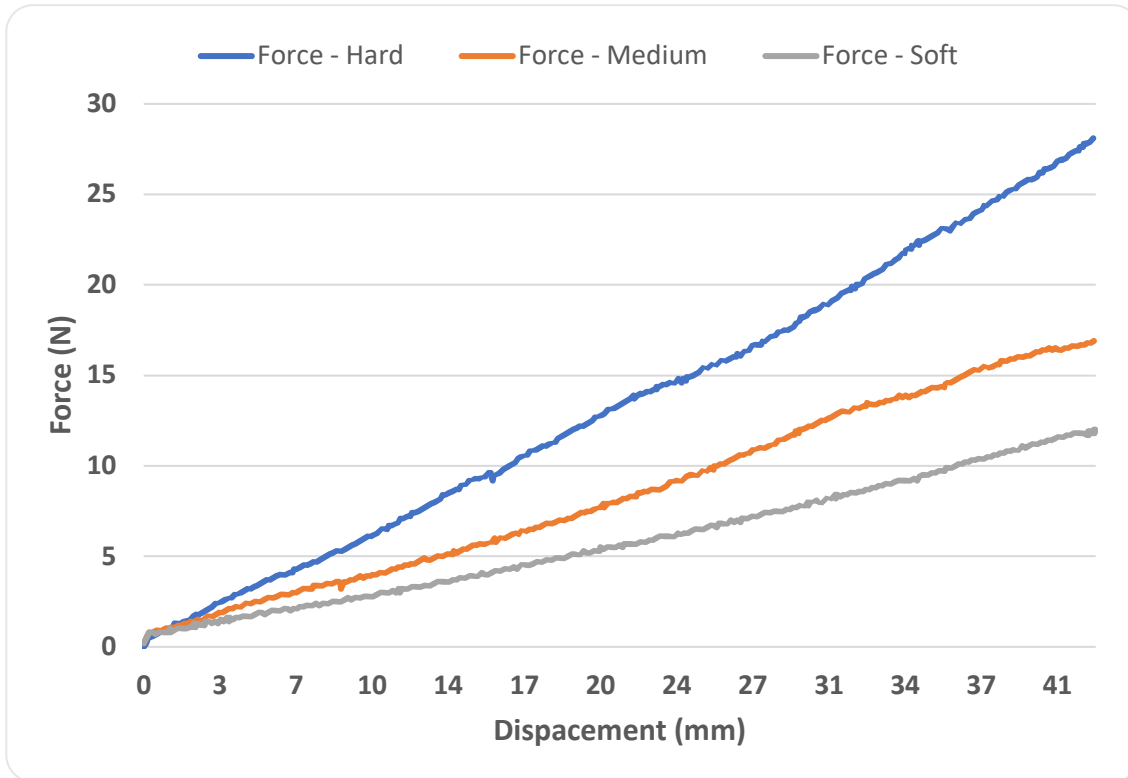


Fig. 72. Actuator compliance.

6.2 Control

A considerable amount of time was spent implementing the control and communication stacks for the leg. ROS manages the control of the overall leg. It can perform the appropriate kinematic calculations and then send the desired position commands to each joint controller (VESC), the desired velocity command to the wheel controller (VESC), and the desired steering angle command to the Steering servo microcontroller. These commands and the feedback data from the joint controllers are published and expected on predefined ROS messages. It is the job of the VESC and microcontroller interface nodes to read the appropriate command messages from ROS and send them to their respective joint controllers, and to publish the data they receive back from the controller to the appropriate ROS messages.

With the ROS VESC and microcontroller interfaces set up to publish to the joint state topics and subscribe to ROS control command topics, the leg can be controlled in Gazebo simulation just as easily as it can be controlled in the real world. For the simulated and real-world control to correlate the leg needs to operate as expected. In the following sections, the control performance of the joints, wheel, and Steering servo will be evaluated.

6.2.1 Actuators

The modified firmware mentioned in section 5.4.2 and used in the actuator motor controllers incorporates a cascaded (series) position control loop, where a velocity control loop runs inside a position control loop. A cascaded control loop, as commonly used in a servo controller, consists of a P controller for the outer position loop, whose output commands the inner PI velocity control loop, whose output commands the motor current. The modified firmware allows for PID control in both the position and velocity loops. However, when both loops use full PID control, the system becomes unstable due to bandwidth constraints. Alternatively, the modified firmware also allows for the motor current to be controlled by a single PID position control loop. When properly tuned, both control loops have near identical characteristics [143].

There are several reasons a cascaded control loop would be used over conventional PID position control in servo type systems: 1) They are simpler to tune because you first tune the velocity P and I gains to give the desired velocity response and, then tune the position P gain to give the desired position response, 2) the velocity and current can be limited independently, and 3) they provide increased stability because each loop can correct errors independently of another loop, meaning one does not have to wait for the error to propagate through the system. A downside of cascaded control is that the outer position loop must have between a 5-10 times lower bandwidth than the inner velocity loop, otherwise there is too much lag and the desired control performance cannot be achieved.

Even though both methods are meant to have near identical characteristics if properly tuned, the cascaded P-PID control loop was unable to be tuned as appropriately as the standard PID control loop. Fig. 73 shows the setpoint change response of the single PID position control loop, and Fig. 74 shows the position change response of the cascaded control loop. Since the normal single PID control loop gave the best results, it was used to carry out the tests in the subsequent chapters.

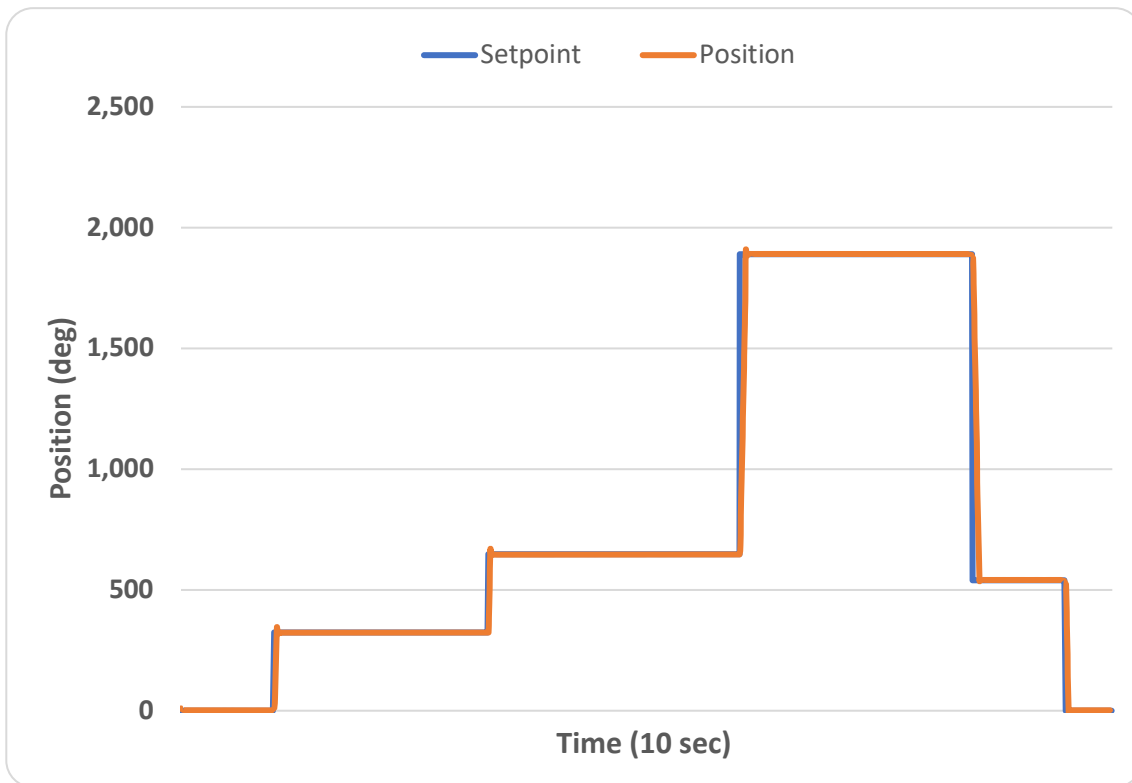


Fig. 73. Single PID control loop setpoint change response.

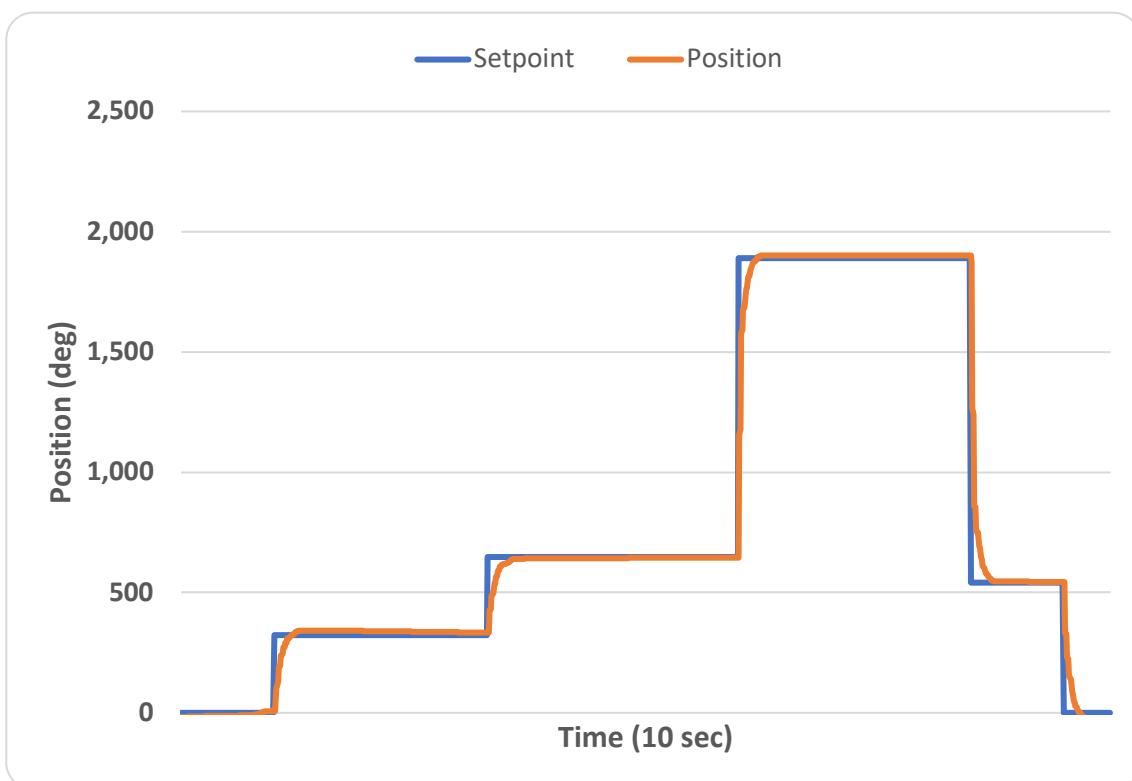


Fig. 74. Cascaded P-PID control loop setpoint change response.

There were several issues with the performance of the actuator position control using standard PID control: 1) Large position changes cause large momentum changes that

put large forces on the leg and actuator than can damage them, 2) the steady-state error was not constant for all rotor positions, 3) the motor was noisy while remaining at the setpoint, and 4) motor position divided by transmission ratio did not equal joint position. The cause and solution to these issues are investigated below.

6.2.1.1 Momentum changes

The large momentum changes are caused by large controller gains. Large controller gains had to be used to move the leg under load to have minimal steady-state error, strong holding torque and good disturbance rejection. The sharp rise time of the single PID loop compared to the cascaded control loop is shown in Fig. 73.

A feature of such aggressive gains and sharp rise times is that the motor has very similar characteristics to that of a stepper motor; the motor will move on tiny position commands (steps). This feature means that a desired movement profile can be generated for the motor to follow that does not cause destructive momentum changes. To test the viability of this feature, a simple ramp movement profile was generated in MATLAB, and incremental position commands were sent to the controller over USB, the results can be seen in Fig. 75.

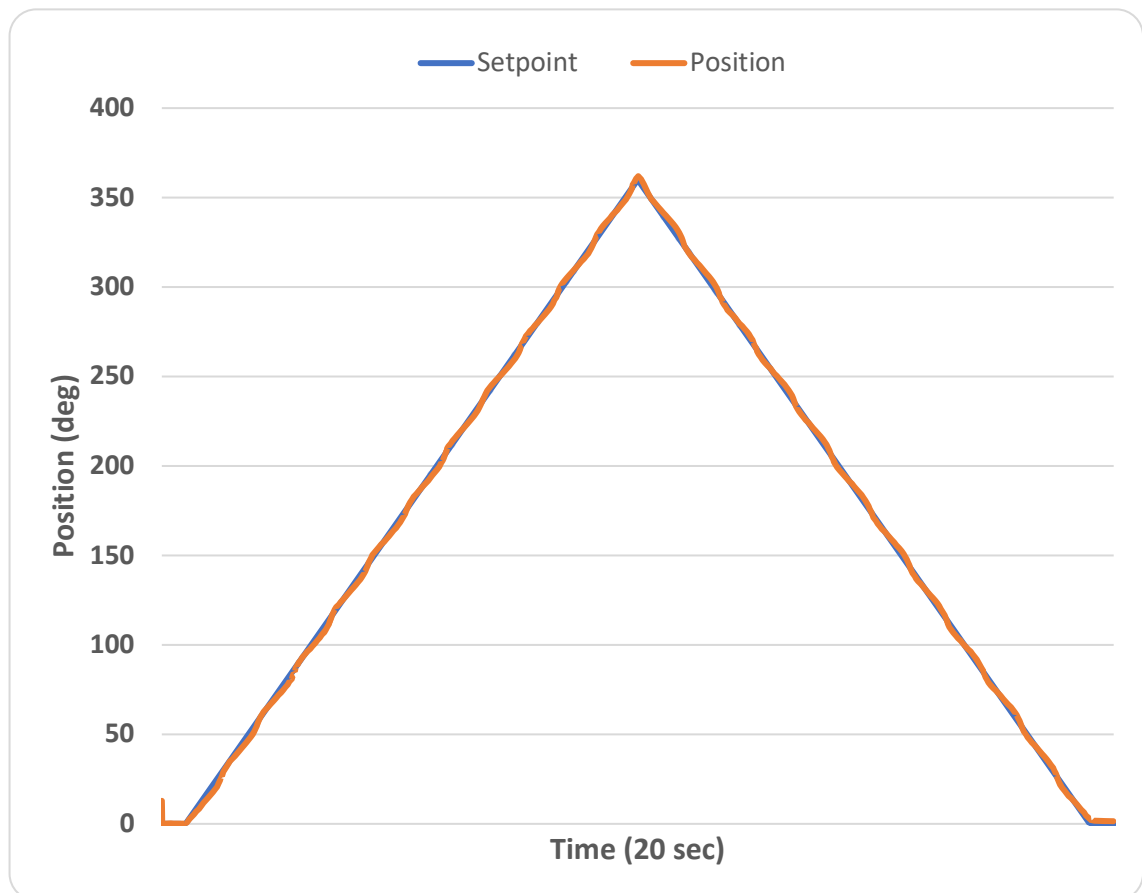


Fig. 75. Actuator motor's ability to follow commanded ramp profile.

The motor followed the profile at low speeds with high but varying precision. The reason it was not able to follow it with the same precision constantly is due to cogging, which is explained in the next section. Additionally, this implementation with MATLAB calculating and sending the profile position commands is only viable for testing. A better option would be for each actuator motor controller to generate the movement profile on the controller from a single endpoint position command; this would avoid saturating the communication bus, especially if CAN bus is used, and it would lower resource usage in ROS.

6.2.1.2 Varying steady-state error

While tuning the position control, it was found that with the same tuning parameters the position control would have a different steady-state error at different positions. Fig. 76 shows the steady-state error at 30 degrees and Fig. 77 shows the steady-state error at 45 degrees; 30 degrees can reach the set point instantly whereas 45 degrees slowly reaches the set point as the integral component of the control loop builds. The reason for this is cogging torque. Cogging torque is caused by the natural attraction the permanent magnets of the rotor have with the phase magnets of the stator. Even though FOC is used, using 10 A to create a magnetic field between two phases results in a weaker magnetic field than applying 10 A to create a magnetic field that aligns with a single phase. This is what causes the varying tracking precision shown in Fig. 75 above.

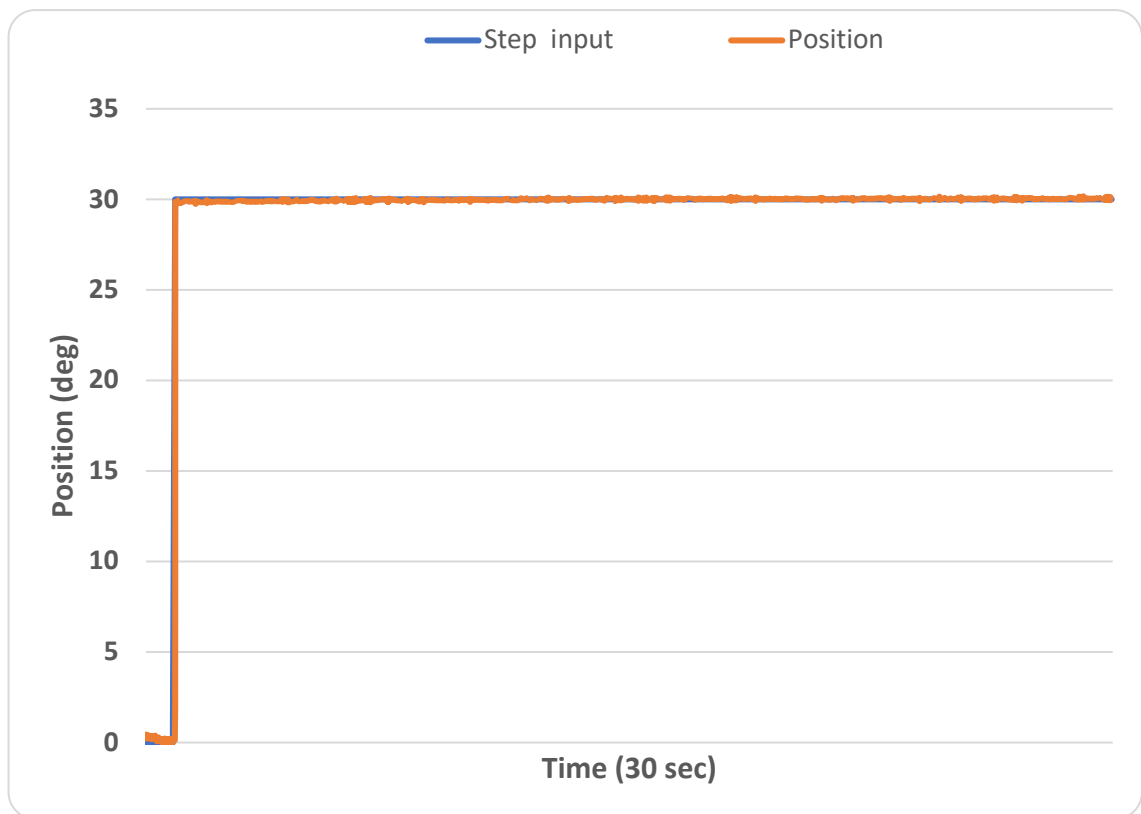


Fig. 76. Steady state error at 30 degrees.

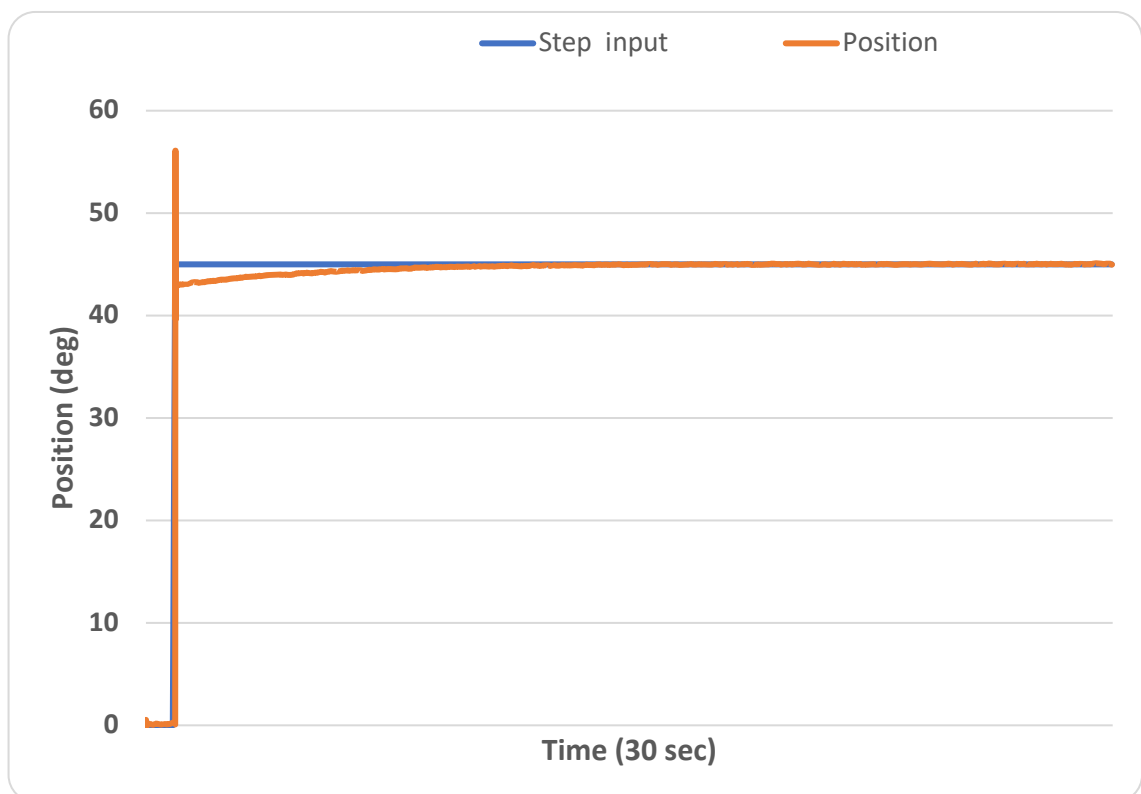


Fig. 77. Steady-state error at 45 degrees.

A Fourier transform of the commanded motor current when the motor follows the position ramp profile from Fig. 75, is shown in Fig. 78. It demonstrates that the commanded current is high and low at harmonics of 12 times a revolution, which correspond exactly to the 12 motor stator slots as they align and un-align with the phase coils. The inverse Fourier transform of these harmonics are shown in Fig. 79 overlaid with the raw measured data. The reproduced sine wave is almost a perfect recreation of the raw measured data without the noise. Since the effects of cogging torque are dependent on position, and its characteristics are now known, it can be compensated for with a feed-forward value into the current control loop.

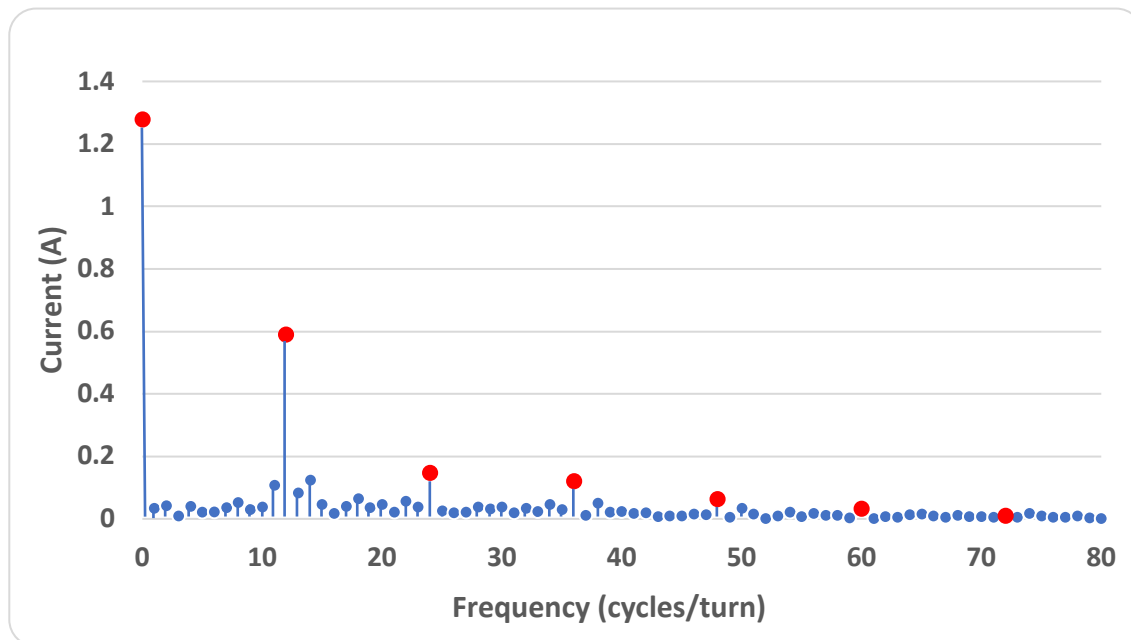


Fig. 78. Fourier transform of motor current while following the ramp profile. The red dots represent the chosen dominant frequencies (harmonics of the stator slots and motor poles).

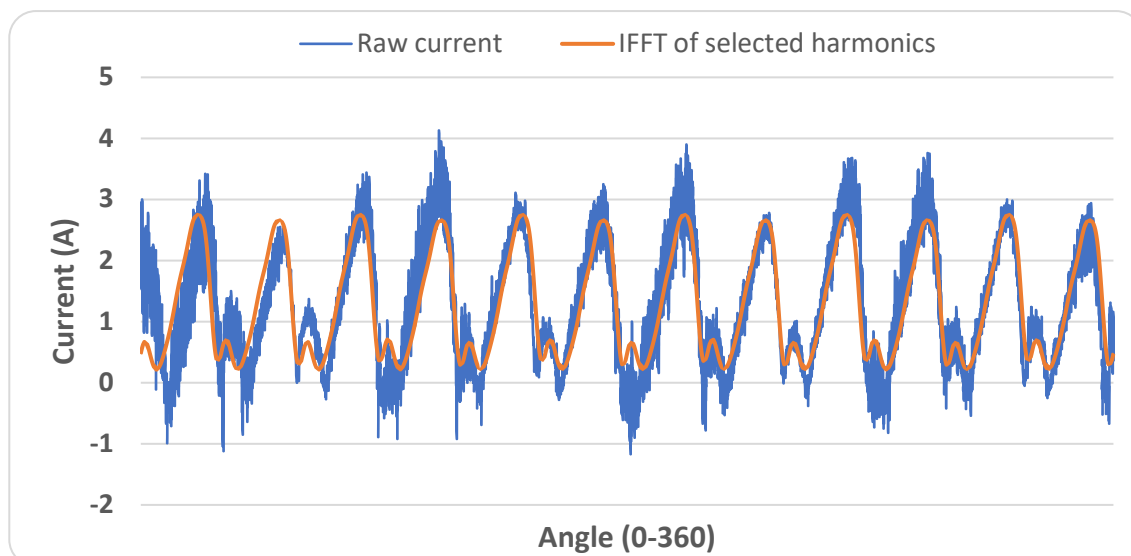


Fig. 79. The blue plot is motor current while following the ramp profile. The orange plot is the inverse Fourier transform of the chosen dominant frequencies shown in Fig. 78.

6.2.1.3 Noisy at set point

The large position controller gains used to make the motor actuator responsive to position commands also makes it responsive to the signal noise from the AS5047 motor encoder. Fig. 80 shows the noisy signal from the encoder, which has a maximum noise of about 0.25 degrees. The controller is always trying to minimise the error, but if the recorded position keeps changing, the error never reaches zero. This means the motor is always trying to move to minimise the error at the same frequency, causing an audible sound. Additionally, this constant noise tracking makes the actuator consume unnecessary energy.

The way to fix this is through filtering. The problem with averaging or second-order filters is that they introduce phase lag into the system and therefore lower the system's response. To overcome this issue, a Phase-locked loop state observer can be used where the position is predicted from velocity. The VESC does use a state observer, but it is currently only used for predicting velocity. To test the effectiveness of an observer at filtering out the encoder noise, one was implemented in excel. Its performance can be seen in Fig. 80.

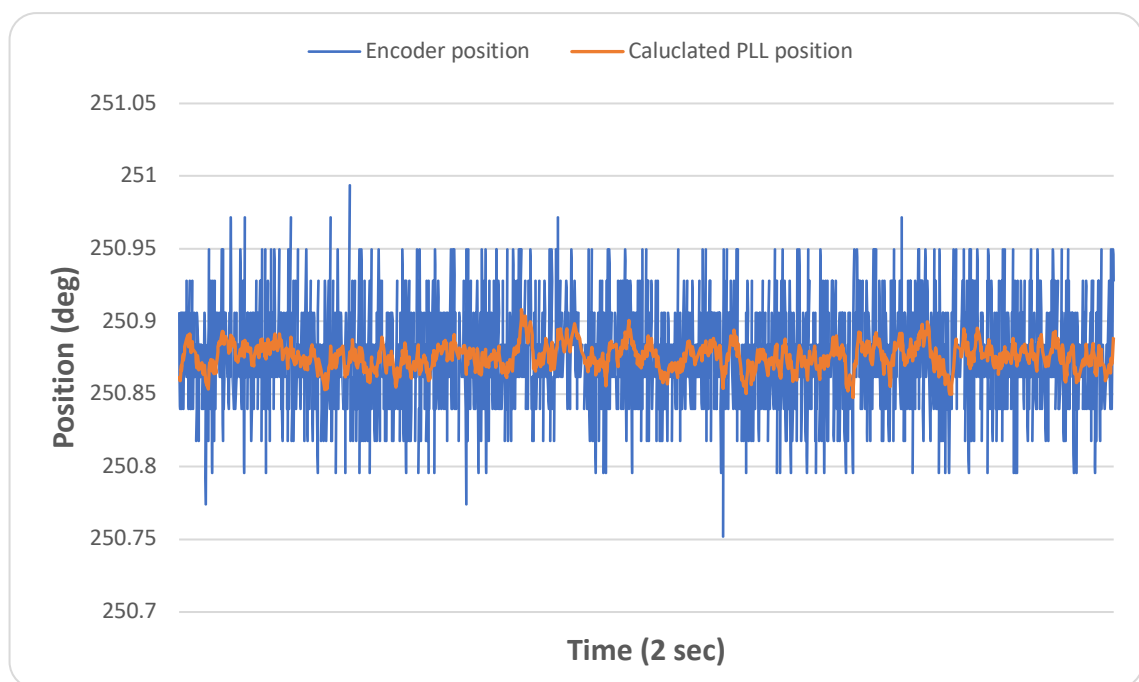


Fig. 80. Raw encoder noise before and after filtering.

6.2.1.4 Joint position

There was a mismatch between the joint position and motor position due to a direction switching delay in the locking mechanism. The motor movement profile and corresponding joint movement can be seen in Fig. 81. The delay is about 18.0 degrees when lifting the load and only about 11.7 degrees when lowering the load. When the locking mechanism switches its locking direction, the joint actuator sticks for a moment

before moving (this can be seen in Fig. 81). The locking mechanism delay appears to be predictable; therefore, it can be compensated for in software.

Further tests were done to see if the locking mechanism can be prevented from sticking, as shown in Fig. 82. It was found that if the direction was changed rapidly, the locking mechanism does not stick, which means software can also be used to remove it. However, as is shown in Fig. 82, this introduced lag. This lag is due to the low communication bandwidth over the USB connection, meaning if this compensation is implemented not externally, but on the controller itself, there will be no noticeable lag.

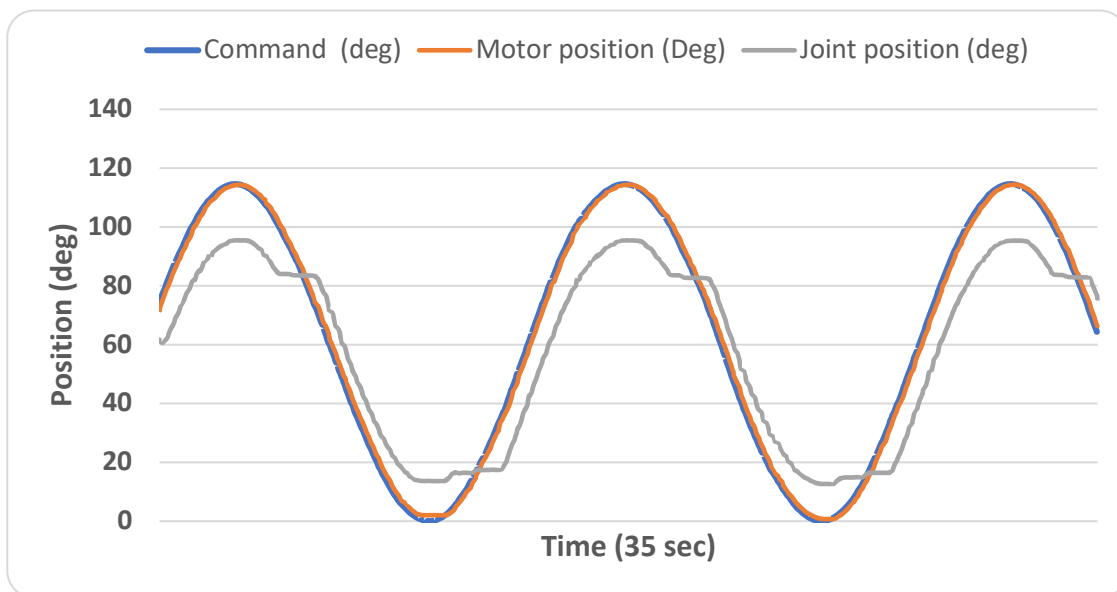


Fig. 81. Relationship between joint position and motor position to a low-frequency sinusoidal command.

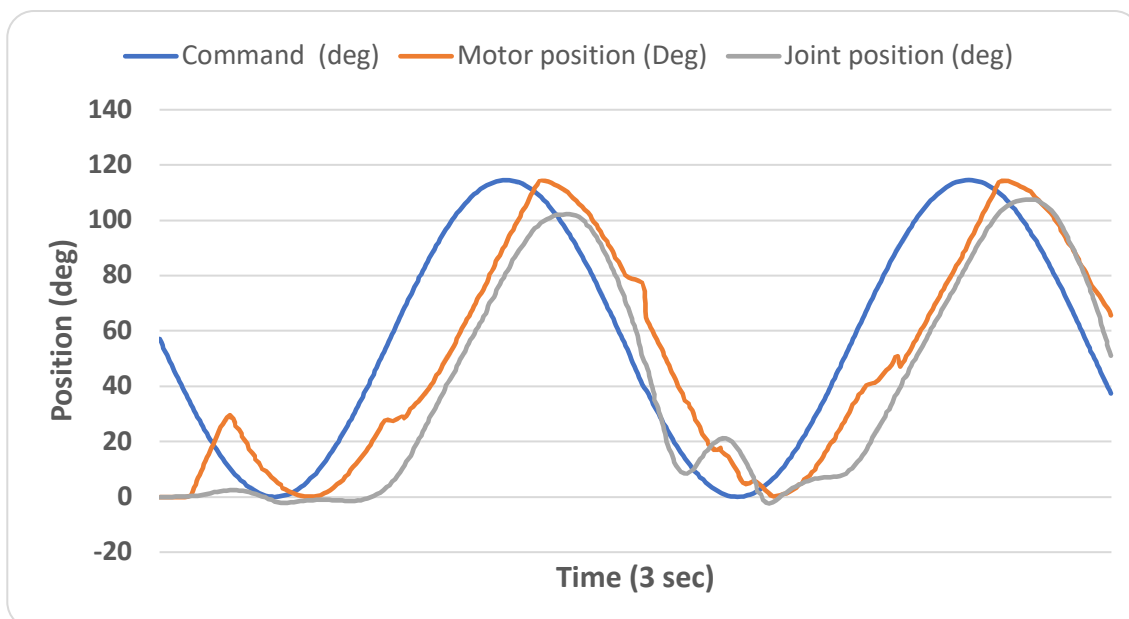


Fig. 82. Relationship between joint position and motor position to a high-frequency sinusoidal command.

6.2.1.5 Conclusion

To improve the performance, controllability, and efficiency of the leg, several of the issues mentioned above should be fixed. A movement profile generator is needed to give the leg smooth and predictable movement characteristics. A filter or phase-locked loop state observer needs to be implemented to smoothen the motor encoder signal to lower motor noise and power usage at steady state. The CALT HAE18U5V12 joint encoder needs to be interfaced directly with the motor controller and an additional control algorithm implemented on the controller to ensure the joint reaches its desired position by compensating for backlash and locking mechanism switching delay. It is believed that cogging torque would not have a significant effect on the performance of the leg due to how little it affects the joint's position after the transmission. Additionally, the positional accuracy required by the leg is not as high as is required by for example a CNC milling machine or 3D printer; meaning that what little effect cogging torque will have on the joint position can be tolerated.

There was not enough time to properly implement the fixes mentioned above. However, the main performance metrics of the leg were able to be tested, and the prototype actuator served its purpose by identifying issues.

While the VESC is extremely versatile, feature-rich, and has an active community which always adds features and fixes issues (which was the reason it was chosen), it is clear that its source code development will stay focused on its intended use in longboards, with limited support for positional control. However, D. Choi [144] has shown that the VESC hardware is capable of being used for robot joint position control, and the firmware can be modified to include a profile generator, and an additional joint encoder can be interfaced with it to accomplish excellent performance in a robotic leg actuator. Unfortunately, since the modified VESC firmware developed by D. Choi [144] used a different encoder interface, it was not possible to try it in the hybrid wheeled leg.

During the design phase of the hybrid wheeled leg, when the VESC was chosen, another open-source ESC called ODrive was just out of its development phase and was sold out when it was needed. ODrive had a small developer community and user base, not as many features, and costs 187 NZD (more than twice as much as the VESC). However, ODrive is intended for position control of BLDC motors, and over the course of this Master's project it has developed a large community and user base, and now incorporates fixes for the issues encountered with the VESC mentioned above, including anti-cogging. The only thing not implemented is compensation for the joint backlash and locking mechanism switch delay. Additionally, due to ODrive's focus on position control and robotics, it has more than one community-supported ROS interface driver.

Going forward, the two options are to spend time implementing all the necessary fixes in the VESC firmware or switch to using the ODrive and only implement compensation for the backlash and locking mechanism switch delay. Additionally, using ODrive means that the actuator can benefit from any additions made to the firmware as it is bound to be position based and any advancements made to the firmware locally can be pushed to GitHub for everyone's benefit.

6.2.2 Steering servo

Steering angle commands are sent to the Arduino from ROS and then the Arduino controls the servo. This intermediate solution worked as expected, although in the future the servo will be controlled directly from the Driven wheel VESC.

6.2.3 Driven wheel

A VESC was used to drive the wheel motor. The VESC is intended for use on electric skateboards and is well suited for controlling the wheel motor. Testing showed the VESC could maintain a constant speed with little variation at high ERPM (= RPM x number of magnet poles) (Fig. 83) and or low ERPM (Fig. 84). The VESC controls the speed in ERPM, and the wheel motor has 14 magnet poles, so the actual set points from Fig. 83 and Fig. 84 are 500 RPM and 17.9 RPM respectively. Speed control may not be applicable in all situations, so current control and duty cycle control are also available.

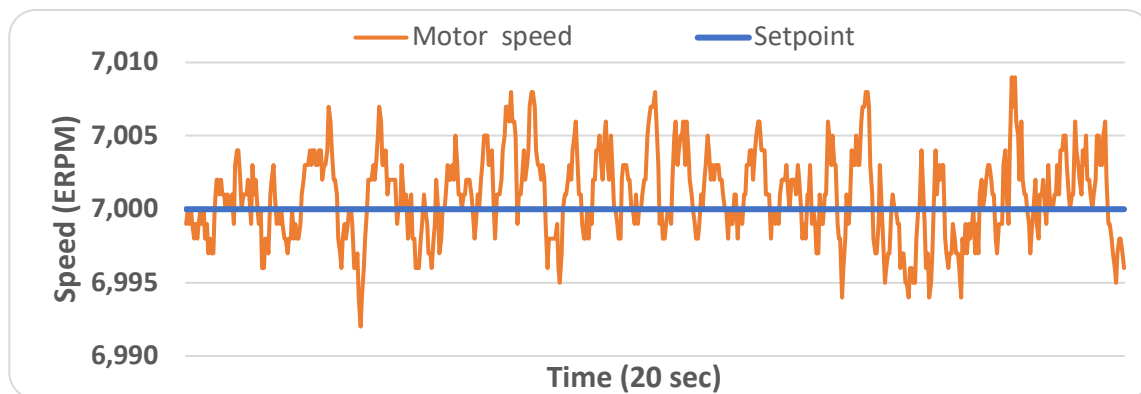


Fig. 83. High ERPM steady-state speed control performance.

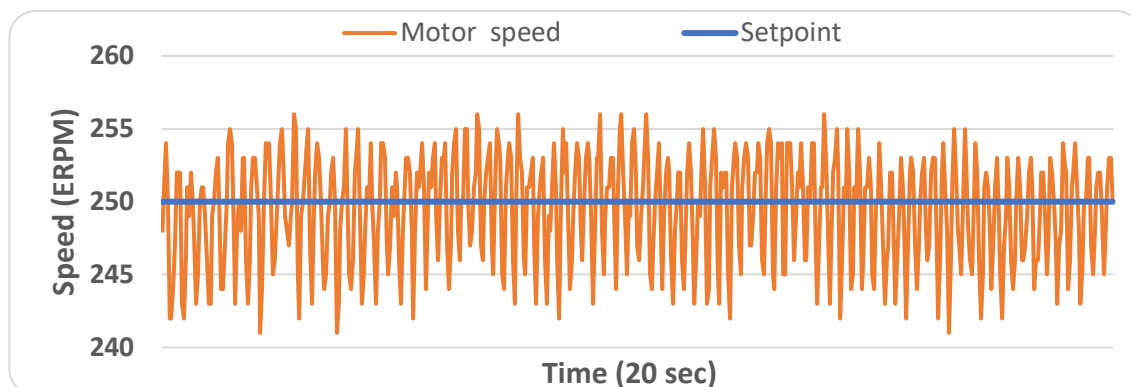


Fig. 84. Low ERPM steady-state speed control performance.

6.2.4 ROS

With ROS, all the DOF were easily turned into a coherent hybrid wheeled leg. The extent of the integration was such that all DOF could be controlled from ROS, and a simulation of the leg could be run in Gazebo. It was not within the scope of this research to develop the kinematic and locomotion algorithms. Fig. 85 shows the leg in a Gazebo simulation. Fig. 86 shows the visualisation of the leg in RVIZ. RVIZ subscribes to the joint state messages that the VESCs and microcontroller publish to and gives you a virtual representation of each joint's current position. Another feature of RVIZ, not tested in this project, is that virtual objects can be placed in RVIZ while physically running the leg, allowing for the development of leg movement trajectories that avoid objects that have not yet been added to the test environment in the real world.

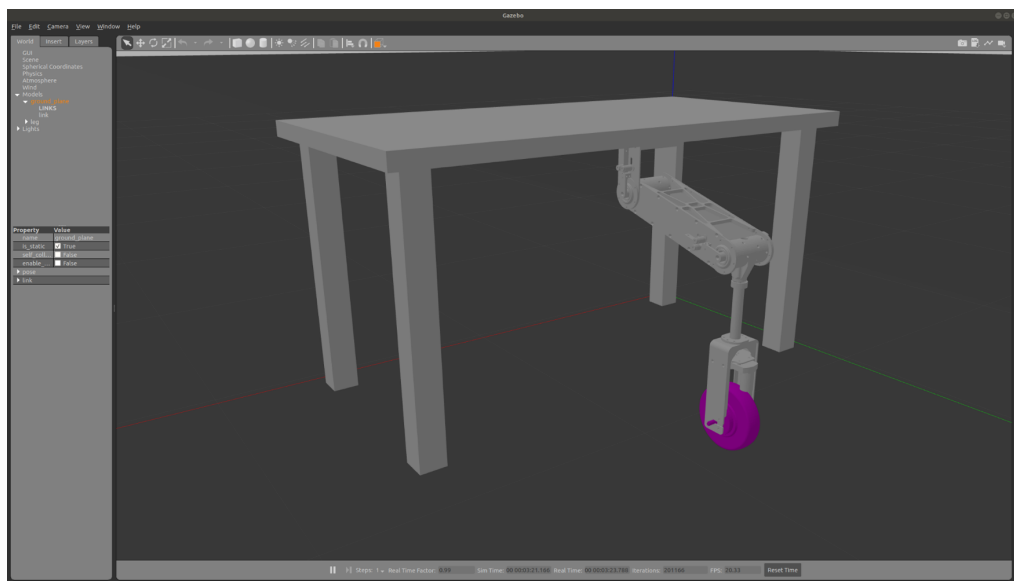


Fig. 85. Leg spawned in a Gazebo simulation.

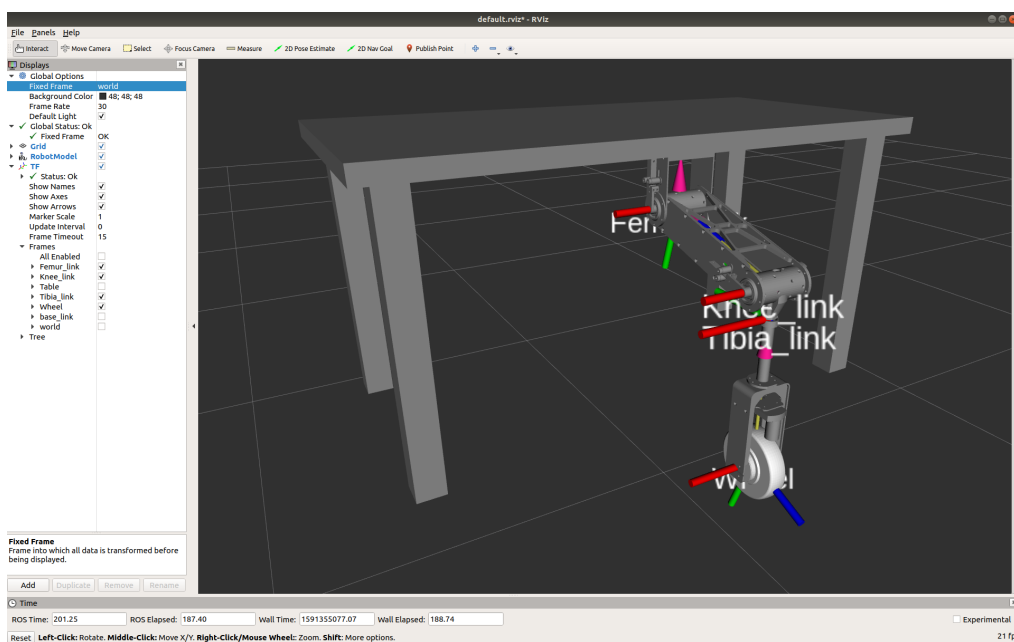


Fig. 86. Leg visualised in RVIZ.

6.3 Actuator performance

The Certa PowerPlus 18 V cordless drill is rated at 50 Nm. However, even though the actuator uses the same motor and gearbox, the actuator was only able to output 23 Nm in testing. The Certa PowerPlus 18 V cordless drill is a cheap, relatively unknown brand of cordless drills. Therefore, it is not surprising that it could not output its stated torque. Fortunately, 23 Nm is enough torque to test most of the leg's functionality.

Unfortunately, there is not enough time left to purchase a high torque drill motor from a known brand and test its torque output.



Fig. 87. The lifting torque of the actuator being tested.

6.4 Cost

There was a 3000 NZD budget to build the leg. The cost of parts and raw materials required to build the custom compliant actuator can be seen in Table 17, and the cost of parts and raw materials required to build the leg can be seen in Table 18.

Table 17. Cost of parts required to build the custom compliant actuator.

Component	Quantity	Type	Total price (NZD)
Motor and gearbox	1	Certa Powerplus 18V brushless drill motor	\$79.00
Motor Driver	1	VESC HW version 4.12	\$78.48
Joint encoder	1	Calt HAE18U5V12 synchronous serial interface (SSI) encoder	\$68.82
Motor encoder	1	AS5047P 14-bit On-Axis Magnetic Rotary Position Sensor	\$16.76
Bearings	2	6808–2RSH 52 mm OD x 40 mm ID x 7 mm	\$100.00
Chassis	1	76.2 mm OD x 63.5 mm ID x 129 mm extruded 6061-T6 aluminium tube	\$11.32
Knee - Tibia link connector	1	76.2 mm OD x 60 mm 6061-T6 aluminium round bar	\$15.82
Through drive stub axle	1	76.2 mm OD x 32.5 mm 6061-T6 aluminium round bar	\$8.57
Non - drive stub axle	1	76.2 mm OD x 24 mm 6061-T6 aluminium round bar	\$6.33
Bearing housings	2	101.6 mm OD x 10 mm 6061-T6 aluminium round bar	\$4.23
Drive link	1	31.8 mm x 31.8 mm aluminium 6061-T6 square bar	\$4.25
Leaf spring	1	2.4 mm x 85 mm x 2 1 mm spring steel sheet	\$2.50
Gearbox mount	1	76.2 mm OD x 13mm 6061-T6 aluminium round bar	\$3.43
Motor holder	1	3D printed PLA	\$0.32
Motor encoder mount	1	3D printed PLA	\$0.40
Joint encoder mount	1	3D printed PLA	\$0.72
Total			\$405.18

Table 18. Cost of parts required to build the leg.

Component	Quantity	Type	Total price (NZD)
Steering motor and gearbox	1	ASMC-04B 12-24 V Servo	\$91.11
Motorised wheel	1	24 V, 350 w hub motor and tire	\$150.50
Motorised wheel Driver	1	VEESC HW version 4.12	\$78.48
Joint Actuator	2	Custom compliant actuator	\$810.36
Motor encoder	1	AS5047P 14-bit On-Axis Magnetic Rotary Position Sensor	\$16.76
Bearings	2	6301-2RSH 37 mm OD x 12 mm ID x 12 mm	\$34.44
Femur link side plates	2	490 mm x 96 mm x 4 mm 6061-T6 aluminium plate	\$33.48
Femur link braces	2	350 mm x 131 mm x 10 mm 6061-T6 aluminium plate	\$69.08
Tibia link Steering axle tube	1	76.2 mm OD x 172 mm 6061-T6 aluminium round bar	\$45.35
Tibia link fork	1	639.98 mm x 70 mm x 4 mm 6061-T6 aluminium plate	\$16.00
Tibia link fork brace	2	211 mm x 116 mm x 3 mm 6061-T6 aluminium plate	\$13.66
Steering servo mount	1	138.14 mm x 94 mm x 3 mm 6061-T6 aluminium plate	\$3.62
Steering axle	1	12 mm OD x 246.8 mm 316 stainless steel round bar	\$5.70
Steering axle adapter	1	40 mm OD x 38 mm 6061-T6 aluminium round bar	\$3.28
Total			\$1,355.06

The cost of parts and raw materials required to build the prototype hybrid wheeled leg was only 1,355 NZD. This is just under half the available budget which meant that spare parts could be purchased in case there was a component failure during testing. This proved advantages when an actuator motor burnt out during testing and there was a spare one to replace it immediately.

At 502 NZD, the available 138 Nm drill motor [133] would push the cost of the leg to 2,200 NZD. While this is within the budget, at the start of the design, it was unclear how many failures there would be or even if the drill motor would work. Therefore, by choosing the Certa Powerplus 18 V brushless drill motor (79 NZD), there was plenty of budget left for a design change if needed.

6.4.1 Comparison to commercial robots

Since building the actuator and leg, only a few commercial actuators and legged robots have become available to give a clear indication of what commercially available offerings will cost. In China, they have started making legged robots based off of the MIT Mini Cheetah robot [145]. The actuators being sold for these robots come in various torque ratings from 18 Nm (562 NZD) to 48 Nm (745 NZD). While the price and torque of these actuators are comparable to the custom compliant actuator developed in this thesis, they do not have any mechanical compliance, which is one of the requirements for the hybrid wheeled leg. It is also unclear if versions capable of close to 147 Nm will become available in the near future, while it is known that 138 Nm cordless drill motors are already available.

The largest and most powerful complete cheetah legged robot clone available from China costs 27,432 NZD [146]. It weighs 24 kg and can carry an additional 15 kg load. Interestingly, its actuators are capable of 72 Nm, but actuators with this output torque intended for the Cheetah legged robot are not available for purchase. The other legged robot that has become available is Spot® from BostonDynamics [147]. It costs 111,929 NZD, weighs 47.6 kg and is capable of carrying a 14 kg payload.

The actuator developed in this thesis can have a 138 Nm output if the correct motor is used as described in section 5.4.2. The actuator then costs 829 NZD. This is 83 NZD more expensive than the most expensive actuator available from China but has 2.87 times the torque, and it has compliance. The entire hybrid wheeled leg developed in this thesis, including 138 Nm actuators, costs 2,200 NZD. This means that a four-legged robot would have 8,800 NZD worth of legs. When considering the 27,432 NZD price of the most powerful robot from China, it leaves 18,632 NZD for the robot chassis to be built. Even with a worst-case 10,000 NZD estimation for the robot chassis and components, there is a 8,632 NZD saving. Performance wise, the robot that is extrapolated from this thesis will be more useful and capable because it is explicitly designed to complete the tasks found on a farm, will be able to carry a heavier payload, and can travel long distances more efficiently because of the wheeled locomotion.

7 Conclusions and Future Work

The literature-investigations of the first objective revealed that:

- Currently the use of robotics in farming is focussed on outdoor crops, orchards, greenhouses, feedlots and dairy sheds because the terrain in these areas is well defined and structured. There is only one research robot intended for outdoor livestock farming because of the steep, undulating and muddy terrain present on these farms.
- The most appropriate binary locomotion type for unstructured terrain is legged locomotion, however it is inefficient and slow, therefore it was identified that a hybrid of wheeled locomotion and legged locomotion would give the robot the efficiency and speed of wheeled locomotion and the excellent unstructured terrain capabilities of legged locomotion making it perfect for use in outdoor livestock farming but also useful in arable farming.
- Driving or walking over unstructured terrain causes a lot of impact loading on a robot. Conventional wheeled locomotion robots use suspension to absorb these impacts, but to absorb these impacts in a legged robot the joint actuators need to have compliance. It was found that a mechanically compliant actuator with adjustable compliance would be the best to use.
- Using a robot middleware would simplify the control of the leg and make testing easier, it also makes the process of scaling from controlling a single leg to four legs simple. The best robot middleware to use would be ROS (Robot Operating System) because it is open source, still currently supported, robot agnostic by design, has well written tutorials, and is the most used robot middleware therefore most sensor and motor controllers have first party or third party driver support.

The second objective was aimed at determining the height and load carry specifications of the leg. It was determined that the task requiring the heaviest equipment is weed spraying and would require each leg to be strong enough to support around 24.7 kg (242 N). Both weed spraying with a delta robot and driving over crops require a robot ground clearance of around 1 m, therefore the leg needs to have an extended length of around 1 m.

After the abovementioned literature investigations and specifications, the third objective of this research was to develop and produce a prototype hybrid wheeled leg intended for use on an agricultural robot based on the learnings from Chapter 2 that met the goals set out in Chapter 1, and agricultural related specifications developed in Chapter 3. In order to meet these goals and specifications, a custom actuator also had to be developed and built.

The prototype designs of the third and fourth objective (hybrid wheeled leg and adjustable mechanically compliant leg actuator) were done using SolidWorks. The length of the leg's links was designed to meet the height requirements, and the structure of the actuator and leg were designed to support the required 24.7 kg (242 N) weight load. However, additional testing was done to determine how the leg would perform under impact loading conditions.

Due to the low budget available for the whole leg, the testing was conducted on the actuator and leg in SolidWorks simulation during the design phase. This identified that: 1) the leaf spring that was used was too small for the required torque output of the final actuator, 2) the actuator bearings were too small to withstand a collision at 5 km/h, and 3) the Femur link braces were not strong enough to withstand a collision at 5 km/h. To fix the issues: 1) a wider and thicker spring can be used because the Motor drive to Spring adapter is designed to take leaf springs that are wider and thicker than what is currently used, 2) it is recommended that roller bearings are used, and the stub axles are made slightly wider to accommodate them, 3) without increasing the leg's weight, topology optimisation was used to develop a new Femur link brace design that could withstand the stresses expected on it during operation. Simulations cannot recreate all the complex interactions that occur in the real-world, therefore further weaknesses can only be identified when the leg is on a robot in an agricultural setting.

For the fifth objective, a physical prototype of the custom compliant actuator was manufactured and assembled. Drivers were found and modified to allow the actuator to be controlled from the chosen middleware. However, the torque testing identified that the actuator was unable to output 50 Nm of torque. This is believed to be down to the cheap Certa PowerPlus 18V cordless drill motor used in the actuator to save costs. The 138 Nm cordless drill motor that is recommended for the next prototype leg actuator is made by Hitachi who are known for their quality. Therefore, it is safe to assume that the recommended drill will be able to output 138 Nm of torque. Positional control testing on the actuator was positive, however, several areas were identified where improvements should be made, and further research needs to be conducted to improve the position control. The identified improvements are software based:

- Implementation of movement profiles for smoother actuator movement.
- Better encoder noise filtering to reduce the steady-state jitter of the motor.
- Implementation of an algorithm to compensate for the joint locking mechanism direction switching delay and tendency to stick as it switches.
- Cogging torque compensation for uniform steady-state error.

While the VESC motor BLDC motor driver used is highly capable and versatile, its intended use is not for position control. Therefore, its position control implementation is basic and resulted in the issues mentioned in section 6.2.1. These could be fixed in software, which would take some time, or another open-source BLDC motor driver called ODrive can be used. ODrive is intended for position control, has ROS support, and has fixes for all but one of the issues stated in section 6.2.1. Additionally, all future software and hardware developments of ODrive will be targeted at improving position control, from which the leg can benefit. Therefore, it is recommended that an ODrive is used for future development of the hybrid wheeled leg.

For the last objective, a physical prototype of the leg was manufacture and assembled. The chosen middleware (ROS) made it easy to get the leg from many individual DOF to a co-ordinated hybrid wheeled leg. A model of the robot was imported from SolidWorks into ROS to allow a visualization of the leg's movements, which also made it possible to simulate the leg. Going forward, a way of simulating the actuator compliance in ROS is needed, and algorithms for optimally controlling the leg with compliance will need to be implemented in ROS and on the actuator controllers.

Lastly, this work showed that a hybrid wheeled leg intended for agriculture could be built for less than 3,000 NZD that met the identified goals and specifications.

8 Bibliography

1. Woodford, K. *Agricultural GDP catches well under one quarter of the agribusiness system. As such it fails to capture the importance of agribusiness to the economy* 2019 [cited 2020 March 14]; Available from: <https://www.interest.co.nz/rural-news/102105/agricultural-gdp-catches-well-under-one-quarter-agribusiness-system-such-it-fails>
2. Tipples, R.S., *New Zealand agricultural employment relations, migration, and 'pledge washing': The new recipe for the 21st century*. 2017.
3. Ang, H.B., *Occupational Stress Among the New Zealand Farmers - A Review*. Labour, Employment and Work in New Zealand, 2010.
4. Robertson, M., *Agricultural productivity in Australia and New Zealand: trends, constraints and opportunities*. Proceedings of the New Zealand Grassland Association, 2010. **72**: p. 51-62.
5. Pow, T., B. Longhurst, and Z. Pow. *The future of NZ dairy farming systems: Self managing cows with access to partial housing*. in *FLRC Workshop 2014*. 2014.
6. Epson. *Why Automate: 5 Ways Robotics Helps Factory Manufacturing Grow [Blog]*. 2018 [cited 2019 February 20]; Available from: <https://blog.epson.com/enterprise/why-automate-5-ways-robotics-helps-factory-manufacturing-grow/>.
7. Wilson, J.N., *Guidance of agricultural vehicles — a historical perspective*. Computers and Electronics in Agriculture, 2000. **25**(1): p. 3-9.
8. Lely®. *Lely Astronaut™*. n.d. [cited 2017 October 2]; Available from: <https://www.lely.com/nz/solutions/milking/astronaut-a4/>
9. GEA Group®. *Automatic Feeding Free Stall Feeder*. n.d. [cited 2017 October 3]; Available from: <http://www.gea.com/en/products/free-stall-feeder.jsp>
10. Abundant Robotics. *Abundant Robotics*. n.d. [cited 2020 June 02]; Available from: <https://www.abundantrobotics.com/>.
11. Agrobot. *Agrobot*. n.d. [cited 2020 June 02]; Available from: <https://www.agrobot.com/>.
12. Rowbot. *Rowbot*. n.d. [cited 2020 June 02]; Available from: <https://www.rowbot.com/>.
13. American Robotics. *American Robotics*. n.d. [cited 2020 June 02]; Available from: <https://www.american-robotics.com/>.
14. Rabbit Tractors. *Rabbit Tractors*. n.d. [cited 2020 June 02]; Available from: <https://www.rabbittractors.com/>.
15. Eckelkamp, M. *A Fully Autonomous Drone For Daily Scouting*. 2017 [cited 2020 June 02]; Available from: <https://www.agprofessional.com/article/fully-autonomous-drone-daily-scouting>.
16. Kessler, S. *Swarms of Teeny Robo-Tractors Will Outmaneuver Tesla's Driverless Cars*. 2020 [cited 2020 June 03]; Available from: <https://onezero.medium.com/swarms-of-teeny-robo-tractors-will-outmaneuver-teslas-driverless-cars-5a7f288e007e>
17. ecoRobotix. *Autonomous Robot Weeder*. n.d. [cited 2019 February 07]; Available from: <https://www.ecorobotix.com/en/autonomous-robot-weeder/>
18. Pedersen, S.M., S. Fountas, and S. Blackmore, *Agricultural robots—Applications and economic perspectives*, in *Service robot applications*. 2008, InTech. p. 369-382.
19. Tullberg, J.N., *Wheel Traffic Effects on Tillage Draught*. Journal of Agricultural Engineering Research, 2000. **75**(4): p. 375-382.
20. Stats NZ. *Farm numbers*. 2018 [cited 2020 June 04]; Available from: http://archive.stats.govt.nz/browse_for_stats/environment/environmental-reporting-series/environmental-indicators/Home/Land/farm-size-and-numbers/farm-numbers-archived-19-04-2018.aspx.
21. Beef + Lamb New Zealand, *Guide to New Zealand cattle farming*, K. Geenty and S. Morris, Editors. 2017, Beef + Lamb New Zealand.
22. James P. Underwood, A.C.F.F.R. *Our Robots*. 2017, December 14 [cited 2018 10 May]; Available from: <https://confluence.acfr.usyd.edu.au/display/AGPub/Our+Robots>.
23. Andrew Hayward. *Meet SwagBot, the Robot Cowboy that Can Herd and Monitor Cattle on Its Own*. 2016, July 18 [cited 2017 20 October]; Available from: <https://modernfarmer.com/2016/07/swagbot/>.

24. Bruzzone, L. and G. Quaglia, *Locomotion systems for ground mobile robots in unstructured environments*. Mechanical Sciences, 2012. **3**(2): p. 49-62.
25. Pratt, G.A., et al. *Stiffness isn't everything*. 1997. Berlin, Heidelberg: Springer Berlin Heidelberg.
26. DeLaval©. *DeLaval VMS™*. n.d. [cited 2017 October 2]; Available from: <http://www.delaval.co.nz/-/Product-Information1/Milking/Systems/Automatic/DeLaval-VMS/>
27. GEA Group©. *Mlone – The Multibox system*. n.d. [cited 2017 October 3]; Available from: <http://www.gea.com/en/products/automatic-milking-robot-mione.jsp>
28. Lely©. *Lely Vector™*. n.d. [cited 2017 2 October]; Available from: <https://www.lely.com/nz/solutions/feeding/vector/>.
29. Veissier, I., et al., *The motivation of cows to walk as thwarted by tethering*. Journal of animal science, 2008. **86**(10): p. 2723-2729.
30. González Sánchez, R., et al., *Navigation Techniques for Mobile Robots in Greenhouses*. Applied Engineering in Agriculture, 2009. **25**: p. 153-165.
31. Jago, J. and M. Woolford. *Automatic Milking Systems: an option to address the labour shortage on New Zealand dairy farms?* in *PROCEEDINGS OF THE CONFERENCE-NEW ZEALAND GRASSLAND ASSOCIATION*. 2002.
32. RobotWorks. *Scott® Milktech* n.d. [cited 2017 October 2]; Available from: <https://www.robots.com/scottcompanies/viewing/scott-milktech>
33. Yaghoubi, S., et al., *Autonomous robots for agricultural tasks and farm assignment and future trends in agro robots*. International Journal of Mechanical and Mechatronics Engineering, 2013. **13**(3): p. 1-6.
34. Blackmore, B., et al. *Development of a deterministic autonomous tractor*. in *Proceedings CIGR*. 2004.
35. Gershgorn, D. *After trying to build self-driving tractors for more than 20 years, John Deere has learned a hard truth about autonomy*. 2017 [cited 2018 May 28]; Available from: <https://qz.com/1042343/after-trying-to-build-self-driving-tractors-for-more-than-20-years-john-deere-has-learned-a-hard-truth-about-autonomy/>.
36. Kassler, M., *Agricultural automation in the new millennium*. Computers and electronics in agriculture, 2001. **30**(1-3): p. 237-240.
37. Gollakota, A. and M.B. Srinivas. *Agribot — A multipurpose agricultural robot*. in *2011 Annual IEEE India Conference*. 2011.
38. Durmuş, H., et al. *The design of general purpose autonomous agricultural mobile-robot: "AGROBOT"*. in *2015 Fourth International Conference on Agro-Geoinformatics (Agro-geoinformatics)*. 2015.
39. Tu, X., *Robust navigation control and headland turning optimization of agricultural vehicles*, in *Agricultural Engineering*. 2013, Iowa State University.
40. Bawden, O.J., *Design of a lightweight, modular robotic vehicle for the sustainable intensification of broadacre agriculture*. 2015.
41. Biber, P., et al. *Navigation system of the autonomous agricultural robot Bonirob*. in *Workshop on Agricultural Robotics: Enabling Safe, Efficient, and Affordable Robots for Food Production (Collocated with IROS 2012)*, Vilamoura, Portugal. 2012.
42. Sander, S. and Deepfield Robotics. *The BoniRob – An Autonomous Mobile Platform for Agricultural Applications*. 2015; Available from: <http://ieeegr.com/ieeegr/Downloads/20150923-Sander-Presentation.pdf>.
43. Nielsen, S., et al. *A low cost, modular robotics tool carrier for precision agriculture research*. in *11th International Conference on Precision Agriculture*. 2012. Indianapolis, Indiana, United States: International Society of Precision Agriculture.
44. Grimstad, L. and P.J. From, *Thorvald II - a Modular and Re-configurable Agricultural Robot*. IFAC-PapersOnLine, 2017. **50**(1): p. 4588-4593.
45. Ion, I., et al., *SOME ASPECTS OF HYDRAULIC DRIVES FOR THE NEW MODEL MERO WALKING ROBOT, APPLIED IN AGRICULTURE AND FORESTRY: Proceedings of the 19th International Conference on CLAWAR 2016*, in *Advances in Cooperative Robotics*. 2016, World Scientific. p. 241-249.
46. Siegwart, R., et al., *Innovative design for wheeled locomotion in rough terrain*. Robotics and Autonomous Systems, 2002. **40**(2): p. 151-162.
47. W Bartlett, P., D. Wettergreen, and W. Whittaker, *Design of the Scarab Rover for Mobility & Drilling in the Lunar Cold Traps*. 2008.

48. Muscato, G., et al., *A prototype of an orange picking robot: past history, the new robot and experimental results*. Industrial Robot: the international journal of robotics research and application, 2005. **32**(2): p. 128-138.
49. Lee, W., et al., *Rough Terrain Negotiable Mobile Platform with Passively Adaptive Double-Tracks and Its Application to Rescue Missions*. Vol. 19. 2005. 1591-1596.
50. Schiele, A., et al., *NanoKhod Exploration Rover - A Rugged Rover Suited for Small, Low-Cost, Planetary Lander Mission*. IEEE Robotics & Automation Magazine, 2008. **15**(2): p. 96-107.
51. Raibert, M., et al., *Bigdog, the rough-terrain quadruped robot*. IFAC Proceedings Volumes, 2008. **41**(2): p. 10822-10825.
52. Kaneko, K., et al. *Humanoid robot hrp-4-humanoid robotics platform with lightweight and slim body*. in *Intelligent Robots and Systems (IROS), 2011 IEEE/RSJ International Conference on*. 2011. IEEE.
53. Huang, Q.-J. and K. Nonami, *Humanitarian mine detecting six-legged walking robot and hybrid neuro walking control with position/force control*. Mechatronics, 2003. **13**(8): p. 773-790.
54. Machado, J.T. and M.F. Silva. *An overview of legged robots*. in *International symposium on mathematical methods in engineering*. 2006. MME Press Ankara, Turkey.
55. Siegwart, R. and I.R. Nourbakhsh, *Introduction to autonomous mobile robots*. Intelligent robots and autonomous agents. 2004, Cambridge, Mass.: MIT Press. ix, 321.
56. Li, Z., et al. *Design and basic experiments of a transformable wheel-track robot with self-adaptive mobile mechanism*. in *2010 IEEE/RSJ International Conference on Intelligent Robots and Systems*. 2010.
57. Luo, Z., et al., *A reconfigurable hybrid wheel-track mobile robot based on Watt II six-bar linkage*. Mechanism and Machine Theory, 2018. **128**: p. 16-32.
58. Fujita, T., T. Sasaki, and Y. Tsuchiya. *Hybrid motions by a quadruped tracked mobile robot*. in *Safety, Security, and Rescue Robotics (SSRR), 2015 IEEE International Symposium on*. 2015. IEEE.
59. Yokota, S., K. Kawabata, and H. Kobayashi, *Development of mobile system using leg-type crawler for rough terrain*. Industrial Robot: An International Journal, 2004. **31**(2): p. 218-223.
60. Hodoshima, R., et al. *Development of track-changeable quadruped walking robot TITAN X-design of leg driving mechanism and basic experiment*. in *Intelligent Robots and Systems (IROS), 2010 IEEE/RSJ International Conference on*. 2010. IEEE.
61. Tadakuma, K., et al. *Mechanical design of the wheel-leg hybrid mobile robot to realize a large wheel diameter*. in *Intelligent Robots and Systems (IROS), 2010 IEEE/RSJ International Conference on*. 2010. IEEE.
62. Wilcox, B.H., et al., *ATHLETE: A cargo handling and manipulation robot for the moon*. Journal of Field Robotics, 2007. **24**(5): p. 421-434.
63. Lu, D., et al. *Design and development of a leg-wheel hybrid robot "HyTRO-I"*. in *2013 IEEE/RSJ International Conference on Intelligent Robots and Systems*. 2013.
64. Schwarz, M., et al. *Hybrid driving-stepping locomotion with the wheeled-legged robot Momaro*. in *2016 IEEE International Conference on Robotics and Automation (ICRA)*. 2016.
65. Zhou, F., et al. *A wheel-track-Leg hybrid Locomotion Mechanism based on transformable rims*. in *2017 IEEE International Conference on Advanced Intelligent Mechatronics (AIM)*. 2017.
66. Michaud, F., et al., *Multi-Modal Locomotion Robotic Platform Using Leg-Track-Wheel Articulations*. Autonomous Robots, 2005. **18**(2): p. 137-156.
67. Bjelonic, M., et al., *Keep Rollin' - Whole-Body Motion Control and Planning for Wheeled Quadrupedal Robots*. IEEE Robotics and Automation Letters, 2019(2): p. 2116-2123.
68. Reid, W., et al. *Actively articulated suspension for a wheel-on-leg rover operating on a Martian analog surface*. in *2016 IEEE International Conference on Robotics and Automation (ICRA)*. 2016.
69. Vanderborght, B., et al., *Variable impedance actuators: A review*. Robotics and Autonomous Systems, 2013. **61**(12): p. 1601-1614.
70. Pratt, G.A. and M.M. Williamson. *Series elastic actuators*. in *Proceedings 1995 IEEE/RSJ International Conference on Intelligent Robots and Systems. Human Robot Interaction and Cooperative Robots*. 1995.
71. Ham, R.V., et al., *Compliant actuator designs*. IEEE Robotics & Automation Magazine, 2009. **16**(3): p. 81-94.
72. Wolf, S., et al., *Variable Stiffness Actuators: Review on Design and Components*. IEEE/ASME Transactions on Mechatronics, 2016. **21**(5): p. 2418-2430.

73. Hollander, K.W., et al., *An efficient robotic tendon for gait assistance*. Journal of Biomechanical Engineering-Transactions of the Asme, 2006. **128**(5): p. 788-791.
74. Migliore, S.A., E.A. Brown, and S.P. DeWeerth. *Biologically Inspired Joint Stiffness Control*. in *Proceedings of the 2005 IEEE International Conference on Robotics and Automation*. 2005.
75. Koganezawa, K. and H. Yamashita. *Three DOF wrist joint - control of joint stiffness and angle*. in *2010 IEEE International Symposium on Industrial Electronics*. 2010.
76. Tonietti, G., R. Schiavi, and A. Bicchi. *Design and Control of a Variable Stiffness Actuator for Safe and Fast Physical Human/Robot Interaction*. in *Proceedings of the 2005 IEEE International Conference on Robotics and Automation*. 2005.
77. Kawamura, S., et al. *Development of passive elements with variable mechanical impedance for wearable robots*. in *Proceedings 2002 IEEE International Conference on Robotics and Automation (Cat. No.02CH37292)*. 2002.
78. Liu, L., S. Leonhardt, and B.J.E. Misgeld, *Design and control of a mechanical rotary variable impedance actuator*. Mechatronics, 2016. **39**: p. 226-236.
79. Choi, J., et al., *A Robot Joint With Variable Stiffness Using Leaf Springs*. IEEE Transactions on Robotics, 2011. **27**(2): p. 229-238.
80. Van Ham, R., et al., *MACCEPA, The mechanically adjustable compliance and controllable equilibrium position actuator: A 3DOF joint with two independent compliances*. 2007. **43**(4): p. 467-474.
81. Hutter, M., et al., *StarLETH: A compliant quadrupedal robot for fast, efficient, and versatile locomotion*, in *Adaptive Mobile Robotics*. 2012, World Scientific. p. 483-490.
82. Colasanto, L., N.G. Tsagarakis, and D.G. Caldwell. *A compact model for the compliant humanoid robot COMAN*. in *2012 4th IEEE RAS & EMBS International Conference on Biomedical Robotics and Biomechatronics (BioRob)*. 2012.
83. Schiavi, R., A. Bicchi, and F. Flacco. *Integration of active and passive compliance control for safe human-robot coexistence*. in *2009 IEEE International Conference on Robotics and Automation*. 2009.
84. ETH Zurich. *ANYdrive*. n.d. [cited 2019 July 13]; Available from: <https://rsl.ethz.ch/robots-media/actuators/anydrive.html>.
85. Elkady, A. and T. Sobh, *Robotics Middleware: A Comprehensive Literature Survey and Attribute-Based Bibliography*. Journal of Robotics, 2012.
86. Kang, S.-C., *Robot development using Microsoft Robotics Developer Studio*. 2011, Boca Raton, FL: CRC Press. 1 online resource (xiii, 273 pages).
87. Collett, T.H., B.A. MacDonald, and B.P. Gerkey. *Player 2.0: Toward a practical robot programming framework*. in *Proceedings of the Australasian conference on robotics and automation (ACRA 2005)*. 2005. Citeseer Citeseer.
88. Nesnas, I.A.D., et al., *CLARAty: Challenges and Steps toward Reusable Robotic Software*. International Journal of Advanced Robotic Systems, 2006. **3**(1): p. 5.
89. Open Robotics. *Robot Operating System (ROS)*. n.d. [cited 2018 January 9]; Available from: <http://www.ros.org/>.
90. YARP. *Yet Another Robot Platform (YARP)*. n.d. [cited 2019 January 20]; Available from: <http://www.yarp.it/>.
91. ROCK. *Robot Construction kit (ROCK)*. n.d. [cited 2019 January 20]; Available from: <https://www.rock-robotics.org/>.
92. DFKI. *German Research Centre for Artificial Intelligence*. n.d. [cited 2019 April 20]; Available from: <https://www.dfki.de/en/web/>.
93. Istituto Italiano di Tecnologia. *Istituto Italiano Di Tecnologia (IIT)*. n.d.; Available from: <https://www.iit.it/>.
94. RobotCub Consortium. *RobotCub Consortium*. n.d. [cited 2019 April 21]; Available from: http://www.robotcub.org/index.php/robotcub/about_us/consortium.html
95. Willow Garage. *Willow Garage*. n.d. [cited 2018 January 09]; Available from: <http://www.willowgarage.com/>.
96. Jensen, K., et al., *Towards an Open Software Platform for Field Robots in Precision Agriculture*. Robotics, 2014. **3**(2): p. 207-234.
97. Dogtooth. *Dogtooth Robot Harvesting Robots*. n.d. [cited 2019 February 04]; Available from: <https://dogtooth.tech/>.

98. Sweeper. *Sweet Pepper Harvesting Robot*. n.d. [cited 2019 February 04]; Available from: <http://sweeper-robot.eu/>.
99. Lehnert, C., et al., *Autonomous Sweet Pepper Harvesting for Protected Cropping Systems*. IEEE Robotics and Automation Letters, 2017. **2**(2): p. 872-879.
100. Mehta, S.S. and T.F. Burks, *Vision-based control of robotic manipulator for citrus harvesting*. Computers and Electronics in Agriculture, 2014. **102**: p. 146-158.
101. BostonDynamics. *SpotMini*. n.d. [cited 2019 February 09]; Available from: <https://www.bostondynamics.com/spot-mini>.
102. Baur, J., et al. *Design and development of a redundant modular multipurpose agricultural manipulator*. in *2012 IEEE/ASME International Conference on Advanced Intelligent Mechatronics (AIM)*. 2012.
103. Universal Robots. *UR5 Robot Arm*. n.d. [cited 2019 February 09]; Available from: <https://www.universal-robots.com/products/ur5-robot/>.
104. Hu, J., et al., *Dimensional synthesis and kinematics simulation of a high-speed plug seedling transplanting robot*. Computers and Electronics in Agriculture, 2014. **107**: p. 64-72.
105. Sipro. *SiAx D3 500 Delta Robot*. n.d. [cited 2019 February 05]; Available from: <https://www.sipro.vr.it/en/delta-robot/delta-robot-SIAX-D3-500.html>
106. igus®. *drylin® Delta Robot: Technical Documentation*. n.d. [cited 2019 February 05]; Available from: https://www.igus.co.nz/contentData/wpck/pdf/global/Delta_Roboter_tech_doc.pdf.
107. *Break feeding*. Ministry for Culture and Heritage.
108. Gallagher. *Posts - Pigtails and Tread-ins*. n.d. [cited 2019 January 10]; Available from: <https://am.gallagher.com/nz/products/1229/posts-pigtails-and-tread-ins>
109. Hirst, R.L., *Seasonal variation of pasture quality on commercial equine farms in New Zealand : a thesis in partial fulfilment of the requirements for the degree of Master of AgriScience (Equine Studies) at Massey University, Palmerston North, New Zealand*. 2011: 2011.
110. Gallagher. *Gallagher power fence systems user manual*. [cited 2019 February 20]; Available from: https://am.gallagher.com/media/4979/3e1978_gallagher_power_fence_systems_user_manual.pdf.
111. Oberti, R., et al., *Selective spraying of grapevines for disease control using a modular agricultural robot*. Biosystems Engineering, 2016. **146**: p. 203-215.
112. Ibex, *Ibex spraying robot*.
113. Adamides, G., et al., *HRI usability evaluation of interaction modes for a teleoperated agricultural robotic sprayer*. Applied Ergonomics, 2017. **62**: p. 237-246.
114. Bakker, T., et al., *Systematic design of an autonomous platform for robotic weeding*. Journal of Terramechanics, 2010. **47**(2): p. 63-73.
115. Bertolini. *Ezi-spot Sprayer: Manual*. n.d.; Available from: <https://www.bertolini.co.nz/media/wysiwyg/manuals/EZI-SPOT%2012%20Volt%20ATV%20Sprayers/Ezispot%20Sprayer%20Manual.pdf>.
116. Blender, T., et al. *Managing a Mobile Agricultural Robot Swarm for a seeding task*. in *IECON 2016 - 42nd Annual Conference of the IEEE Industrial Electronics Society*. 2016.
117. Greentech Robotics Ltd. *SeedSpider Metering System*. n.d.; Available from: <https://greentechrobotics.com/wp-content/uploads/metering-unit.pdf>.
118. Leon Cook Silos. *Typical Grain Bulk Densities and Angles of Repose*. n.d.; Available from: <http://www.leoncooksilos.com.au/Typical%20Grain%20Bulk%20Densities%20and%20Angles%20of%20Repose.pdf>.
119. Technologies, T.U.o.S.F.o.E.a.I. *Agriculture and the Environment: Research*. n.d. [cited 2019 February 04]; Available from: <https://sydney.edu.au/engineering/our-research/robotics-and-intelligent-systems/australian-centre-for-field-robotics/agriculture-and-the-environment.html>.
120. Allen, R.G., et al. *Crop evapotranspiration - Guidelines for computing crop water requirements - FAO Irrigation and drainage paper 56*. 1998; Available from: [http://www.fao.org/3/X0490E/x0490e0b.htm#chapter%206%20%20etc%20%20single%20crop%20coefficient%20\(kc\)](http://www.fao.org/3/X0490E/x0490e0b.htm#chapter%206%20%20etc%20%20single%20crop%20coefficient%20(kc))
121. Young, S.L. and D.K. Giles, *Targeted and Microdose Chemical Applications*, in *Automation: The Future of Weed Control in Cropping Systems*, S.L. Young and F.J. Pierce, Editors. 2014, Springer Netherlands: Dordrecht. p. 139-147.

122. Parker Hannifin Corporation. *Energy Efficiency in Hydraulics*. 2009; Available from: https://www.parker.com/literature/Hydraulic%20Controls%20Europe/Brochures/HY11-3338UK_Energy%20efficiency%20HMI09.pdf
123. Rivera-Rosario, H.T. and J.S. Powell, *Installation torque tables for noncritical applications*. 2017.
124. Juvinall, R.C. and K.M. Marshek, *Fundamentals of Machine Component Design, 5th Edition*. 2011: Wiley.
125. Akin, J.E. *Impact Load Factors for Static Analysis*. n.d.; Available from: <https://www.clear.rice.edu/mech403/HelpFiles/ImpactLoadFactors.pdf>.
126. Shop4486048 Store. *Wheel hub motor*. n.d. [cited 2018 September 08]; Available from: https://www.aliexpress.com/item/32918096554.html?spm=a2g0o.productlist.0.0.19675665QnFN3J&algo_pvid=2a4e2286-dfe1-4299-a6e6-936c18cb1bd6&algo_expid=2a4e2286-dfe1-4299-a6e6-936c18cb1bd6-1&btsid=0ab6f82315969547126346787e2c3e&ws_ab_test=searchweb0_0,searchweb201602_,searchweb201603
127. Ma, B., et al., *Analysis of vehicle static steering torque based on tire–road contact patch sliding model and variable transmission ratio*. *Advances in Mechanical Engineering*, 2016. 8(9): p. 1687814016668765.
128. Engineering toolbox. *Friction coefficients*. 2004 [cited 2019 July 20]; Available from: https://www.engineeringtoolbox.com/friction-coefficients-d_778.html
129. C-Life Store. *Steering Servo*. n.d. [cited 2019 January 12]; Available from: https://www.aliexpress.com/item/33059208314.html?spm=a2g0o.productlist.0.0.879c4153RxNxO0&algo_pvid=e2af6392-11f2-4400-804b-f4461cc0eab3&algo_expid=e2af6392-11f2-4400-804b-f4461cc0eab3-0&btsid=0ab50f6115969560714151689e8e51&ws_ab_test=searchweb0_0,searchweb201602_,searchweb201603
130. SKF. *Equivalent static bearing load*. n.d. [cited 2018 December 13]; Available from: <https://www.skf.com/group/products/rolling-bearings/principles-of-rolling-bearing-selection/bearing-selection-process/bearing-size/size-selection-based-on-static-load>
131. SKF. *Loads - Single row deep groove ball bearings*. n.d. [cited 2018 December 12]; Available from: <https://www.skf.com/group/products/rolling-bearings/ball-bearings/deep-groove-ball-bearings/loads#cid-467046>
132. *Components of the ANYdrive actuator*. n.d. [cited 2020 January 10]; Available from: <https://image.slidesharecdn.com/ethroboticspresent-190316013749/95/robotics-of-quadruped-robot-7-638.jpg?cb=1552700570>
133. Hikoki NZ Ltd. *Hitachi 138Nm cordless drill*. n.d. [cited 2019 December 15]; Available from: <https://www.hikoki.co.nz/shop/new-products/36v-138nm-driver-drill/>
134. Certa. *Certa 18v cordless drill*. n.d. [cited 2017 November 20]; Available from: <https://www.dicksmith.co.nz/dn/buy/certa-powerplus-18v-brushless-drill-skin-only/>
135. Calt Sensor. *Calt HAE18U5V12 SSI encoder*. n.d. [cited 2018 August 10]; Available from: <https://www.aliexpress.com/item/1214295061.html?spm=2114.12010615.8148356.2.6ec97f14Ty30uU>.
136. ams AG. *AS5047P encoder datasheet*. 2016; Available from: https://ams.com/documents/20143/36005/AS5047P_DS000324_2-00.pdf/a7d44138-51f1-2f6e-c8b6-2577b369ace8.
137. ams AG. *AS5047P Adapter Board manual*. 2015; Available from: https://media.digikey.com/pdf/Data%20Sheets/Austriamicrosystems%20PDFs/AS5047P-TS_EK_AB.pdf.
138. Fröjd, R. *Multi turn VESC position control Firmware*. n.d. [cited 2018 November 03]; Available from: <https://github.com/raess1/vesc-FW>
139. MIT. *MIT racecar VESC ROS driver*. n.d. [cited 2018 April 15]; Available from: <https://github.com/mit-racecar/vesc>.
140. MIT. *MIT racecar project*. n.d. [cited 2018 December 06]; Available from: <https://racecar.mit.edu/>.
141. Fröjd, R. *VESC to ROS hardware interface*. n.d. [cited 2018 November 05]; Available from: https://github.com/raess1/vesc_hardware_interface.
142. vedder, B. *VESC V4.12*. 2015 [cited 2017 November 13]; Available from: <http://vedder.se/2015/01/vesc-open-source-esc/>.

143. Ellis, G., in *Observers in Control Systems*, G. Ellis, Editor. 2002, Academic Press: San Diego. p. 173-212.
144. Choi, D., *Development of Open-Source Motor Controller Framework for Robotic Applications*. IEEE Access, 2020. **8**: p. 14134-14145.
145. Katz, B., J.D. Carlo, and S. Kim. *Mini Cheetah: A Platform for Pushing the Limits of Dynamic Quadruped Control*. in *2019 International Conference on Robotics and Automation (ICRA)*. 2019.
146. rosymaker store. *MIT Mini Cheetah robot clone*. n.d. [cited 2020 July 28]; Available from: https://www.aliexpress.com/item/4000388454741.html?spm=a2g0o.productlist.0.0.737d639fXtHHHG&algo_pvid=7ccf352c-9016-4a88-a75f-06898e1c24a7&algo_expid=7ccf352c-9016-4a88-a75f-06898e1c24a7-11&btsid=0ab6f82415959306156317955e7f59&ws_ab_test=searchweb0_0,searchweb201602_,searchweb201603
147. BostonDynamics. *Spot legged robot* n.d. [cited 2020 July 28]; Available from: <https://www.bostondynamics.com/spot>